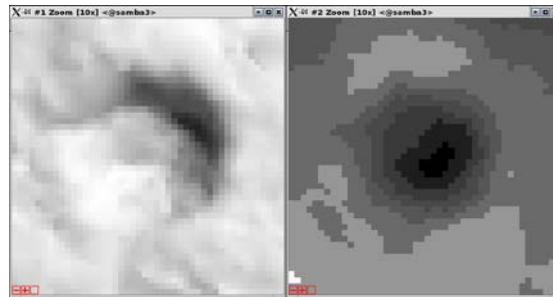


Application of remote sensing in management of cultural heritage

Project Report 2010



Note no

SAMBA/11/11

Authors

Øivind Due Trier (ed., NR), Trude Aga Brun (VFK), Lars Gustavsen (NIKU), Kjetil Loftsgarden (KHM), Lars Holger Pilø (OFK), Arnt-Børre Salberg (NR), Rune Solberg (NR), Knut Harald Stomsvik (STFK), Christer Tønning (VFK)

Date

14 March 2011



Norsk Regnesentral

Norsk Regnesentral (Norwegian Computing Center, NR) is a private, independent, non-profit foundation established in 1952. NR carries out contract research and development projects in the areas of information and communication technology and applied statistical modeling. The clients are a broad range of industrial, commercial and public service organizations in the national as well as the international market. Our scientific and technical capabilities are further developed in co-operation with The Research Council of Norway and key customers. The results of our projects may take the form of reports, software, prototypes, and short courses. A proof of the confidence and appreciation our clients have for us is given by the fact that most of our new contracts are signed with previous customers.

Front page photo

Pitfall trap in Nord-Fron Municipality, Oppland County. Hillshade and elevation image, resolution of 0.2 m, generated from lidar height measurements with 10 hits per m² on average. *In situ* photography by Lars Holger Pilø.

Title	Application of remote sensing in management of cultural heritage – Project report 2010
Authors	Øivind Due Trier (NR, ed.), Trude Aga Brun (VFK), Lars Gustavsen (NIKU), Kjetil Loftsgarden (KHM), Lars Holger Pilø (OFK), Arnt-Børre Salberg (NR), Rune Solberg (NR), Knut Harald Stomsvik (STFK), Christer Tønning (VFK)
Affiliations	Norwegian Computing Center (NR), Vestfold County Administration (VFK), The Norwegian Institute for Cultural Heritage Research (NIKU), The Museum of Cultural History at the University of Oslo (KHM), Oppland County Administration (OFK), Sør-Trøndelag County Administration (STFK)
Quality assurance	Rune Solberg
Date	14 March 2011
Year	2011
Publication number	SAMBA/11/11

Abstract

The project was started in 2002 with the overall aim of developing a cost-effective method for surveying and monitoring cultural heritage sites on a regional and national scale. The project focuses on the development of automated pattern recognition methods for detecting and locating cultural heritage sites. The working assumption is that cultural heritage sites with no visual apparent manifestations above ground may be detectable in satellite images due to alterations in the spectral signature of the bare soil or of uniform vegetation growing there (crops). A software prototype, *CultSearcher*, has been developed to provide computerized assistance in the analysis of satellite images. In particular, the software marks possible sites for further inspection by an archaeologist.

This note describes the achievements of the project during 2010. With the new satellite Worldview-2, we were able to make many new acquisitions of multispectral satellite images of 0.5 m resolution. In these images, the software *CultSearcher* was able to detect several ring-shaped crop marks and soil marks, many of which are likely to be previously unknown leveled grave mounds.

The *CultSearcher* software has been enhanced in three major ways: (1) fewer false detections are made, (2) it can make detections in aerial orthophoto of ground resolution 10-60 cm, and (3) it can detect pitfall traps in lidar height measurements, provided the point density is sufficiently high.

Keywords	Crop marks, soil marks, pitfall traps, Quickbird, Worldview-2, lidar, ring edge detection, pit detection
Target group	Archaeologists, remote sensing researchers.
Availability	Open
Project number	220 449 CultSearcher2010
Research field	Earth observation
Number of pages	139
© Copyright	Norsk Regnesentral

Contents

List of figures.....	7
List of tables	15
1 Introduction.....	17
2 Data and methods.....	19
2.1 Remote sensing images.....	19
2.1.1 New Worldview-2 satellite images	19
2.1.2 Archive Quickbird imagery	30
2.1.3 Aerial orthophoto.....	31
2.1.4 Airborne lidar height measurements.....	32
2.2 Automatic detection of circular soilmarks and cropmarks.....	34
2.2.1 New improvements of automatic detection of circular soilmarks and cropmarks.....	34
2.2.2 Tangent filter response	35
2.2.3 Disc-based match criterion	35
2.2.4 Normalized difference vegetation index.....	36
2.2.5 Texture classification	36
2.2.6 Other improvements of the ring detection algorithm.....	37
2.2.7 Evaluation of the new improvements of the automatic detection of circular soilmarks and cropmarks	37
2.3 Crop mark and soil mark detection in aerial orthophoto.....	39
2.4 Visual inspection of satellite images.....	40
2.5 Automatic detection of pitfall traps in lidar height images	41
2.5.1 Introduction	41
2.5.2 Preprocessing of LAS files.....	41
2.5.3 Detection method.....	41
2.5.4 Manual inspection	44
2.5.5 Analysis of reduced point sampling density.....	44
3 Results.....	45
3.1 Automatic detection of possible crop marks in optical images.....	45
3.1.1 Detections in Worldview-2 images in Vestfold.....	46
3.1.2 Detailed assessment of Vestfold detections	67
3.1.3 Detections in Worldview-2 images in Oppland County.....	89

3.1.4	Detections in Worldview-2 images in Sør-Trøndelag	108
3.1.5	Detections in the Quickbird image of Gardermoen of 29 July 2003	114
3.1.6	Detections in aerial ortophotos in Vestfold	121
3.2	Automatic detection of pitfall traps in lidar data.....	123
3.2.1	Field inspection of pitfall traps.....	125
3.2.2	Detection of pitfall traps in reduced versions of lidar data	133
4	Discussion.....	135
4.1	Detection of circular soil marks and crop marks in optical images	135
4.2	Detection of pitfall traps in lidar data	135
4.3	Point density of lidar data	135
5	Concluding remarks	137
	References	139
	References for soil and crop mark detection method.....	139
	References for detection methods on lidar data.....	139

List of figures

Figure 1. The Brunlanes image from 16 July 2010.	19
Figure 2. The Brunlanes image of 7 August 2010.....	20
Figure 3. The Granavollen image of 24 July 2010.	21
Figure 4. The Granavollen image of 7 August 2010.	22
Figure 5. The Lågendalen image of 7 August 2010.	23
Figure 6. The Marum image of 7 August 2010. For this image, we have eight multispectral bands.	24
Figure 7. The Ørland image of 5 June 2010. For this image, we have eight multispectral bands.	25
Figure 8. The Ørland image of 19 August 2010.	26
Figure 9. The Sandefjord image of 7 August 2010.	27
Figure 10. The Tjølling image of 7 August 2010.	28
Figure 11. The Worldview-2 acquisition of Tjølling of 7 August 2010. The red polygon indicates the portion of the image that is purchased.	29
Figure 12. Archive Quickbird image from 29 July 2003, of an area surrounding, but not including, the Gardermoen airport north of Oslo.	30
Figure 13. Aerial ortophotos covering the Tjølling image. Top: northern part, with the Store Sandnes detection located in the red square. Bottom: southern part, with the Fjellvik location in the red square. Note that the ortophotos are mosaics of different dates of acquisition.	31
Figure 14. Lidar image 32-1-503-169-07, displayed with hillshading.....	32
Figure 15. Lidar image 32-1-503-169-06, also displayed with hill shading.	33
Figure 16: Ring edge template with radius equal to 16 pixels (left) , and the corresponding tangent template (right) at a given angle.....	35
Figure 17. Pit template. White pixels are +1, black pixels are -1, and grey pixels in between. The medium grey pixels outside the white ring edge are exactly zero, thus not contributing to the convolution value. This particular pit template has a radius of 17 pixels, or 3.4 m.....	42
Figure 18. Elongation for four pitfall traps (left) and six false detections (right). Top row: hillshaded DEM, second row: elevation image, with contrast adjusted for visualization, third row: 25% blobs for detections, fourth to seventh rows: descriptions, major axis, radii, and elongations.	44
Figure 19. Examples of obvious misclassifications. Top row, from left: parallel wheel tracks plus some strong spots, turning wheel tracks, forest within agricultural mask, texture in field with other crop (e.g., potato). Bottom row, from left: single tree with shadow, field island, green cereal field, many single strong spots	45
Figure 20. The ten most plausible of the crop mark detections in Vestfold images of 2010. First row from top to bottom: 1-4, Tjølling image of 7 August. Note that there are three detections in	

the second subimage. Second row: 1, from Brunlanes image of 16 July 2010. 2, from Brunlanes image of 7 August. 3, from Lågendalen image of 7 August. 4, from Marum image of 7 August. For details, see the below subsections on each image..... 46

Figure 21. Top: detection no. 1 in the Tjølling image of 7 August 2010, at Eide. Bottom: the crop mark at Eide is not visible in the 2002 orthophoto. 47

Figure 22. Detections nos. 2 (upper left of the three), 3 (upper right), and 8 (lower) in the Tjølling image of 7 August 2010, at Store Sandnes. 48

Figure 23. Top: the 2010 detections nos. 2, 3, and 8 can be seen in the 2009 Quickbird image, albeit obscured by thick haze Bottom: detection no. 3 is clearly visible in the aerial orthophoto of 15 July 2002. 49

Figure 24. Top: detection no. 4, near Fjellvik. This crop mark was also detected in the Quickbird image of 24 July 2009. Bottom: the cropmark at Fjellvik is barely visible in the 2002 ortophoto.50

Figure 25. Top: Detection no. 5, at Nedre Klåstad. This crop mark was also detected in the Quickbird image of 24 July 2009, and an aerial orthophoto of 15 July 2002. Middle: Detection no. 6, bottom: detection no. 7..... 51

Figure 26. Top: detection no. 9, a dark spot. Middle: detection no. 10, a very weak detection. Bottom: Detection no. 11, at Huseby. 52

Figure 27. Detections nos. 12 (top), 13 (middle), and 14 (bottom). Detections nos. 13 and 14 are manual detections that are missed by CultSearcher..... 53

Figure 28. Detection no. 15, several crop marks that are not detected by CultSearcher. Note that the rings are very faint in the panchromatic image. 54

Figure 29. Detection no. 1 in the 16 July 2010 Brunlanes image 54

Figure 30. Detections nos. 2 (top), 3 (middle) and 4 (bottom) in the Brunlanes image of 16 July 2010..... 55

Figure 31. Detections nos. 5 (top) and 6 (bottom) in the 16 July 2010 image of Brunlanes..... 56

Figure 32. Detections nos. 1 (top) and 2 (bottom) in the Brunlanes image of 7 August 2010. ... 57

Figure 33. Detections nos. 3 (top), 4 (middle), and 5 (bottom) in the Brunlanes image of 7 August 2010. 58

Figure 34. Detections nos. 6 (top), 7 (middle), and 8 (bottom) in the Brunlanes image of 7 August 2010. 59

Figure 35. Detections nos. 9 (top), 10 (middle), and 11 (bottom) in the Brunlanes image of 7 August 2010. Detections nos. 10 and 11 were detected manually but missed by CultSearcher.60

Figure 36. Detection no. 12 in the Brunlanes image of 7 August 2010, a manual detection missed by CultSearcher. 61

Figure 37. Detection nos. 1 (top), 2 (middle), and 3 (bottom) in the image of Lågendalen of 7 August 2010. Detection no. 3 was detected manually but missed by CultSearcher..... 62

Figure 38. Four manual detections that were missed by CultSearcher in the Lågendalen image of 7 August 2010. Top: detections nos. 4-6, a group of three rings. Bottom: detection no 7..... 63

Figure 39. Detection no. 1 in the Marum image of 7 August 2010..... 64

Figure 40. Detection no. 1 in the Sandefjord image of 7 August 2010.	64
Figure 41. Detections nos. 2 (top), 3 (middle), and 4 (bottom) in the 7 August 2010 image of Sandefjord.	65
Figure 42. Detections nos. 5 (top), 6 (middle), and 7 (bottom) in the 7 August 2010 image of Sandefjord.	66
Figure 43. Detection no. 1 and two nearby grave mounds (Askeladden IDs 76,929 and 9,323).67	
Figure 44. Close-up of the Worldview-2 image with detection no. 1 and two nearby grave mounds.	68
Figure 45. Detection no 1. (labeled 53 in the image) together with manual detections done by visual inspection of the satellite image by the archaeologist.	68
Figure 46. Detections nos. 2, 3, and 8, and surrounding heritage sites at Hem in Larvik municipality.	69
Figure 47. Combined lidar/optical image. The leftmost part of the area is displayed as a lidar height relief image, while the rest of the area is displayed as the Worldview-2 optical satellite image. Two grave fields are indicated as red outlines. Detections nos. 2, 3, and 6 are clearly seen as a group of three bright rings, a little bit below the center of the combined image.	70
Figure 48. Detection no. 4 (orange dot) and surrounding cultural heritage sites marked with red dots.	71
Figure 49. Detection no. 4, at Fjellvik.	71
Figure 50. Top: detection no. 5, and surrounding cultural heritage sites. Bottom: Detection no. 5 (labeled 70) and two manual uncertain detections.	72
Figure 51. Top: detection 7 and the nearby registered cultural heritage sites. Bottom: detection 7 in the satellite image, and a nearby cultural heritage site from the Askeladden database.	74
Figure 52. Top: detection no. 1 and surrounding cultural heritage sites. Bottom: detection no. 1 in the satellite image.	75
Figure 53. Top: overview map showing detection 2 and its surrounding heritage sites. Bottom: Detection no. 2 in the satellite image.	76
Figure 54. Top: detection 1 and surrounding registered cultural heritage sites. Bottom: Detection no. 1 in the satellite image.	77
Figure 55. Top: detection no. 1 (labeled 21 by manual registrator) alongside manually registered crop marks nos. 22 and 23. Number 22 is marked out as certain whilst number 23 is marked as an uncertain detection. Bottom: Detection 1 in constellation with manual detected crop marks south west and north east of detection 1.	78
Figure 56. Detection 2 and surrounding cultural heritage sites.	79
Figure 57. Detection 2 with an unclosed ringditch and what seems like a conserved central (a bit askew to the north) grave inside ringditch.	80
Figure 58. Manual detection no. 1, in the Brunlanes images. Left:: image of 16 July 2010, right: image of 7 August 2010.	82

Figure 59. Manual detections nos. 14-18, in the Brunlanes images. Top: from 16 July 2010, bottom: from 7 August 2010.	82
Figure 60. Manual detections nos. 19 (top), 22 (middle), and 42 (bottom), in the Brunlanes images. Left column: from 16 July 2010, right column: from 7 August 2010.	83
Figure 61. Manual detections nos. 43, in the Brunlanes image (top), 67-69, in the Tjølling image(middle), and 100, in the Lågendalen image; all images of 7 August 2010.	84
Figure 62. A manually detected grave field with five circles (nos. 14-18). This gravefield lies in connection with registered gravefield ID 52459 and ID 70769. The latter is a excavated ironage grave (flatmarksgrav).	86
Figure 63. The same grave field as in Figure 62, with the satellite image replaced by a lidar height relief image in the left part of the illustration. Note the heaps, which are grave mounds in the forest, and the lines, which are roads.	87
Figure 64. Manual detection no. 33 and surrounding registered cultural heritage sites. ID 141980 and 141984 are leveled remains of housing (cooking pits, fireplace, postholes), while ID 141981 is a leveled grave.	87
Figure 65. Manually detected ring ritches, detections nos. 62-64. To the south: a gravefield (ID 68437). and to the west: a gravemound (ID 68436).....	88
Figure 66. Detection no. 1 in the Granavollen image of 24 July 2010.	89
Figure 67. Detections nos. 2 (top), 3 (middle), and 4 (bottom) in the Granavollen image of 24 July 2010.	90
Figure 68. Detections nos. 70 (top) and 71 (bottom) in the 24 July 2010 image of Granavollen.91	
Figure 69. Detection no. 1 in the Granavollen image of 7 August 2010.	92
Figure 70. Detections nos. 2 (top), 3 (middle), and 4 (bottom) in the Granavollen image of 7 August 2010.	93
Figure 71. A ring that was missed by CultSearcher is located about 200 m north-west of detection no. 3.	94
Figure 72. Detection no. 5 in the Granavollen image of 7 August 2010.	94
Figure 73. Manual detection no. 1 at Hvinden vestre in 24 July image. The circular pattern may be due to tractor track turns.	96
Figure 74. Manual detection no. 1 at Hvinden vestre in 7 August image. The circular pattern may be due to tractor track turns.....	96
Figure 75. Detection no. 2, in the 24 July image, with circular patterns at Blakstad, possibly of modern origin. They are clearly visible in a digital orthophoto of 7 May 2010 (Figure 77).	97
Figure 76. Detection no. 2 at Blakstad in Worldview-2 image of 7 August 2010.	97
Figure 77. Top: Circular patterns at Blakstad in orthophoto of 7 May 2010, with 10 cm ground resolution. Bottom: Close-up of four of the circular patterns at Blakstad.	98
Figure 78. Detection no. 3 at Horgen nord in 24 July image. The detection is located 25 m south-east of a grave mound with Askeladden ID 71136.	99

Figure 79. Detection no. 3 at Horgen nord in 7 August image.....	99
Figure 80. Detection no. 6 at Staksrud in the 24 July image. There are several tractor track turns in the area.....	100
Figure 81. Detection no. 6 at Staksrud in the 7 August image.....	100
Figure 82. Detection no. 12 at Gisleberg in the 24 July image. The detection is located 100 m south of burial mounds with Askeladden ID 23040.....	101
Figure 83. Detection no. 12 at Gisleberg in the 7 August image.	101
Figure 84. Detection no. 14 at Hov in the 24 July image. The detection is inside a known burial mound site, with Askeladden ID 52695.....	102
Figure 85. Detection no. 14 at Hov in the 7 August image.	102
Figure 86. Detection no. 27, a circular pattern at Hov søndre in the 24 July image.....	103
Figure 87. Detection no. 27 at Hov søndre.	103
Figure 88. Detection no. 28 at Røisum nordre in the 24 July image. The detection is located 60 m south of a cultural heritage site with Askeladden ID 22975. The detection is probably modern.....	104
Figure 89. Detection no. 28 at Røisum nordre in the 7 August image.....	104
Figure 90. Detection no. 31, two circular patterns at Askim Nordre in the 24 July image.	105
Figure 91. Detection no. 31 in the 7 August image.....	105
Figure 92. Detection no. 34, a circular pattern at Dvergsten in the 24 July image.	106
Figure 93. Detection no. 34 at Dvergsten in the 7 August image.	106
Figure 94. Detection no. 1 in the Ørland image of 5 June 2010.	108
Figure 95. Detections nos. 2 (top) and 3 (bottom) in the Ørland June image.....	109
Figure 96. Left: Detection no. 4, at Vik, in the Ørland June image. Right: the new detection at Vik, superimposed on a Quickbird image from 7 August 2007, which shows a leveled grave field including an elongated grave mound.	109
Figure 97. Left: detection no. 5, at Berg, in the Ørland June image. Right: the crop mark is less visible in the August image.....	110
Figure 98. Detections nos. 1 (top), 2 (middle), and 3 (bottom) in the Ørland image of 19 August 2010.....	111
Figure 99. Detection no. 4 in the 19 August image of Ørland.	112
Figure 100. Detection no. 1 in the Gardermoen image of 29 July 2003.	114
Figure 101. Detections nos. 2 (top), 3 (middle), and 4 (bottom) in the Gardermoen image.of 29 July 2003.	115
Figure 102. Detections nos. 5 (top), 6 (middle), and 7 (bottom) in the Gardermoen image of 29 July 2003.	116
Figure 103. Detections nos. 8, (top), 9 (middle), and 10 (bottom) in the 29 July 2003 image of Gardermoen.	117

Figure 104. Detections nos. 11 (top), 12 (middle), and 13 (bottom) in the 29 July 2003 image of Gardermoen.	118
Figure 105. Detections nos. 14, (top), 15 (middle), and 16 (bottom) in the Gardermoen image of 29 July 2003.	119
Figure 106. Detections nos. 17 (top), 18 (middle), and 19 (bottom) in the Gardermoen image of 29 July 2003.	120
Figure 107. Detection no. 1 in the aerial orthophoto of 15 July 2002 of parts of Vestfold.	121
Figure 108. Detections nos. 2 (top), 3 (middle), and 4 (bottom) in the aerial orthophoto of 15 July 2002.	122
Figure 109. Detections at road edges.	124
Figure 110. The top 27 detections in image 32-1-503-169-6, with the strongest detection enlarged. The detections are labeled in order from the strongest (1) to the weakest (27).	124
Figure 111. The top 6 detections in image 32-1-503-169-7, with the strongest detection enlarged. The detections are labeled in order from the strongest (1) to the weakest (6).	125
Figure 112. This and the following five figures show the top 12 detections in image 32-1-503-169-6. For each detection, the hill shade image is above left, the elevation image is above right, and the field image is below. In the elevation image, each gray tone level represents a separate integer elevation value in feet (0.3048 m). This figure: detections nos. 1 (left) and 2 (right).	126
Figure 113. Detections nos. 3 (left) and 4 (right).	126
Figure 114. Detections nos. 5 (left) and 6 (right).	127
Figure 115. Detections nos. 7 (left) and 8 (right).	127
Figure 116. Detections nos. 9 (left) and 10 (right).	128
Figure 117. Detections nos. 11 (left) and 12 (right).	128
Figure 118. This and the two next figures show five less clear detections. However, all five were confirmed by field inspection. Here: detections nos. 13 (left) and 14 (right).	129
Figure 119. Detections nos. 16 and 17.	129
Figure 120. Detection no. 19. This detection was not found during the initial visual inspection of the laser data, but detected by CultSearcher, and confirmed in the field.	130
Figure 121. False detections. Nos. 15 (left) , 21 (middle), and 22 (right).	130
Figure 122. False detections: detections nos. 23 (left) and 24 (right).	131
Figure 123. False detections: detections nos. 25 (left) and 26 (right).	131
Figure 124. False detections: nos. 18 (bottom left), 20 (bottom middle) and 27 (bottom right). Top left: the three false detections are located in the same small valley. Top right: section of the small valley, with a large river and a sunlit tree-covered hillside in the background.	132
Figure 125. Detection rates as a function of point density, relative to the full resolution dataset.	134
Figure 126. Four pitfall traps at nine different point densities. From left to right: original dataset with 7.3 ground points per m ² , reduced dataset with 3.6 points per m ² , 1.8 points per m ² , 0.73,	

0.29, 0.15, 0.073, 0.036, and 0.007 points per m². A green frame indicates that the pitfall trap is detected at this resolution, while a red frame indicates that it is not detected. 136

List of tables

Table 1. Worldview-2 acquisitions made during the summer of 2010.	20
Table 2. Point sampling densities, in points per square meter, for the original and the 19 reduced density versions.	33
Table 3. Evaluated features for confirmed detections.	38
Table 4. Crop mark detections in the 7 August 2010 Tjølling image. The first five, the eighth and the eleventh are clear detections. The remaining five detections are weak or doubtful.	48
Table 5. CultSearcher detections for the Brunlanes image of 16 July 2010.	54
Table 6. Cultsearcher detections in the 7 August 2010 Brunlanes image. Abbreviations: det. no. = detection number, diam. = diameter, vis. det. = visual detection, aut. det. = automatic detection, conf. a. d. = confirmed automatic detection.	57
Table 7. CultSearcher detections in the Lågendalen image of 7 August 2010.	61
Table 8. Detections in the Marum image.	63
Table 9. CultSearcher detections in the Sandefjord image.	64
Table 10. Certain manual detections in the Vestfold images of 2010. Auto ID refers to the detection id in Table 4-Table 9, with manual detections from those tables in parentheses.	81
Table 11. Uncertain manual detections in the Vestfold images of 2010.	85
Table 12. Possible manual detections in the Vestfold images of 2010.	86
Table 13. Cultsearcher detections in the Granavollen image of 24 July 2010.	89
Table 14. CultSearcher detections in the Granavollen image of 7 August 2010.	92
Table 15. Manual detections in the two Granavollen images. The four most promising detections are ranked 1-4. The remaining five detections are more uncertain.	95
Table 16. Automatic detections (aut. det.), confirmed automatic detections (conf.a.d.) and manual detections (man.det.) in the Ørland image of 5 June 2010.	108
Table 17. CultSearcher detections in the Ørland image of 19 August 2010.	110
Table 18. CultSearcher detections in the Gardermoen image.	114
Table 19. Detections in Tjølling area of the 2002 Vestfold ortophoto acquisitions.	121
Table 20. Default values for advanced pit search parameters.	123
Table 21. CultSearcher detections of pits in the lidar height image 32-1-503-169-6. The shaded rows are removed manually before field work.	123
Table 22. The result of the field inspection. The green rows denote valid detections, and the pink rows denote false detections. The detections are sorted by <i>normalized correlation</i> , the 6th column.	132

Table 23. Detection results on reduced point density datasets. Detection categories are from a manual inspection of the detection results on the full resolution dataset, with '9' being a certain true detection of a cultural heritage pit, '5' being in doubt, and '1' being a certain false detection. Categories 2-3 are probable false detections, with something resembling a pit. Categories 6-8 are probable cultural heritage pits. 133

1 Introduction

The increasingly intensive use and modification of the landscape resulting from modern demands for efficient infrastructure and land use (agricultural production, mining, energy sources, leisure/tourism facilities, etc.) exerts growing pressure on cultural heritage in the landscape. In order to match the political intentions of updated and sustainable cultural heritage management, it is necessary to develop a cost-effective method for locating and monitoring cultural heritage sites. In recognition of this, a project was started in 2002 with the overall aim of developing a cost-effective method for surveying and monitoring cultural heritage sites on a regional and national scale.

The early stage of the project focused on the development of automated methods, such as pattern recognition, for detecting and locating cultural heritage sites. The working assumption is that cultural heritage sites with no visual apparent manifestations above ground may be detectable in satellite images due to alterations in the spectral signature of the bare soil or of uniform vegetation growing there (crops). During the last project years the aim was to develop a software prototype, CultSearcher, to provide computerized assistance in the analysis of satellite images. In particular, the software marks possible sites for further inspection by an archaeologist. The detection method has focused on identifying circular crop marks and soil marks in agricultural fields, which may indicate the presence of a leveled grave mound.

CultSearcher is further developed during the 2010 project. The ring detection method is improved to reduce the number of false detections, and is applied on ten new Worldview-2 images, acquired in 2010. Further, CultSearcher is adjusted to also accept digital orthophoto of ground resolution 10-60 cm as input. Also, CultSearcher is extended to search for pitfall traps in lidar height images.

The rest of this report is organized as follows. Chapter 2 describes the remote sensing images and the improvements and extensions of the detection algorithms. In Chapter 3, the results of automatic detection methods on the remote sensing images are described. The results are discussed in Chapter 4. The report ends with concluding remarks in Chapter 5.

2 Data and methods

2.1 Remote sensing images

This section describes new satellite images, archive aerial orthophoto, and new lidar height images, used for automatic detection of some kinds of cultural heritage.

2.1.1 New Worldview-2 satellite images

During the 2010 project, a number of new Worldview-2 acquisitions have been made (Figure 1- Figure 11, Table 1).



Figure 1. The Brunlanes image from 16 July 2010.

Table 1. Worldview-2 acquisitions made during the summer of 2010.

Name	County	Date	Area	0.5 m pan	2.0 m MS	
					4 band	8 band
Brunlanes	Vestfold	16 July 2010	79km ²	x	x	
Brunlanes	Vestfold	7 August 2010	79km ²	x	x	
Granavollen	Oppland	24 July 2010	86km ²	x	x	
Granavollen	Oppland	7 August 2010	86km ²	x	x	
Lågendalen	Vestfold	7 August 2010	40km ²	x	x	
Marum	Vestfold	7 August 2010	39km ²	x	x	x
Sandefjord	Vestfold	7 August 2010	80km ²	x	x	
Tjølling	Vestfold	7 August 2010	78km ²	x	x	
Ørland	Sør-Trøndelag	5 June 2010	46km ²	x	x	x
Ørland	Sør-Trøndelag	19 August 2010	78km ²	x	x	



Figure 2. The Brunlanes image of 7 August 2010.



Figure 3. The Granavollen image of 24 July 2010.



Figure 4. The Granavollen image of 7 August 2010.



Figure 5. The Lågendalen image of 7 August 2010.



Figure 6. The Marum image of 7 August 2010. For this image, we have eight multispectral bands.



Figure 7. The Ørland image of 5 June 2010. For this image, we have eight multispectral bands.



Figure 8. The Ørland image of 19 August 2010.



Figure 9. The Sandefjord image of 7 August 2010.



Figure 10. The Tjølling image of 7 August 2010.

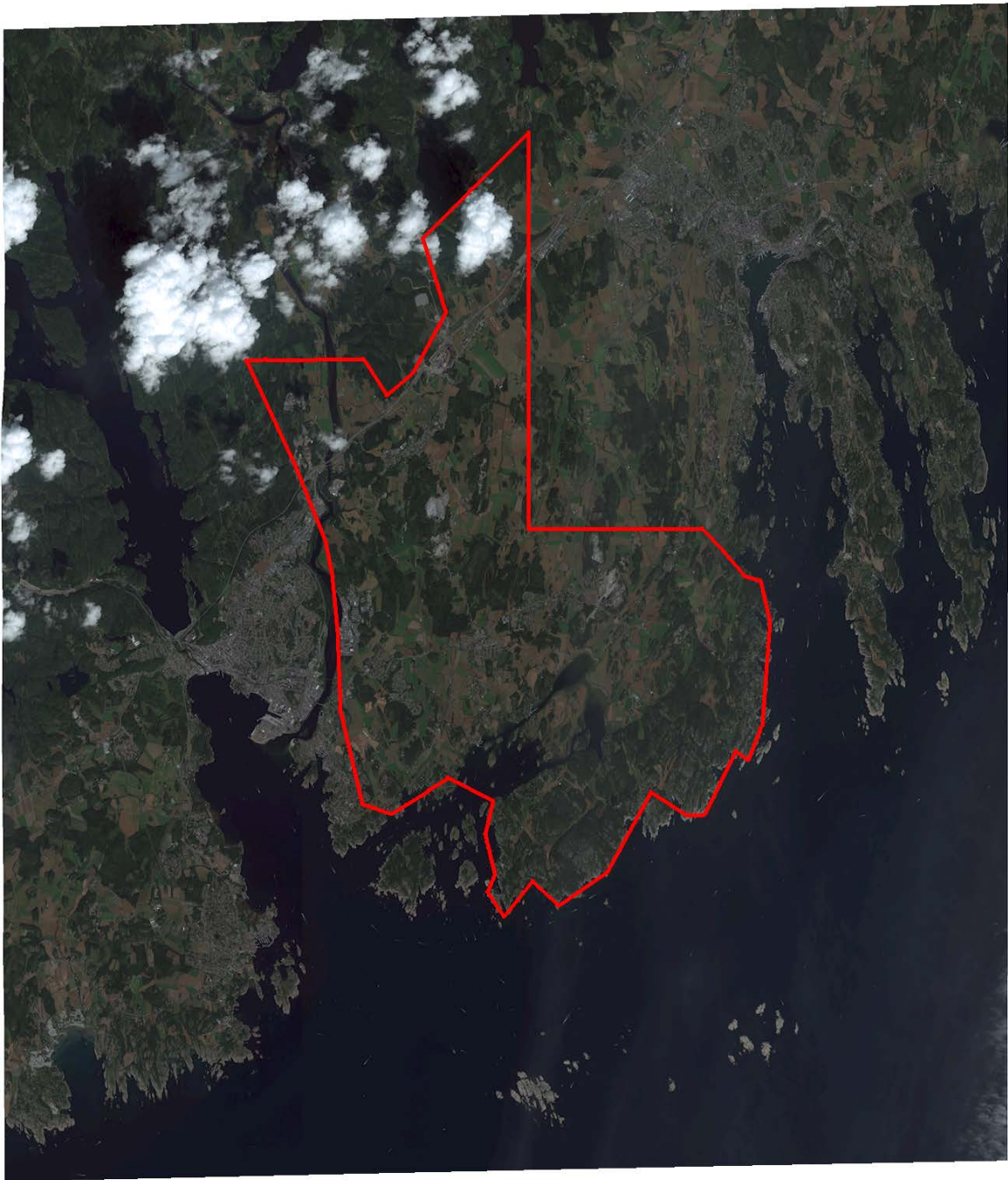


Figure 11. The Worldview-2 acquisition of Tjølling of 7 August 2010. The red polygon indicates the portion of the image that is purchased.

2.1.2 Archive Quickbird imagery

In addition to this year's Worldview-2 acquisitions, an archive Quickbird image of Gardermoen of 29 July 2003 (Figure 12) has been included for processing.



Figure 12. Archive Quickbird image from 29 July 2003, of an area surrounding, but not including, the Gardermoen airport north of Oslo.

2.1.3 Aerial orthophoto

At www.norgebilder.no, privileged users may log in and download aerial orthophotos. For some areas, several acquisitions are available. Most acquisitions are in May, June and early July, too early for crop marks to have developed. However, the scanned analogue RGB aerial images of 2002 of most of Vestfold are from late July and early August. Aerial images, covering most of the Tjølling satellite image, were downloaded (Figure 13).



Figure 13. Aerial orthophotos covering the Tjølling image. Top: northern part, with the Store Sandnes detection located in the red square. Bottom: southern part, with the Fjellvik location in the red square. Note that the orthophotos are mosaics of different dates of acquisition.

2.1.4 Airborne lidar height measurements

The project has acquired lidar height measurements from some municipalities in Gudbrandsdalen, Oppland County, at different point densities. In 2010, experiments were conducted on one dataset: Olstappen. The experiments will continue on the other datasets in 2011.

2.1.4.1 Olstappen dataset

For an area surrounding the lake Olstappen in Nord-Fron municipality, Oppland County, the data was acquired by helicopter, with a minimum of 10 emitted laser pulses per m². This terrain is dominated by open pine forest, allowing a large proportion of hits from the ground. The dataset is divided into 600 m x 800 m tiles (Figure 14-Figure 15). This area is known to contain many pitfall traps that were used in moose hunting 500-2000 years ago.

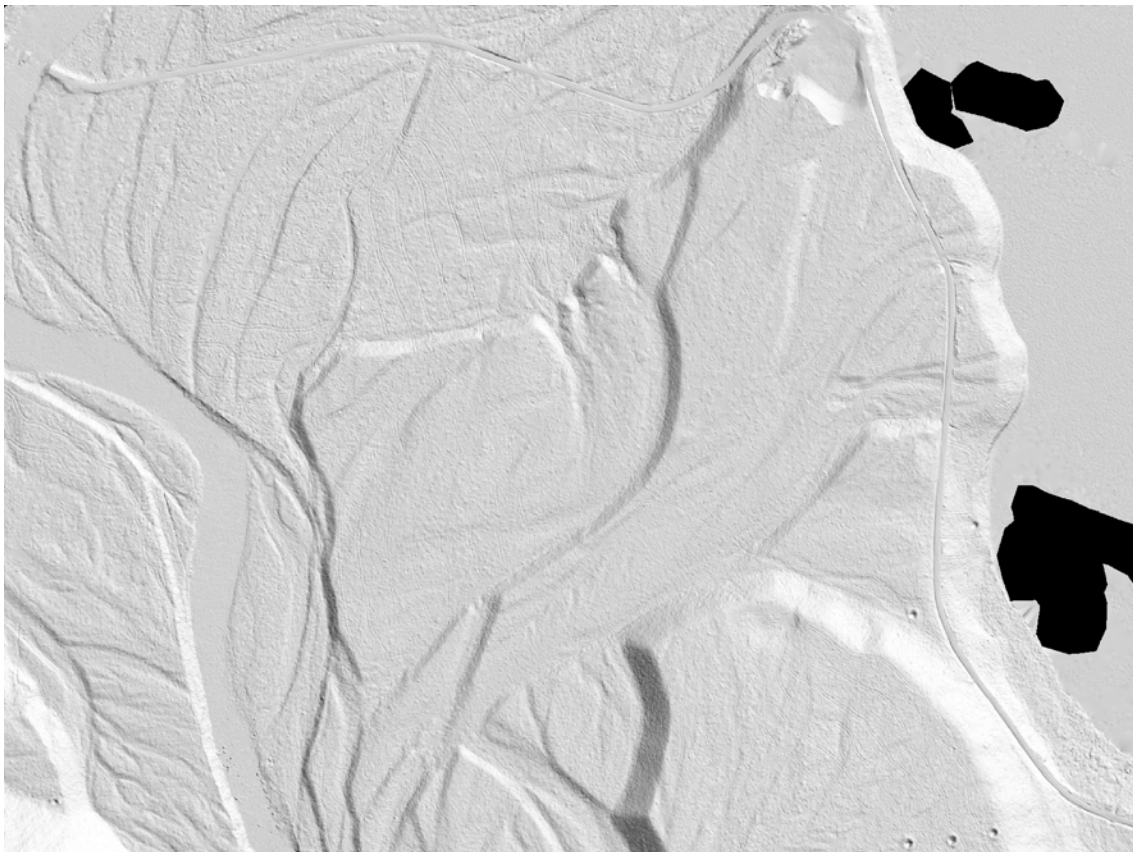


Figure 14. Lidar image 32-1-503-169-07, displayed with hillshading.



Figure 15. Lidar image 32-1-503-169-06, also displayed with hill shading.

2.1.4.2 Reduced point density versions of the Olstappen dataset

In order to simulate the effect of acquiring lidar at lower point density, reduced point density versions of the Olstappen dataset is produced as follows. For each ground reflection, a number between 0.0 and 1.0 is drawn randomly from a uniform distribution. Then, for each point sampling factor, a ground reflection is kept if the associated random number is below the sampling factor. For example, if the point sampling factor is 0.1, then only ground reflections with random numbers below 0.1 are included. For each ground reflection, the associated random number is drawn only once, so that if the ground reflection is included at a specific point sampling factor, then it is included for all higher point sampling factors as well.

20 point sampling factors were used, from 1.0 to 0.001, resulting in point sampling densities between 7.277 and 0.007 points per m² (Table 2).

Table 2. Point sampling densities, in points per square meter, for the original and the 19 reduced density versions.

Point sampling factor	1	0.9	0.8	0.7	0.6	0.5	0.4	0.3	0.25	0.2
Point sampling density	7.277	6.549	5.822	5.094	4.366	3.638	2.911	2.183	1.819	1.455
Point sampling factor	0.15	0.1	0.08	0.06	0.04	0.02	0.01	0.005	0.003	0.001
Point sampling density	1.092	0.728	0.582	0.437	0.291	0.146	0.073	0.036	0.022	0.007

2.2 Automatic detection of circular soilmarks and cropmarks

In 2008, the ring detection algorithm contained the following steps.

1. Compute a locally contrast enhanced image
2. Convolve the contrast enhanced image with a ring template with radius r .
3. Threshold the convolved image to get ring candidates
4. Repeat steps 2-3 for different radii.

In 2009, the ring detection was modified, resulting in the following steps.

1. Compute a locally contrast enhanced image
2. Convolve the contrast enhanced image with a ring edge template with radius r .
3. Threshold the convolved image to get ring edge candidates
4. Repeat steps 2-3 for different radii.
5. Combine ring pairs having the same center but different radii, to form *strong ring indications*. The ring pairs must be of opposite direction. For each strong ring indication, compute the distance between the ring pair centers and the difference in radii.
6. All remaining ring edges are weak ring indicators.
7. For all ring indicators, compute a number of pattern recognition features.

2.2.1 New improvements of automatic detection of circular soilmarks and cropmarks

In 2010, several new features were added to the ring detection methodology derived in 2009. The aim was to reduce the number of false detections that occur when CultSearcher was applied to an image covering a large scene. The new features are based on:

- Comparisons of the ring filter response with a tangent filter response. This criterion is introduced to remove some false detections due to tracks from tractors and agriculture machinery.
- Use of a disc-based match criterion. This criterion is introduced mainly to remove false detections due to tree shadows and single trees located in the field.
- Normalized difference vegetation index (NDVI). This criterion is introduced to remove false detections that may occur in areas with dense green vegetation.
- Texture classification of the ground where the ring is situated. This criterion is introduced to detected areas that are not interesting with respect to detection of crop or soil marks.

Tuning of CultSearcher to the new features, as well as a re-tuning of the existing ones, were done on a training set consisting of 25 ring shaped objects that could be cultural heritages and

1654 false ring detections. The training set was created from the Lågen 2003, Gardermoen 2003, Tjølling 2009 and Tjølling 2010 images.

2.2.2 Tangent filter response

The tangent filter response is the maximum response (over all angles) of the line edge filter acting as the tangent of a circle at a given angle (Figure 16). The length of the tangent line filter is equal to the corresponding diameter of the circle. Given we have a candidate ring edge at radius r we apply the corresponding tangent edge filter for all angles, and select the maximum response over all angles, i.e.

$$y_T = \max_{\phi} |y(\phi, r)|,$$

where $y(\phi, r)$ denotes the response of the tangent edge filter at radius r and angle ϕ . The maximum response y_T is then compared to the ring edge detection, and the corresponding ring edge detection is deleted if

$$y_R - 0.5\|R(r)\|^2 < y_T - 0.5\|T(r, \phi_{max})\|^2$$

$$\left(y_R - 0.5\|R(r)\|^2 \right) - \left(y_T - 0.5\|T(r, \phi_{max})\|^2 \right) > threshold$$

where $R(r)$ denotes the ring edge template at radius r , and $T(r, \phi_{max})$ denotes tangent edge template at radius r and angle ϕ_{max} . The threshold may be different for single detections and ring pair detections.

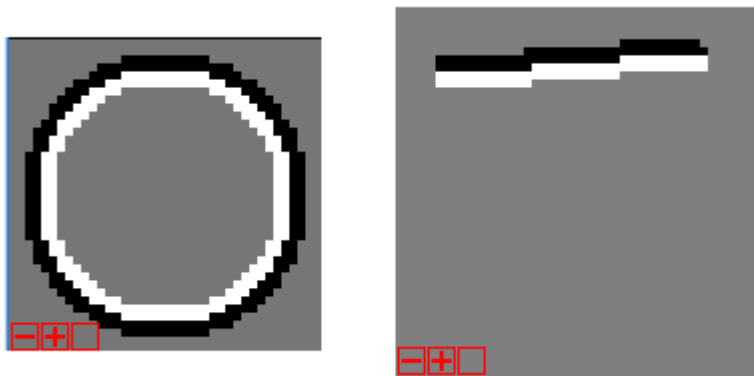


Figure 16: Ring edge template with radius equal to 16 pixels (left) , and the corresponding tangent template (right) at a given angle.

2.2.3 Disc-based match criterion

A disc-based match criterion is constructed from the Cauchy-Schwarz (CS) divergence by comparing samples taken from the centre of the detected ring to samples of the surroundings of the detected ring. The CS divergence is defined as (Jensen et al., 2010)

$$CS = -\log \left[\frac{\int p_1(x) p_2(x) dx}{\sqrt{\int p_1^2(x) dx \int p_2^2(x) dx}} \right]$$

where $p_1(x)$ and $p_2(x)$ denotes the probability density function (PDF) of samples taken at the ring centre and surroundings, respectively. The PDFs are estimated using Parzen's density estimator for the intensity values extracted from corresponding areas in the panchromatic image.

If CS is higher than a given threshold the detected ring edge most likely correspond to a disc-based object, like a trees shadow or a single tree.

2.2.4 Normalized difference vegetation index

The normalized difference vegetation index, NDVI (e.g., see Campbell, 2006; Townshend et al, 1985; Aase and Siddoway, 1981), is a simple numerical indicator that can be used to analyse remote sensing measurements, and assess whether the target being observed contains live green vegetation or not. The NDVI is defined as:

$$NDVI = \frac{NIR - R}{NIR + R}$$

where NIR and R denotes the near infrared and red band, respectively.

Since crop marks are often best visible in the late summer in cereal fields, the NDVI may be used to reduce the number of false detections. The NDVI is often much lower in mature cereal fields than for other green vegetation, like e.g. potato plants. Thus, by deleting ring edge detections in high NDVI areas the number of false alarms may be reduced.

Please note that crop marks may be visible in high NDVI areas as well, and the use of NDVI as a feature for suppressing false detections should be used with caution. Other factors that influences the NDVI is atmospheric effects, cloud, soil effects, and anisotropic effects.

The actual composition of the atmosphere (in particular with respect to water vapour and aerosols) can significantly affect the measurements made in space. Hence, the latter may be misinterpreted if these effects are not properly taken into account (as is the case when the NDVI is calculated directly on the basis of raw measurements). In particular thin clouds (such as the ubiquitous cirrus) can significantly contaminate the measurements. More over the NDVI may depend on the particular anisotropy of the target and on the angular geometry of illumination and observation at the time of the measurements, and hence on the position of the target of interest within the swath of the instrument or the time of passage of the satellite over the site.

2.2.5 Texture classification

Texture is a powerful feature for classifying the content a given area on the ground. Many texture classification schemes exists, and we have chosen the method proposed by Varma and Zisserman (2004), which is a texture classification scheme based on directional filtering of the image, to classify the surroundings of a detected ring. The filters applied are the so-called MR8 filter bank (Varma and Zisserman, 2004).

The method is based on filtering of the image with each of the filters in the MR8 filter bank. After processing the filter responses for rotation invariance, an 8 dimensional feature vector is constructed for each pixel. Within each texture class up to 10 sub-classes is constructed by a K-means clustering strategy, and each pixel in the image is then classified to one of the sub-classes. Then, within a small patch, of say 25×25 m², a histogram model of the sub-classes is constructed.

Training data selected from the following field types in the Tjølling 2010 image

- Class 1 – Forest
- Class 2 – Green medium rugged vegetation
- Class 3 – Mature cereal
- Class 4 - Ploughed

and texture models were constructed by following the approach suggested by Varma and Zisserman (2004).

Then, for each ring edge detection we classify the texture of an 25×25 m² area around the detected ring centre, by first filtering the image patch with MR8 filter bank, classifying each pixel in the patch, constructing a model, and comparing the model with the models constructed from the training set.

In order to apply the new proposed features to improve the ring detection, they need to be evaluated on a data set consisting of both true and false ring detections. The ground truth of the ring detections in the training data set were determined by experienced archaeologists.

2.2.6 Other improvements of the ring detection algorithm

The computational speed and memory consumption of the ring detection algorithm was improved by:

- Implementing an efficient search algorithm for identifying overlapping rings. The new algorithm uses the pixel coordinates directly instead of computing the Euclidean distance between the detect ring centers.
- Applying a linear interpolation, instead of a cubic interpolation, for computing the Cauchy-Schwarz and Laplacian features.

2.2.7 Evaluation of the new improvements of the automatic detection of circular soilmarks and cropmarks

For the confirmed detections in the images Tjølling 2010-08-07, Brulanes 2010-07-16, Brulanes 2010-08-07, Granavollen 2010-07-24, Granavollen 2010-08-07, Ørland 2010-06-05, and Ørland 2010-08-19, the following features were computed (Table 3):

- NDVI
- tangent match
- texture class

We observe that texture appears to be a strong feature (Table 3). All but one true ring detection were classified to texture Class 3 (mature cereal). This indicates that texture is an interesting feature in order to remove false detections. Furthermore, when comparing the tangent match criterion we observed that for single ring detections, this is larger than 10 for all cases. For double rings no such relationship is observed. However, due to the small number of true single

ring detections, more evaluations are needed in order to quantify this threshold. From the table we observe that NDVI is a weak feature. The NDVI value is as high as 0.8 for one ring detection, which in many cases correspond to highly green vegetation. The disc-based match criterion was not evaluated.

Some of the rings found by visual inspection were not detected by CultSearcher due to their size being too large. CultSearcher did not look for rings larger than 10 m in diameter.

Table 3. Evaluated features for confirmed detections.

Location	X (pixel)	Y (pixel)	Ring pair	NDVI	Tangent match	Texture class
Tjølling 2010-08-07	16982,00	20097,00	1	0,36	46,85	3
	18834,00	19378,00	1	0,52	-18,10	3
	18884,00	19369,00	1	0,51	19,38	3
	20111,00	25284,00	1	0,31	-3,75	3
	16387,00	21727,00	1	0,33	-72,16	3
	10274,00	20284,00	0	0,34	20,97	3
	18851,00	19408,00	0	0,52	45,00	3
	9573,00	20687,00	0	0,39	36,40	3
Brulanes 2010-07-16	20250,00	21853,00	1	0,49	44,64	3
	17267,00	17039,00	1	0,72	4,03	3
Brulanes 2010-08-07	19202,00	19759,00	1	0,79	38,09	3
	11499,00	13044,00	1	0,29	-2,21	3
	17266,00	17042,00	1	0,29	-8,10	3
	21885,00	18861,00	1	0,55	-17,91	3
	21790,00	21505,00	0	0,31	12,19	3
Granavollen 2010-07-24	18417,00	21347,00	0	0,63	19,67	3
	23529,00	20048,00	0	0,69	21,33	3
Granavollen 2010-08-07	23712,00	19747,00	1	0,63	33,76	2
	10613,00	7294,00	0	0,72	16,23	3
Ørland 2010-06-05	15451,00	11469,00	1	0,23	-37,18	3
	10361,00	1779,00	0	0,41	23,39	3
	5647,00	7327,00	0	0,32	24,08	3
Ørland 2010-08-19	4708,00	15822,00	1	0,72	24,49	3
	11715,00	18985,00	0	0,61	10,42	3

2.3 Crop mark and soil mark detection in aerial orthophoto

The same method that is used on very high resolution satellite images (Worldview-2 and Quickbird) is also used on aerial orthophoto. Only a few preprocessing steps are necessary in order to bring the images into a form suitable to the ring detection algorithm.

The ground resolution of the orthophoto used in this study is 0.2 m. For other sets of images available from Norge i bilder (www.norgebilder.no) or elsewhere, the resolution could be 0.1 m, 0.25 m, or 0.5 m. Further, the images are optimized for viewing on computer screens, with eight bits per color, and no near infrared band. The ring detection method was developed for satellite images with 0.5 m or 0.6 m ground resolution and a panchromatic band with 11 bits of information. Initial studies indicated that merely creating panchromatic versions of the aerial images with eight bit per pixel and 0.2 m ground resolution gave poor results. Therefore, the following preprocessing steps are used to bring the aerial orthophoto of 0.2 m ground resolution into a suitable form for the ring detection method:

1. Convert all byte values to floating point values
2. Convert the 0.2 m RGB image to HSV (hue, saturation, value)
3. Take the value band of the HSV image as the 0.2 m panchromatic image.
4. In the 0.2 m panchromatic image, aggregate non-overlapping blocks of 3 x 3 pixels to form 0.6 m pixels and save this 0.6 m ground resolution, floating point panchromatic image
5. In the 0.2 m float-valued RGB image, and for each of the three bands: red, green, and blue, aggregate 3 x 3 pixels to form a 0.6 m ground resolution, floating point RGB image. This image is very useful for manual inspection of the detection results.

2.4 Visual inspection of satellite images

The main aim of the visual inspection is to consider whether detections made by the CultSearcher program are true or false, and to report on any crop marks that CultSearcher could not detect. The images are visually inspected using the imagery software ENVI 4.7. Attributes for any crop marks are reported as UTM coordinates, diameter and any relevant comments. Following the visual inspection, the results are compared with the results from the CultSearcher program. Where CultSearcher has detected crop marks thought to be of archaeological interest, a similar description to the visually detected crop marks is employed.

2.5 Automatic detection of pitfall traps in lidar height images

2.5.1 Introduction

In 2010, the scope of the project is extended to include airborne lidar data for the purpose of detecting cultural heritage sites. Bewley et al. (2005) used a digital elevation model (DEM) derived from lidar height measurements to map previously unknown details of the Stonehenge World Heritage Site. The height accuracy of the lidar measurements was able to reveal details that had been previously overlooked and regarded as 'no visible surface expression'. Devereux et al. (2005, 2008) explored the possibilities of varying the sun elevation and illumination direction when hill-shading the lidar DEM, and noted that some structures may be missed by human interpretation if only one illumination direction is used. They further demonstrated that by using only the ground surface reflectances of the lidar pulses, in effect removing the forest vegetation from the DEM, a very detailed elevation model of the ground was obtained. For the particular study site, more detail was apparent in the DEM than could be seen in the existing archaeological map. Hesse (2010) subtracted a smoothed version of the ground surface DEM from the original to obtain a local height model, thus enhancing local detail and suppressing the large-scale terrain. The local height model could be viewed directly as a grey scale image. It was often an advantage to view both the local height model and a hill-shade model of the original ground surface DEM to get the landscape context when doing visual interpretation. Hesse further noticed that some archaeological structures, such as burial mounds, can be confused with natural phenomena such as small natural hills, wood piles, and patches of low vegetation. Coluzzi et al. (2010) used full-waveform lidar to better discriminate between low vegetation and structures of archaeological interest.

2.5.2 Preprocessing of LAS files

The lidar data is available as LAS files containing up to four returns per emitted laser pulse. Each return contains an x,y,z coordinate in UTM zone 32, and a class label denoting if it is a ground, vegetation, or building point. We are only interested in the ground points, and prefer to do the detection on a regular grid (image) rather than arbitrary points. The following steps are used to convert the LAS files to a 0.2 m xy -resolution height image with floating point height values in meters.

1. Create a triangulation of all the ground returns
2. Convert the triangulation to a digital elevation model (DEM) with 0.2 m ground resolution in the x - and y -coordinates, and floating point-valued height values in meters.

2.5.3 Detection method

The detection method uses the following main steps, similarly to the ring detection method for soil marks and crop marks in optical images:

1. Convolve the image with templates of varying sizes. Threshold each convolution result to obtain detections.
2. Merge detections that are closer than a distance threshold, keeping the strongest detections.
3. For each detection, compute features that measure the deviation from an ideal model, using different measures than the convolution in step 1.

4. Remove detections that have feature values outside prescribed intervals.

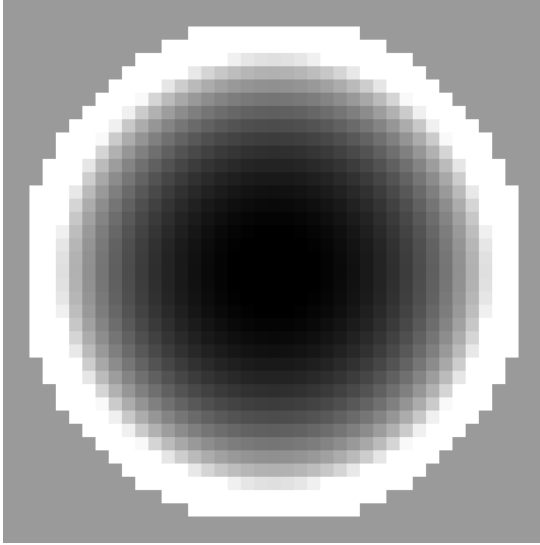


Figure 17. Pit template. White pixels are +1, black pixels are -1, and grey pixels in between. The medium grey pixels outside the white ring edge are exactly zero, thus not contributing to the convolution value. This particular pit template has a radius of 17 pixels, or 3.4 m.

Each pit template in step 1 is a hemisphere with a ring edge (Figure 17). We used 12 pit templates with radii from 6 to 17 pixels, that is, 1.2 to 3.4 meters, each template having 1 pixel (0.2 m) larger radius than the next smaller.

In step 2, for each detection, if another detection is closer than the first detection's radius, the two detections are merged, keeping the stronger of the two detections. The distance between two detections is measured between their centers.

In step 3, the following features are computed:

- Normalized correlation value, that is, the correlation value divided by the radius
- Average pit depth, measured as the height difference between the lowest point inside the pit and the average height on the ring edge outside the pit.
- Minimum pit depth, measured as the height difference between the lowest point inside the pit and the lowest point on the ring edge.
- Standard deviation of height values on the ring edge
- Root mean square deviation from a perfect hemisphere
- Root mean square deviation from a perfect V-shaped pit
- For each pit, a threshold is defined as the value that separates the pixels inside the pit into two groups, the 25% of the pixels that are darker than the threshold, and the 75% that are brighter. Use this threshold to extract a dark blob from a square image centered on the pit, with sides equal to six times the radius. This is called the 25%-blob. If this results in a compact, central blob inside the pit, connected to a larger blob outside the

pit, with only a few connecting pixels on a ring just outside the pit, then the central blob is separated from the outside blob. From the extracted blob, the following features are computed:

- Offset: distance from pit center to the blob's center
 - Major axis length, defined below in Section 2.5.3.1
 - Elongation, defined as major axis divided by radius.
- Similarly to above, extract the 50%-blob and compute offset, major axis and elongation from that blob as well

With true pits labeled, one can then sort the pit detections on one feature at a time, to determine suitable thresholds that seem to be able to separate at least some false detections from the true detections. The thresholds should not be set too tight, as this may lead to true pits being removed by mistake in another dataset. In the event that one has a large number of training samples, one may use a feature selection method (e.g., Somol et al., 1999) and multivariate statistical analysis (e.g., Hastie et al., 2009) to design a classifier.

We used the two tiles in Figure 14 and Figure 15 as a guide in selecting a subset of the features and setting thresholds. Tight thresholds would have been

- normalized correlation > 4.5
- minimum depth > 0.4
- average depth > 0.75
- RMS u-shape < 0.075
- RMS v-shape < 0.075
- 25% blob elongation < 1.5

However, by setting the thresholds too tight, one may risk losing some true detections. Further, the datasets with reduced sampling density will probably need looser thresholds. So, we used:

- normalized correlation > 2.0
- minimum depth > 0.1
- average depth > 0.5
- RMS u-shape < 0.1
- RMS v-shape < 0.1
- 25% blob elongation < 4

2.5.3.1 Major and minor axis, and elongation of a raster object

The major axis of an object can be computed from the central moments as (Prokop and Reeves, 1992):

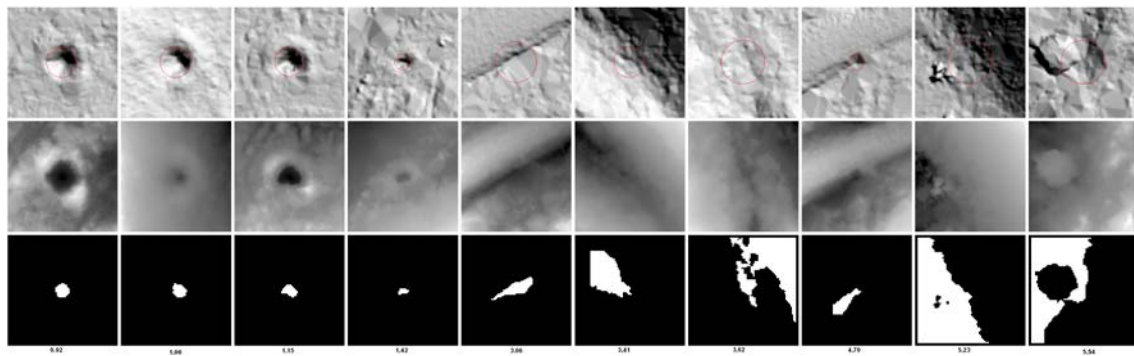
$$\alpha = 2 \sqrt{\frac{2(\mu_{20} + \mu_{02} + \sqrt{(\mu_{20} - \mu_{02})^2 + 4\mu_{11}^2})}{\mu_{00}}}$$

Here, μ_{pq} is the central moment of order $p+q$.

The minor axis is defined as

$$\beta = 2\sqrt{\frac{2(\mu_{20} + \mu_{02} - \sqrt{(\mu_{20} - \mu_{02})^2 + 4\mu_{11}^2})}{\mu_{00}}}$$

The elongation is usually defined as $e = \alpha / \beta$. However, for our purpose, we have a more stable measure of the minor axis in the form of the pit radius r . Ideally, we should scale the radius r by a constant c to get the elongation: $e = \alpha / cr$. However, for the 25% blob, $e = \alpha / r$ is an acceptable estimate, although this elongation can be slightly less than 1 (Figure 18).



Pitfall trap	Pitfall trap	Pitfall trap	Pitfall trap	Road edge	Valley	Valleys meet	Road edge	Foothill	Rock in slope
a=11.04	12.00	12.68	8.52	32.91	40.87	61.51	28.19	88.95	94.15
r=12.00	12.00	11.00	6.00	16.00	12.00	17.00	6.00	17.00	17.00
e=0.92	1.00	1.15	1.42	2.06	3.41	3.62	4.70	5.23	5.54

Figure 18. Elongation for four pitfall traps (left) and six false detections (right). Top row: hillshaded DEM, second row: elevation image, with contrast adjusted for visualization, third row: 25% blobs for detections, fourth to seventh rows: descriptions, major axis, radii, and elongations.

2.5.4 Manual inspection

All detections are labeled with a code from 1 through 9, with 9 meaning a certain detection, 5 meaning being in doubt, and 1 meaning a clear misclassification. 2-3 mean probable misclassifications, but somehow resembling a pit. 4 is not used. 6-8 mean probable detections.

2.5.5 Analysis of reduced point sampling density

In order to study the effect of reduced point density, the detection performance on the reduced versions are compared with the detection performance on the original version. All automatic detections in the full resolution are labeled as described above. Then, for each reduced sampling density, the automatic detections are compared with the automatic detections on the full resolution as follows. For each detection in the full resolution, the closest detection in the reduced resolution is located. If the distance between their centers is less than 2 m, then the detection is counted as 'found' in the reduced version.

3 Results

3.1 Automatic detection of possible crop marks in optical images

This section describes possible crop mark detections in satellite and aerial images. First, detections in new optical Worldview-2 satellite images, acquired during the summer of 2010, are described. A number of uncertain detections are included in addition to the more plausible ones. The shortlists of detections are edited versions of the lists of automatic detections from CultSearcher. The editing consists of removing obvious false detections (Figure 19) by visual inspection guided by CultSearcher. Section 3.1.1 describes detection of possible crop marks in the Wordview-2 satellite images of Vestfold. This is the county that had the highest number of image acquisitions during 2010, and also the highest number of plausible crop mark detections of the participating counties.

Also, detections on an older Quickbird satellite image of Gardermoen are described in Section 3.1.5, since we have now been able to run CultSearcher on the entire image.

The archaeologists contribute as follows. Lars Gustavsen does a visual inspection of the Vestfold 2010 images, and a verification of the shortlists of automatic detections by CultSearcher on the same images in Section 3.1.1. In Section 3.1.2, Christer Tønning and Trude Aga Brun do a detailed assessment of the automatic detections by CultSearcher, followed by a visual inspection, on the same Vestfold images. In this way, the Vestfold images are investigated twice. In Section 3.1.3, Kjetil Loftsgarden verifies the shortlist of automatic detections on two images of Granavollen in Oppland County, and also does a visual inspection of these images. Two image acquisitions of Ørland are available, and shortlists of the automatic detections in these are verified by Knut Harald Stomsvik in Section 3.1.4.



Figure 19. Examples of obvious misclassifications. Top row, from left: parallel wheel tracks plus some strong spots, turning wheel tracks, forest within agricultural mask, texture in field with other crop (e.g., potato). Bottom row, from left: single tree with shadow, field island, green cereal field, many single strong spots

3.1.1 Detections in Worldview-2 images in Vestfold

A number of new detections of possible crop marks have been made in the six Worldview-2 images that were acquired during July and August. Of the ten most plausible detections (Figure 20), six of them were in the Tjølling image. Therefore, the detections in the Tjølling image are presented first, followed by the other images in alphabetical order.

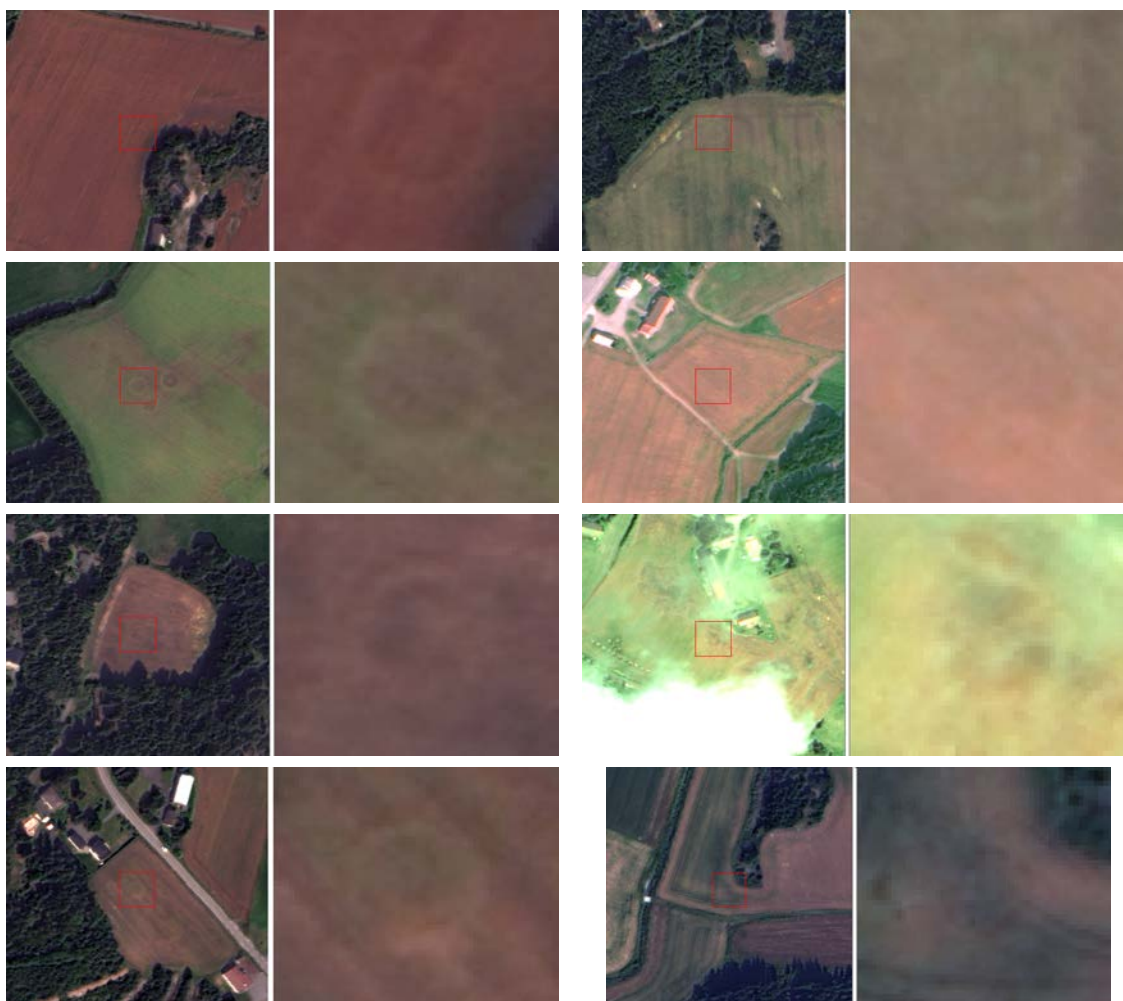


Figure 20. The ten most plausible of the crop mark detections in Vestfold images of 2010. First row from top to bottom: 1-4, Tjølling image of 7 August. Note that there are three detections in the second subimage. Second row: 1, from Brunlanes image of 16 July 2010. 2, from Brunlanes image of 7 August. 3, from Lågendalen image of 7 August. 4, from Marum image of 7 August. For details, see the below subsections on each image.

3.1.1.1 Tjølling, 7 August 2010

In the Worldview-2 image of Tjølling of 7 August 2010 (Figure 10), archaeologist Lars Gustavsen visually detects eight circular crop marks. CultSearcher automatically makes 64 detections. Of these, obvious false detections (Figure 19) are removed. The remaining 12 detections (Table 4) are forwarded to archaeologist Lars Gustavsen for visual inspection. Eight of these are confirmed as true detections. In total, ten true crop marks detections are found by the combined visual and automatic detection method. In addition, an area containing several circular crop marks is detected by Christer Tonning (detection no. 15 in Table 4)

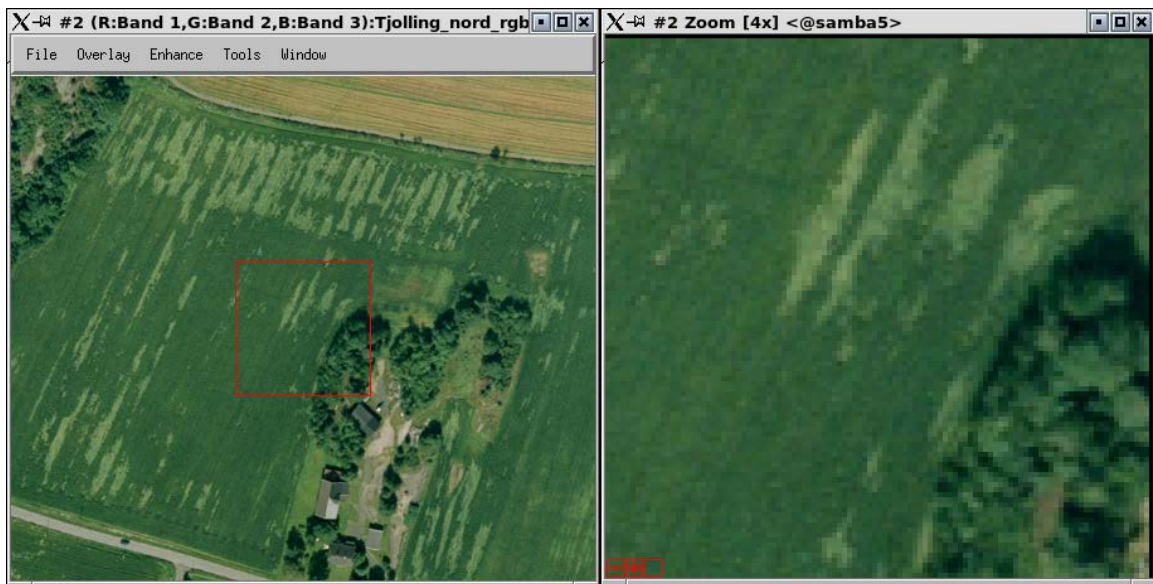


Figure 21. Top: detection no. 1 in the Tjølling image of 7 August 2010, at Eide. Bottom: the crop mark at Eide is not visible in the 2002 orthophoto.

Table 4. Crop mark detections in the 7 August 2010 Tjølling image. The first five, the eighth and the eleventh are clear detections. The remaining five detections are weak or doubtful.

det. no.	UTM zone 32		diam. [m]	vis. insp.	aut. det.	conf. a.d.	Farm name	Comment
	east	north						
1	568029	6547342	13	x	x	x	Eide	
2	568955	6547701	13	x	x	x	Store Sandnes	Very close to detections nos. 3 and 8
3	568980	6547706	17	x	x	x	Store Sandnes	Also detected in 2002 ortophoto.
4	569594	6544748			x	x	Fjellvik	Detected in 2009 Quickbird image
5	567732	6546527	15	x	x	x	Nedre Klåstad	Detected in 2009 Quickbird image and 2002 orthophoto
6	563417	6550829			x			
7	564675	6547248			x			Weak ring
8	568964	6547686	12	x	x	x	Store Sandnes	Only inner ring edge detected.
9	561552	6551963			x			Dark spot
10	564074	6545075			x			Very weak ring
11	564325	6547047	13	x	x	x	Huseby	
12	560864	6552166			x			Doubtful detection
13	563610	6544996	18	x				
14	563902	6546584	8	x				Possible crop mark
15	563212	6546632		x				Several rings



Figure 22. Detections nos. 2 (upper left of the three), 3 (upper right), and 8 (lower) in the Tjølling image of 7 August 2010, at Store Sandnes.



Figure 23. Top: the 2010 detections nos. 2, 3, and 8 can be seen in the 2009 Quickbird image, albeit obscured by thick haze
 Bottom: detection no. 3 is clearly visible in the aerial orthophoto of 15 July 2002.



Figure 24. Top: detection no. 4, near Fjellvik. This crop mark was also detected in the Quickbird image of 24 July 2009. Bottom: the cropmark at Fjellvik is barely visible in the 2002 orthophoto.



Figure 25. Top: Detection no. 5, at Nedre Klåstad. This crop mark was also detected in the Quickbird image of 24 July 2009, and an aerial orthophoto of 15 July 2002. Middle: Detection no. 6, bottom: detection no. 7.



Figure 26. Top: detection no. 9, a dark spot. Middle: detection no. 10, a very weak detection. Bottom: Detection no. 11, at Huseby.



Figure 27. Detections nos. 12 (top), 13 (middle), and 14 (bottom). Detections nos. 13 and 14 are manual detections that are missed by CultSearcher.



Figure 28. Detection no. 15, several crop marks that are not detected by CultSearcher. Note that the rings are very faint in the panchromatic image.

3.1.1.2 Brunlanes image of 16 July 2010

Prior to looking at the automatic detections, no detections are made by visual inspection by the archaeologist. CultSearcher automatically detects 54 potential crop marks. Of these, six are forwarded to the archaeologist for verification (Figure 29-Figure 31). The archaeologist regards one of these as a true detection of a leveled grave mound, and another of these a possible detection.

Table 5. CultSearcher detections for the Brunlanes image of 16 July 2010.

det. no.	UTM zone 32		diam. [m]	vis. insp.	aut. det.	conf. a.d.	Farm name	Comment
	east	north						
1	557131	6538118	15		x	x		True detection
2	555640	6540525	10		x	x		Possible detection
3	551384	6537651			x			
4	552918	6540502			x			
5	558947	6538425			x			
6	556411	6540068			x			



Figure 29. Detection no. 1 in the 16 July 2010 Brunlanes image



Figure 30. Detections nos. 2 (top), 3 (middle) and 4 (bottom) in the Brunlanes image of 16 July 2010.



Figure 31. Detections nos. 5 (top) and 6 (bottom) in the 16 July 2010 image of Brunlanes.

3.1.1.3 Brunlanes image of 7 August 2010

The archaeologist visually detects five crop marks. CultSearcher automatically detects 67 potential crop marks. Nine of these are forwarded to the archaeologist for visual inspection, and the archaeologist regards three of these as true detections, and two as possible detections of leveled grave mounds. In total, five true detections and three possible detections are made (Table 6).

Table 6. Cultsearcher detections in the 7 August 2010 Brunlanes image. Abbreviations: det. no. = detection number, diam. = diameter, vis. det. = visual detection, aut. det. = automatic detection, conf. a. d. = confirmed automatic detection.

det. no.	UTM zone 32		diam. [m]	vis. det.	aut. det.	conf. a. d.	Farm name	Comment
	east	north						
1	556607	6539165	14	x	x	x		
2	552756	6542522	18		x	x		Also a possible ring to the east of this.
3	555639	6540523	15	x	x	x		Broken ring. Central grave?
4	557949	6539614	11		x	x		Possible
5	555326	6540889			x			
6	553812	6540592			x			
7	554905	6538398			x			
8	557901	6538292	12		x	x		Possible
9	557522	6543286			x			
10	554550	6540975	20	x				Very thin, central grave
11	557126	6538111	15	x				
12	555790	6540022	26	x				Very thin, possible.

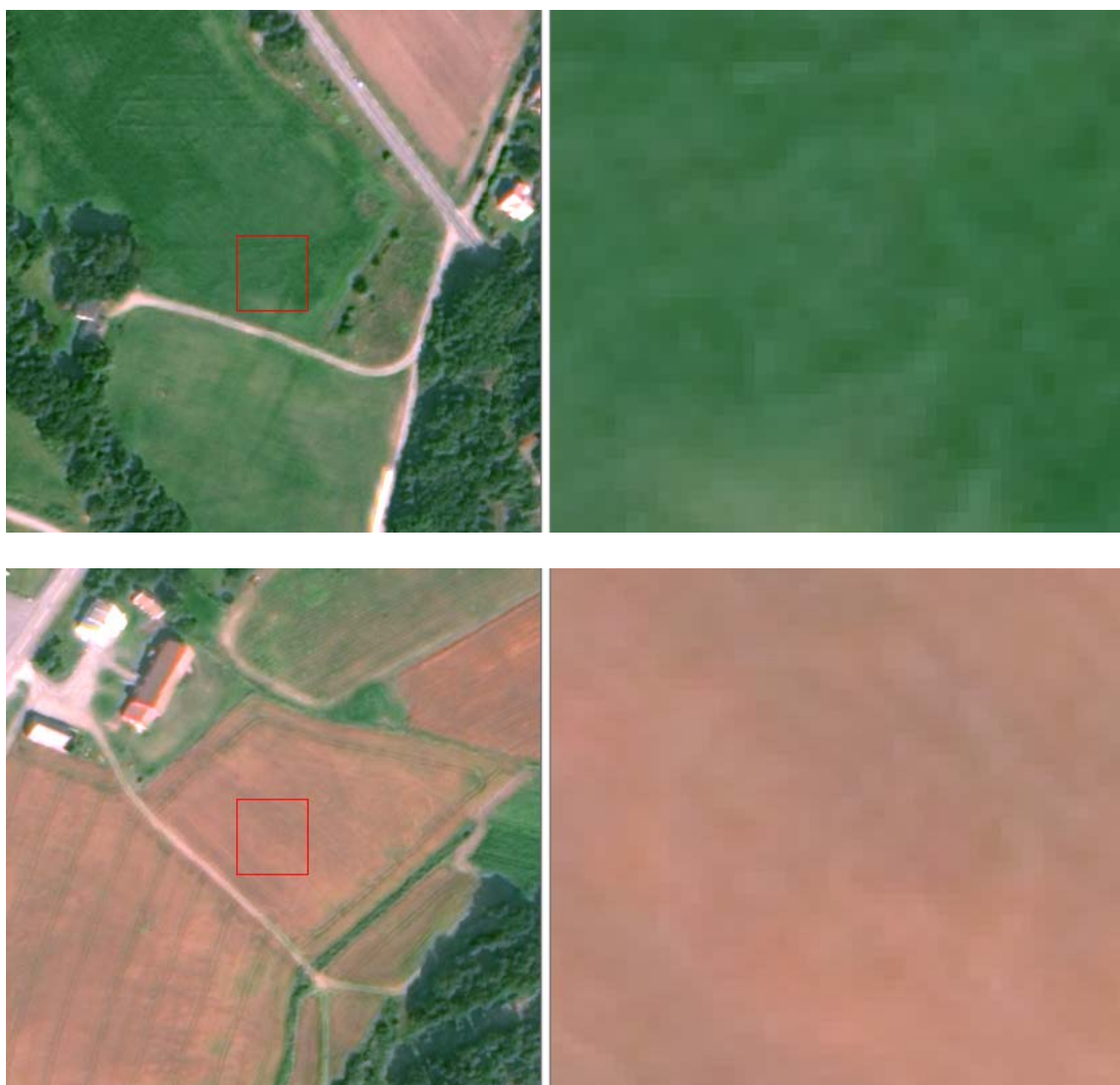


Figure 32. Detections nos. 1 (top) and 2 (bottom) in the Brunlanes image of 7 August 2010.



Figure 33. Detections nos. 3 (top), 4 (middle), and 5 (bottom) in the Brunlanes image of 7 August 2010.



Figure 34. Detections nos. 6 (top), 7 (middle), and 8 (bottom) in the Brunlanes image of 7 August 2010.



Figure 35. Detections nos. 9 (top), 10 (middle), and 11 (bottom) in the Brunlanes image of 7 August 2010. Detections nos. 10 and 11 were detected manually but missed by CultSearcher.



Figure 36. Detection no. 12 in the Brunlanes image of 7 August 2010, a manual detection missed by CultSearcher.

3.1.1.4 Lågendalen image of 7 August 2010

During visual inspection by the archaeologist, five crop marks are detected. CultSearcher automatically detects 15 potential crop marks, and two of them are forwarded to the archaeologist. The archaeologist regards these as possible true detections, but as they are partially covered by clouds they were difficult to investigate further. In total, five true detections and two possible detections of circular crop marks from leveled grave mounds are made (Figure 37-Figure 38, Table 7).

Table 7. CultSearcher detections in the Lågendalen image of 7 August 2010.

det. no.	UTM zone 32		diam. [m]	vis. det.	aut. det.	conf. a.d.	Farm name	Comment
	east	north						
1	558739,5	6558792,5			x	x		Possible detection, but difficult to assess due to clouds
2	557563,5	6561815,5			x	x		Possible detection, but difficult to assess due to clouds
3	555326,0	6562452,0	21,0	x				
4	555265,0	6562294,0	13,0	x				Cluster of 3 rings
5	555264,0	6562283,0	12,0	x				Cluster of 3 rings
6	555277,0	6562275,0	17,0	x				Cluster of 3 rings
7	555488,0	6563409,0	22,0	x				

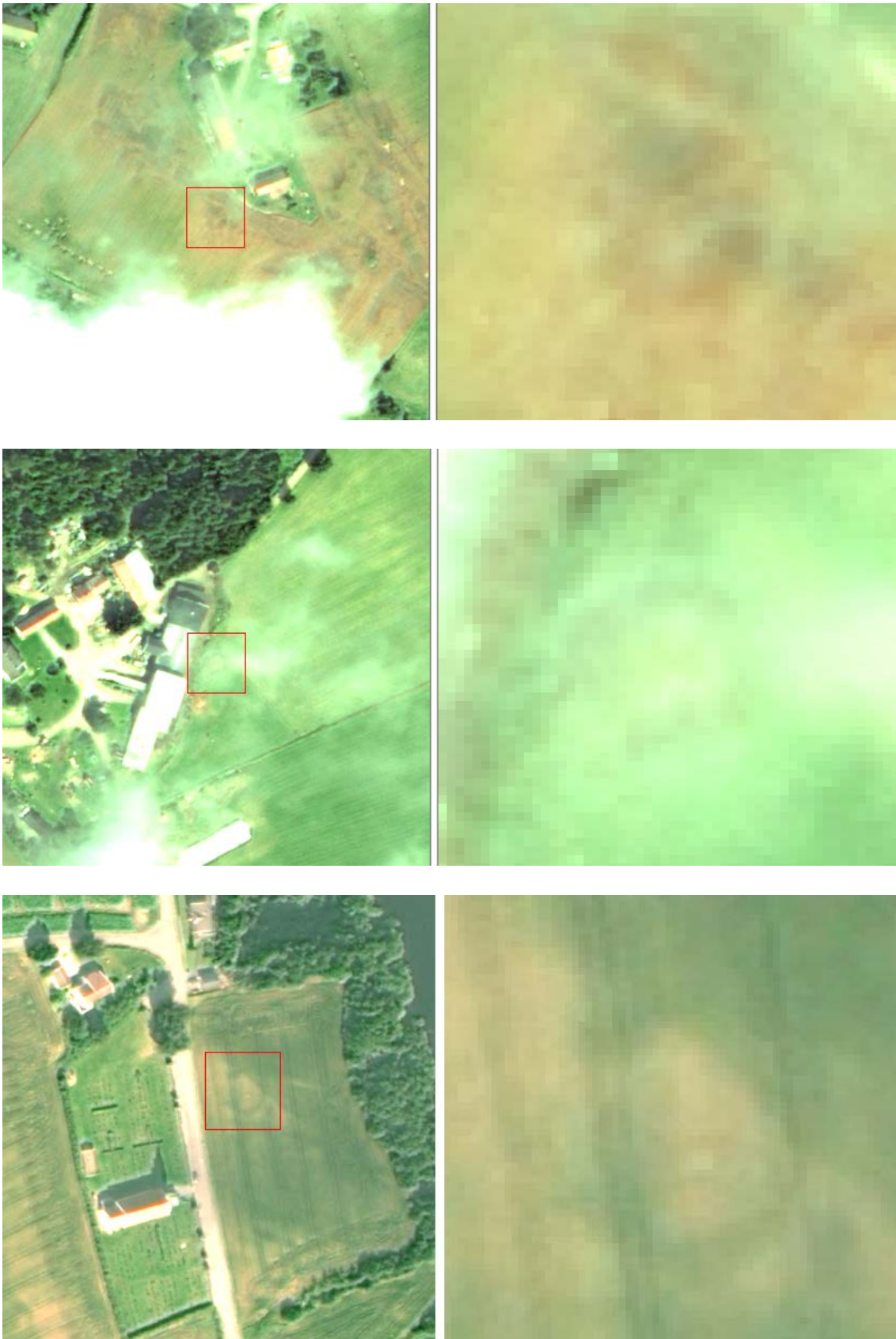


Figure 37. Detection nos. 1 (top), 2 (middle), and 3 (bottom) in the image of Lågendalen of 7 August 2010. Detection no. 3 was detected manually but missed by CultSearcher.



Figure 38. Four manual detections that were missed by CultSearcher in the Lågendalen image of 7 August 2010. Top: detections nos. 4-6, a group of three rings. Bottom: detection no 7.

3.1.1.5 Marum image of 7 August 2010

No crop marks of archaeological interest are visually detected during the visual inspection. CultSearcher automatically detects 8 potential crop marks, of which one is forwarded to the archaeologist (Figure 39, Table 8). This detection is considered false.

Table 8. Detections in the Marum image.

CultSearcher detection no.	UTM zone 32		Comment by archaeologist
	east	north	
1	565963	6549989	False detection



Figure 39. Detection no. 1 in the Marum image of 7 August 2010.

3.1.1.6 Sandefjord image of 7 August 2010

No crop marks of archaeological interest are detected by visual inspection by the archaeologist. CultSearcher automatically detects 119 potential crop marks, and 7 of them are considered as interesting and checked by the archaeologist (Table 9). None of these are considered true.

Table 9. CultSearcher detections in the Sandefjord image.

CultSearcher detection no.	UTM zone 32		Comment by archaeologist
	east	north	
1	576916.5	6566716.5	False detection
2	575450.5	6566749.0	False detection
3	573501.0	6564126.5	False detection
4	569981.0	6560967.0	False detection
5	574895.0	6570661.5	False detection
6	570199.5	6560392.5	False detection
7	568480.0	6557231.0	False detection



Figure 40. Detection no. 1 in the Sandefjord image of 7 August 2010.



Figure 41. Detections nos. 2 (top), 3 (middle), and 4 (bottom) in the 7 August 2010 image of Sandefjord.

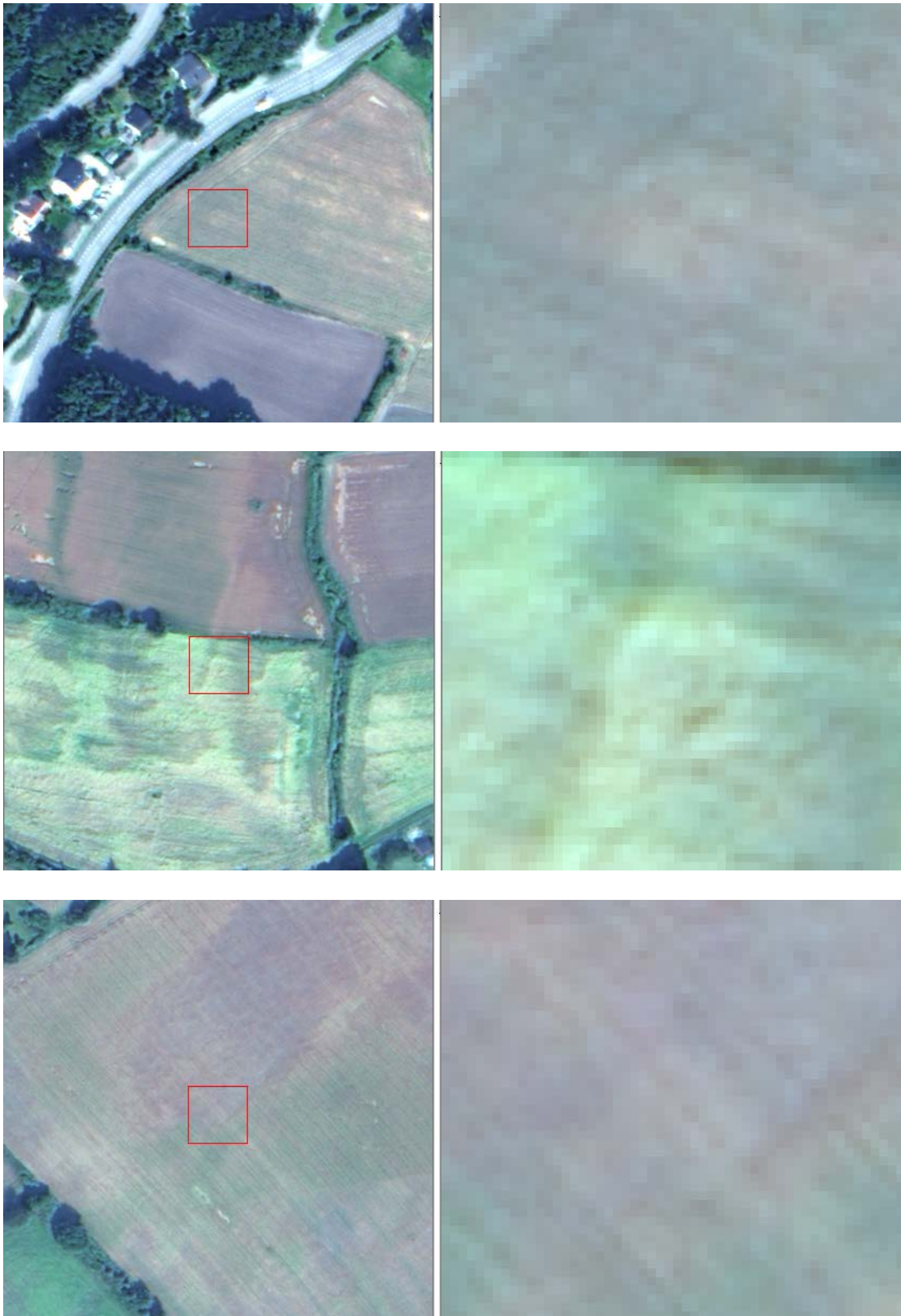


Figure 42. Detections nos. 5 (top), 6 (middle), and 7 (bottom) in the 7 August 2010 image of Sandefjord.

3.1.2 Detailed assessment of Vestfold detections

3.1.2.1 Tjølling 7 August 2010

Of the original 12 detections made by CultSearcher, 7 detections are certain cultural heritage sites.

Detection 1 Eide GBNR 1085/3 N6547341.5 E568029. This detection is in itself very convincing, showing the remains of an overplown grave mound in the form of a preserved/partially preserved ring ditch. The cultural heritage context surrounding detection 1 is rich. 42 meters south by southeast of detection 1 lies 2 grave mounds (Figure 43-Figure 44). North and west lies furthermore grave fields and singular grave mounds. In the bottom left of the map (Figure 43) is also the location for the finding of the Klåstad viking ship in the 1970s (ID 9326 Funnsted). This is a certain detection by CultSearcher, and this find is not previously known. Seen in context with the two grave mounds close by in the east it is clear that this most likely is one continuous grave field which has been partially destroyed. This suspicion was further strengthened under the manual visual inspection of the satellite image, where further five possible overplown grave mounds were found (Figure 45).

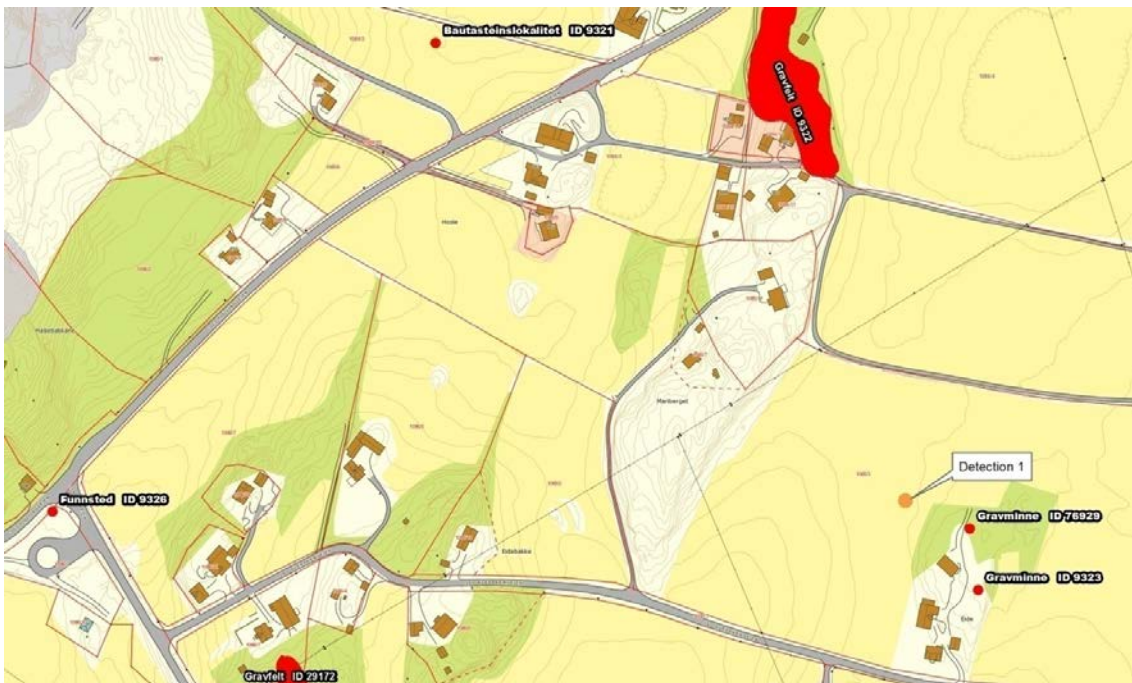


Figure 43. Detection no. 1 and two nearby grave mounds (Askeladden IDs 76,929 and 9,323).



Figure 44. Close-up of the Worldview-2 image with detection no. 1 and two nearby grave mounds.

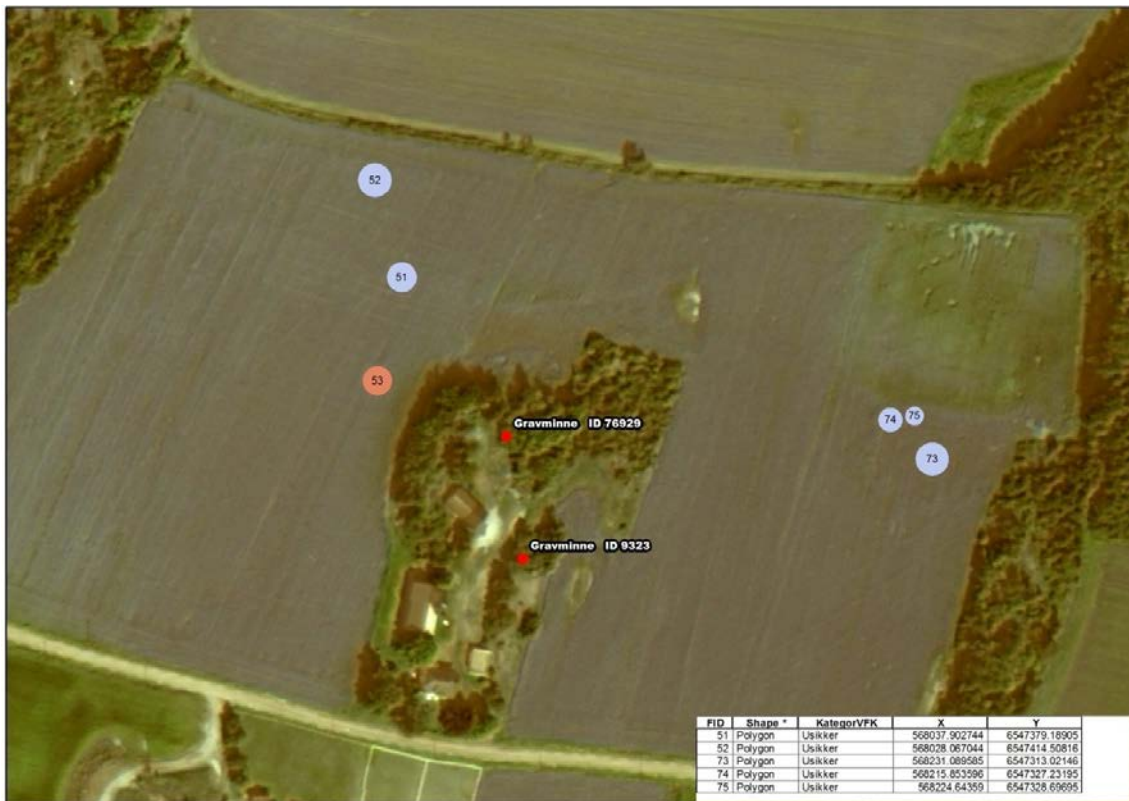


Figure 45. Detection no. 1. (labeled 53 in the image) together with manual detections done by visual inspection of the satellite image by the archaeologist.

Detections nos. 2, 3 and 8, Hem østre, GBNR 1092/5 N 6547705.5 E 568980. These detections are the most distinct cropmarks observed in the datasets in 2010. Detection 2 lies close to and in connection with detection 3 and 8, which are equally distinct. These three detections represents the remaining ring ditches which originally surrounded the now overplown grave mounds.

211 meters west of these three detections and in a small forest patch lies a large grave field consisting of at least 12 similarly sized gravemounds (ID 38735). 265 meters north west of the detections is another grave field consisting of three stone circles and 4 gravemounds. Archaeological excavations of stone circles in Norway has shown that these are graves.

Detections 2, 3 and 8 are certain cultural heritage sites and these are not previously known. These detections lies in an area densely populated by cultural heritage sites as shown in map 4. While manually investigating the satellite these three detections were also flagged by the archaeologist as certain cropmarks.

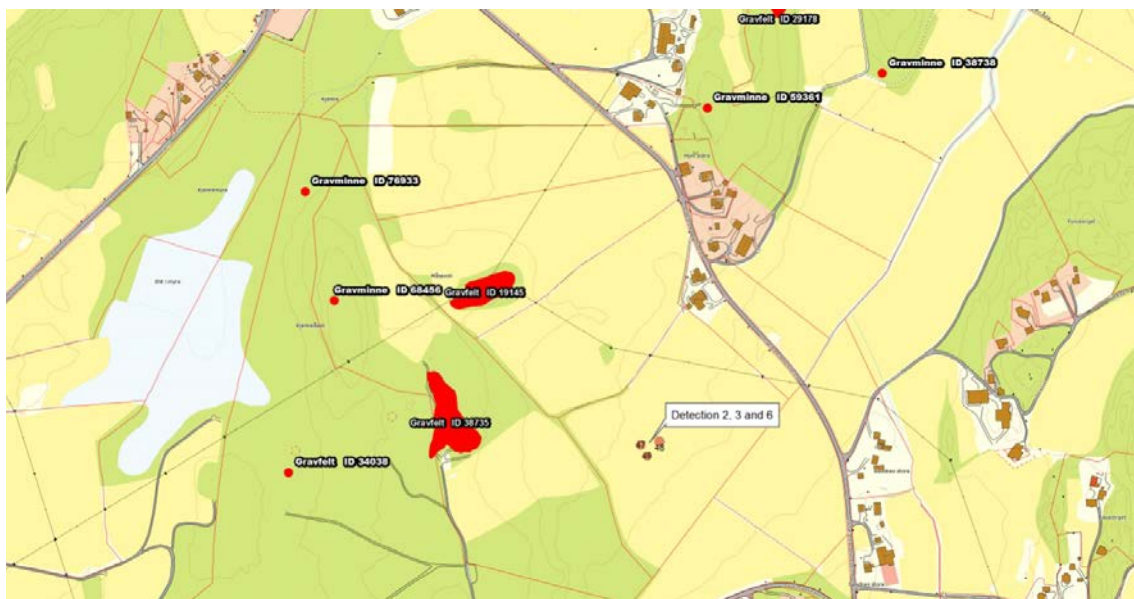


Figure 46. Detections nos. 2, 3, and 8, and surrounding heritage sites at Hem in Larvik municipality.

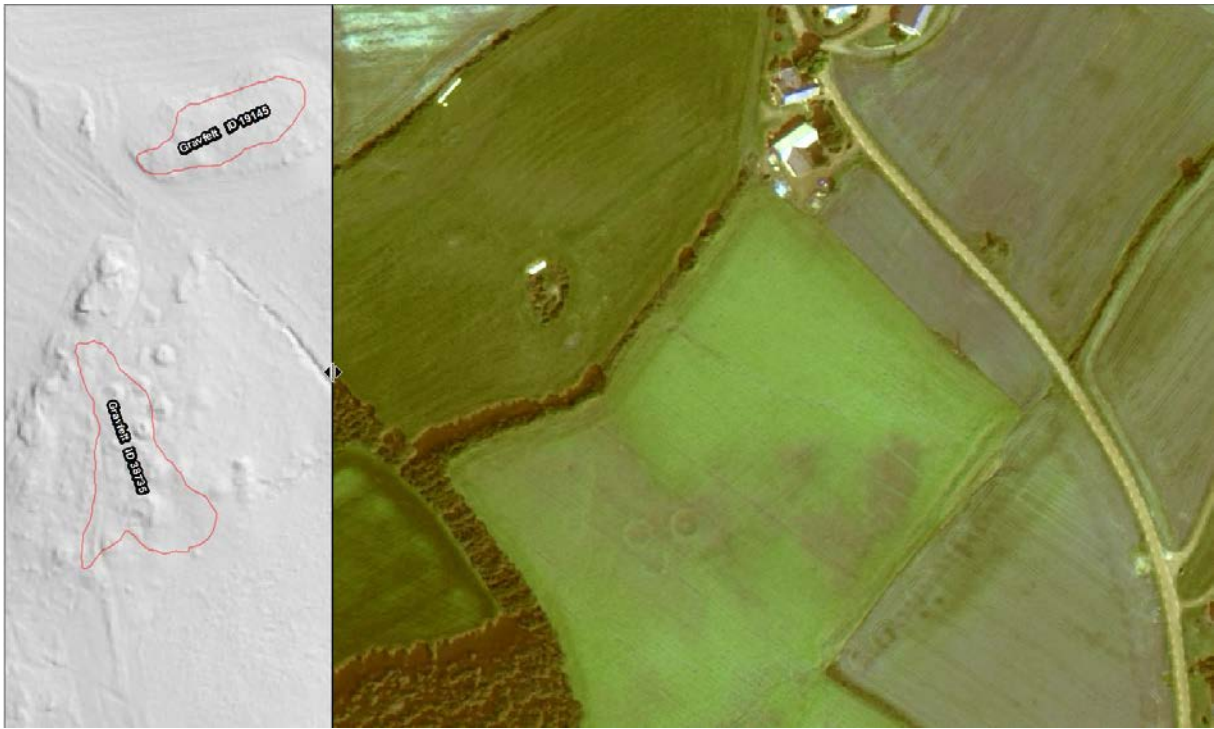


Figure 47. Combined lidar/optical image. The leftmost part of the area is displayed as a lidar height relief image, while the rest of the area is displayed as the Worldview-2 optical satellite image. Two grave fields are indicated as red outlines. Detections nos. 2, 3, and 6 are clearly seen as a group of three bright rings, a little bit below the center of the combined image.

Detection no. 4, Fjellvik, GBNR 1106/1, N 6544748, E 569593.5. This detection is in itself quite convincing as a crop mark, showing the ring ditch of an over plowed grave mound. But it is situated far from other registered heritage sites, and its placement is on a field lying in between two ridges of forest. This is not a typical placement in the landscape for grave mounds or grave fields. Our evaluation of the detection is that it should be classified as a certain ring ditch, but with slight reservations concerning the certainty. This is a new detection done by CultSearcher, and has also been pinpointed by the archaeologist during manual search.

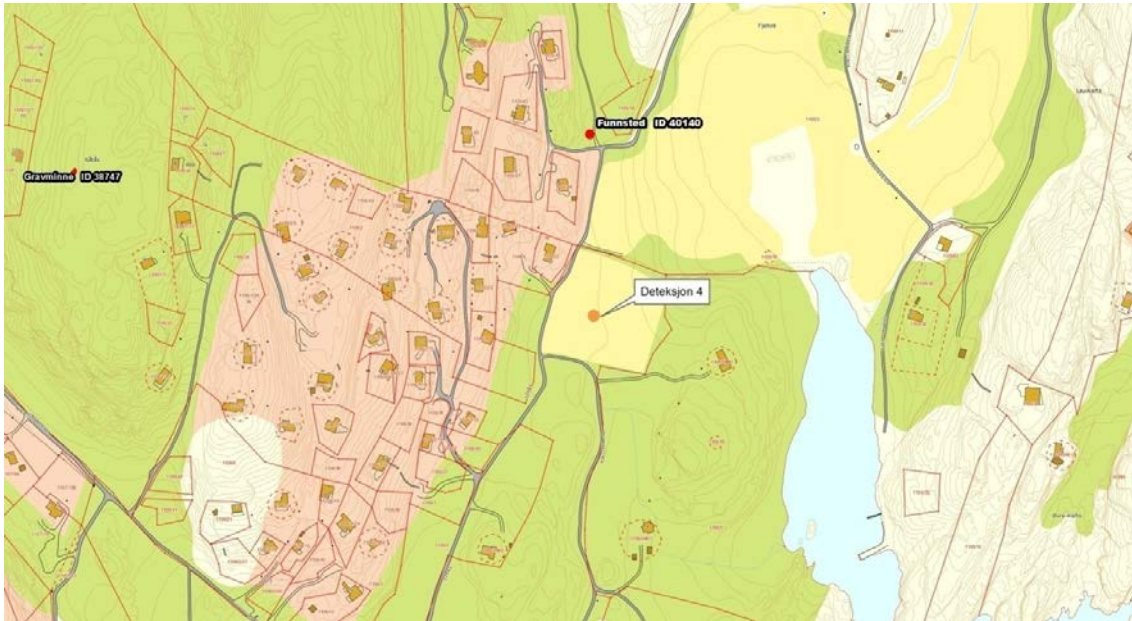


Figure 48. Detection no. 4 (orange dot) and surrounding cultural heritage sites marked with red dots.



Figure 49. Detection no. 4, at Fjellvik.

Detection no. 5, Klåstad nedre, GBNR 1087/1, N 6546526.5, E 567731.5. Very strong detection of a circular ringditch. The cultural heritage context surrounding detection 5 is substantial. Approximately 240 m north west of the detection lies three registered grave mounds (ID 9328, 9327 and 38733). All of these are quite fragmented due to modern housing and infrastructure. Surrounding the detection to the southeast, east and north east lies further three sites (ID 48762, 58885 and 48749, Figure 50). This detection was also flagged during manually searching the satellite images, further two ring ditches was discovered by archaeologist (Figure 50).

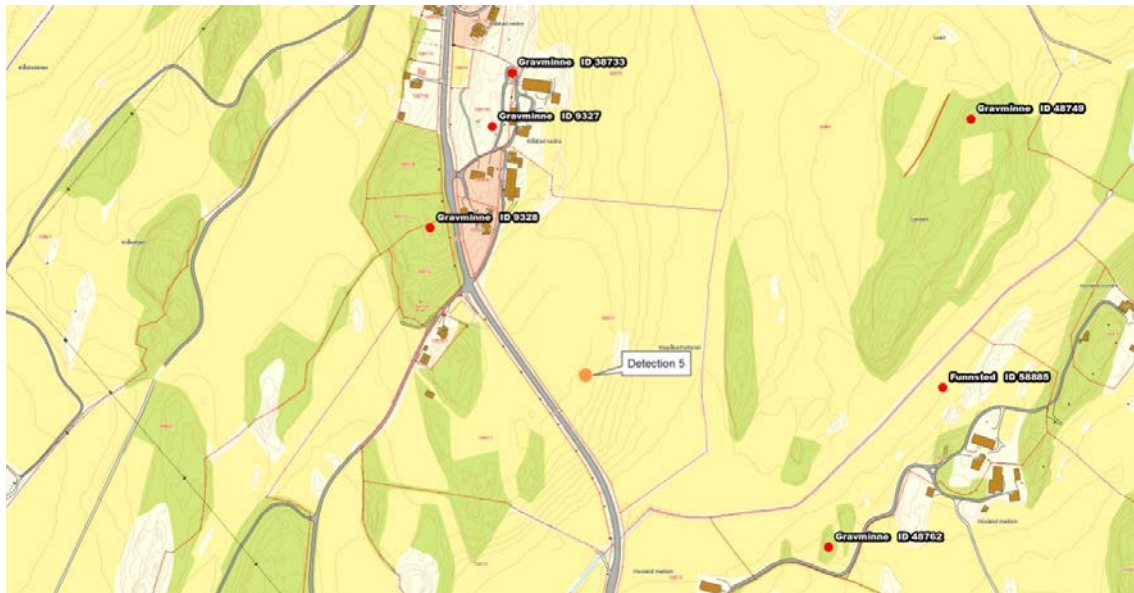


Figure 50. Top: detection no. 5, and surrounding cultural heritage sites. Bottom: Detection no. 5 (labeled 70) and two manual uncertain detections.

Automatic detection no. 5 and manual detections nos. 71 and 72 are new detections not previously known. Manual detections nos. 71 and 72 are not certain detections, but highly plausible.

Detection no. 7, Huseby, GBNR 1032/17, N 6547046.5, E 564324.5. Detection 7 is a solid detection of a ringditch belonging to a over plown grave mound. Detection 7 was also discovered during manual detection. The detection is situated at Tjøllingvollen in Larvik, which is a site densely populated with cultural heritage sites, primarily dated to iron age. The closest cultural heritage site lies 50 meters south east of detection (ID 129621). This is a site consisting of cooking pits, probably belonging to a housing area.



Figure 51. Top: detection 7 and the nearby registered cultural heritage sites. Bottom: detection 7 in the satellite image, and a nearby cultural heritage site from the Askeladden database

3.1.2.2 Brunlanes 07162010

Of the original 6 detections by CultSearcher, 2 are true detections.

Detection 1 Rugland Vestre, GBNR 4034/1 N 6538117.5 E 557131. This detection is quite strong in the dataset, showing the ring ditch of an over plown grave mound. The surrounding cultural heritage sites are situated between 300-600 meters from detection 1. Lidar data from the forest to the north of the detection is inconclusive due to dense vegetation.

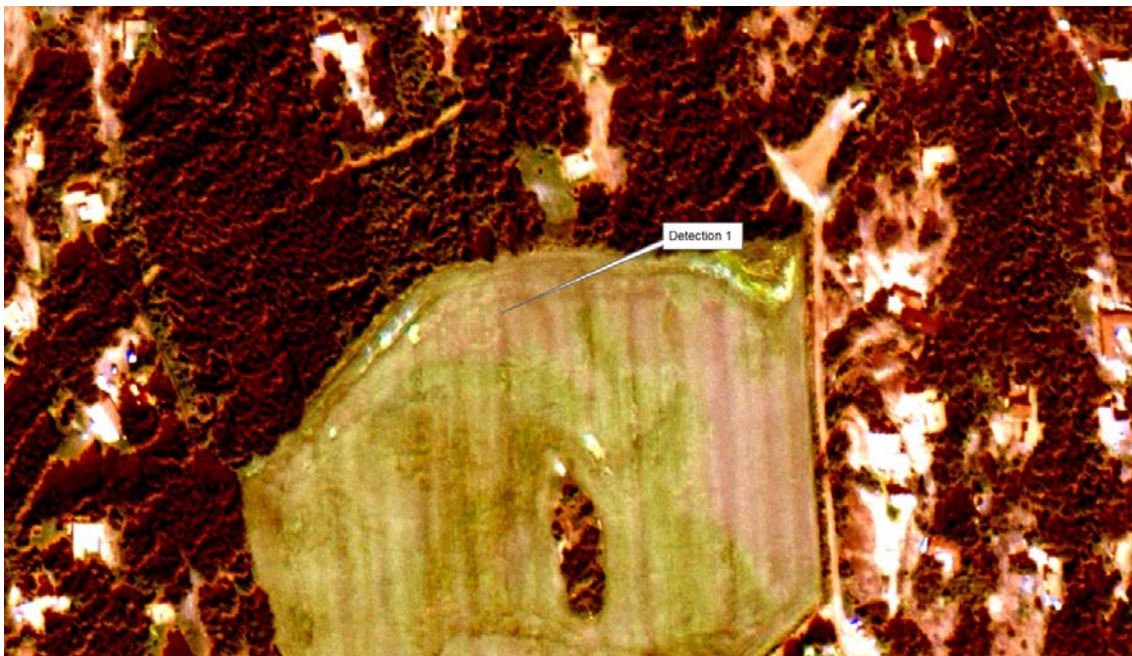


Figure 52. Top: detection no. 1 and surrounding cultural heritage sites. Bottom: detection no. 1 in the satellite image.

Detection 1 is a clear detection but should be considered with some reservations as a singular detection far from other registered sites. This is a new detection done by CultSearcher, and was also flagged by manual observer.

Detection 2 Foldvik Nordre GBNR 4025/1 N 6540524.5 E 555639.5. Quite strong detection showing ringditch from over plown grave mound. As detection 1, this detection lies a good stretch (700-800 m) from nearby registered cultural heritage sites. Should be considered with reservations.

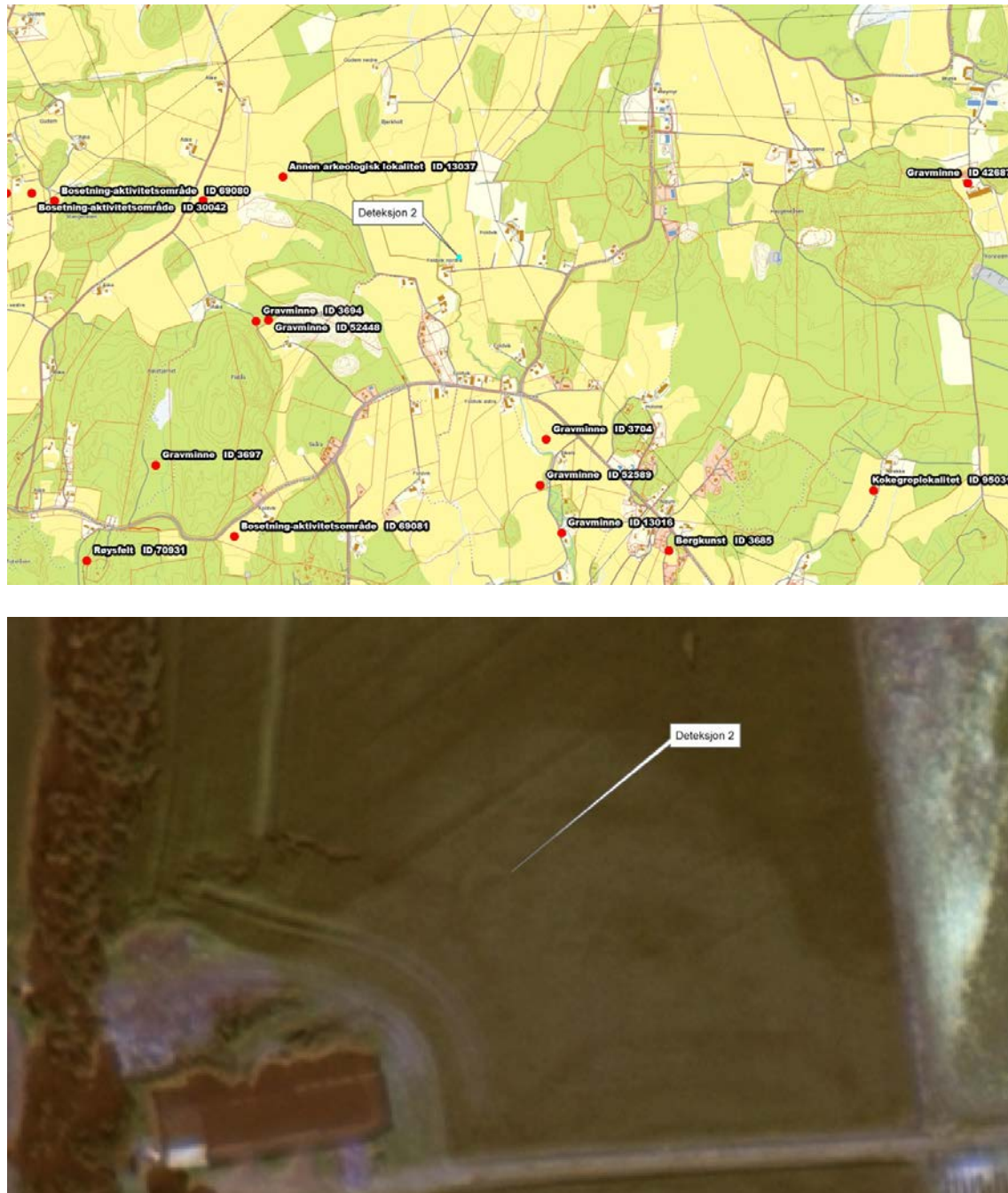


Figure 53. Top: overview map showing detection 2 and its surrounding heritage sites. Bottom: Detection no. 2 in the satellite image.

3.1.2.3 Brunlanes 08072010

Of the original 9 detections by CultSearcher, one is confirmed as an overplow ringditch (detection 1) and one is more uncertain (detection 2) and will need further investigations. The other 7 detections were discarded as false detections.

Detection 1 Halle GBNR 4013/2 N 6542522 E 552755.5. This detection is very lucid and strong. Shows a crop mark from an over plow grave mound. South and southwest of detection lies two grave mounds (ID 32706 and 52470). Detection two was also detected during manual registration alongside further 6 crop marks of over plow gravemounds, and a larger area showing cropmarks of unclear context (24).

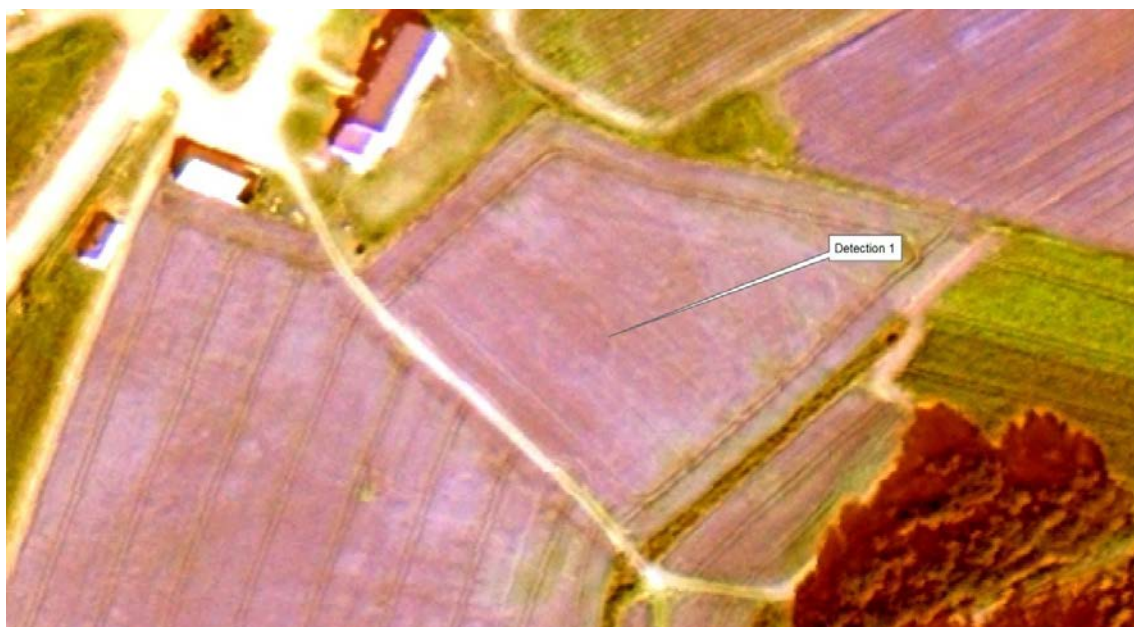


Figure 54. Top: detection 1 and surrounding registered cultural heritage sites. Bottom: Detection no. 1 in the satellite image.

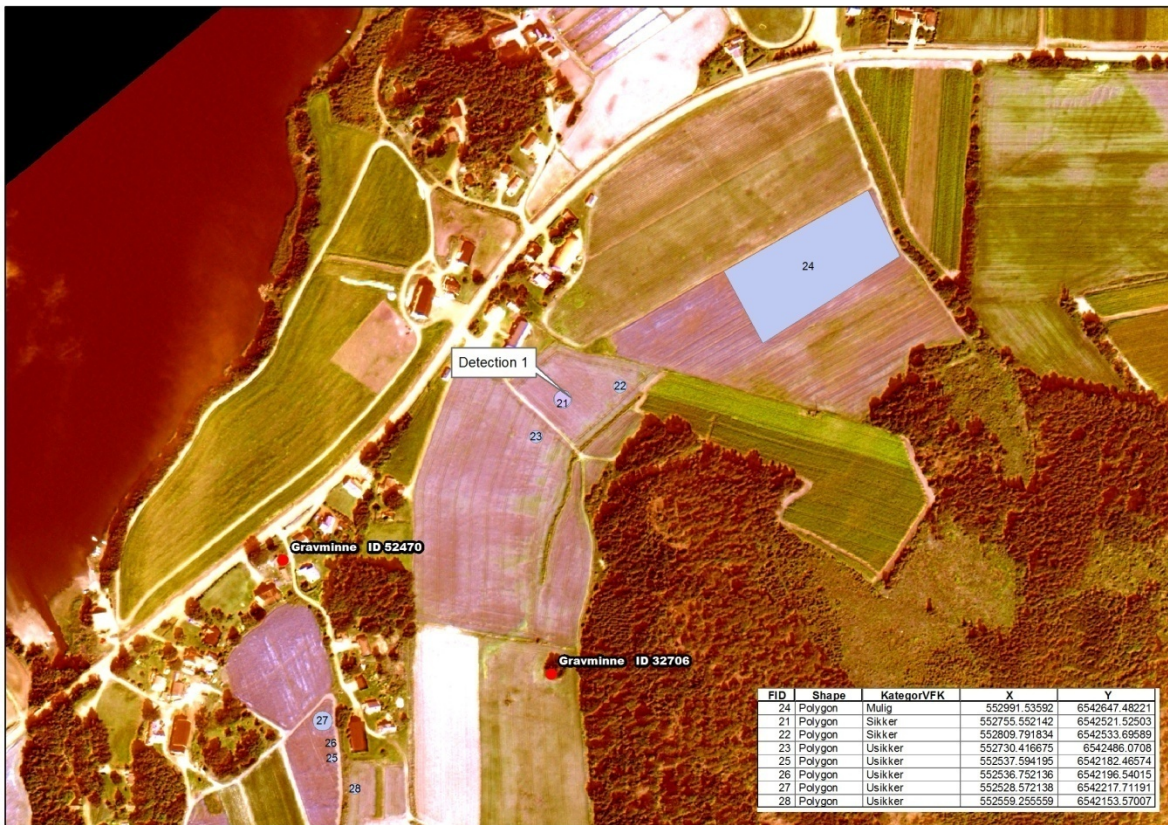
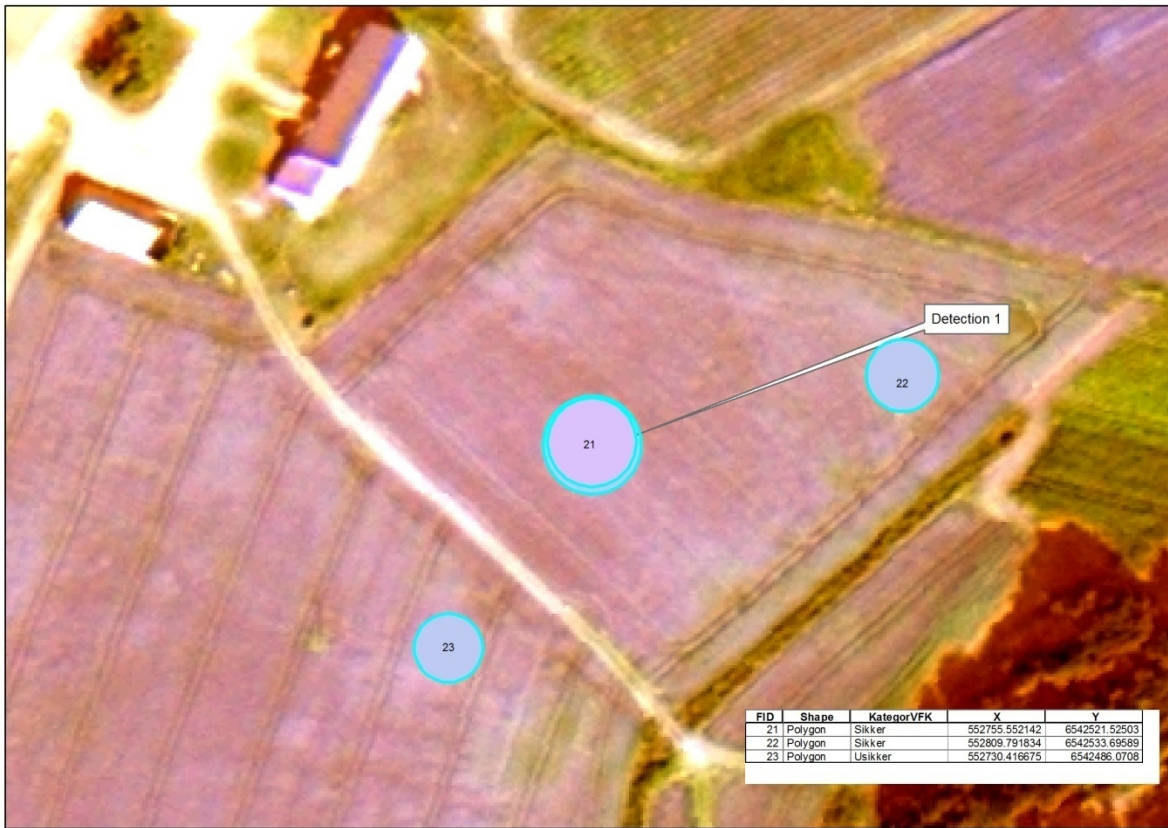


Figure 55. Top: detection no. 1 (labeled 21 by manual registrator) alongside manually registered crop marks nos. 22 and 23. Number 22 is marked out as certain whilst number 23 is marked as an uncertain detection. Bottom: Detection 1 in constellation with manual detected crop marks south west and north east of detection 1.

Detection 2 Foldvik nordre GBNR 4025/1 N 6540523 E 555639. Fairly clear detection of ringditch from an over plown gravemound. This detection seems quite promising concerning a possible conserved central grave, shiplike in shape. But this detection should be investigated further on more satellite images and aerial photos, and possibly also with field investigations before concluding this observation. This location was also shown as a detected site by CultSearcher in the Brulanes 07162010 image, but was not very good in this image. Surrounding cultural heritage sites are located quite far off (Figure 56).

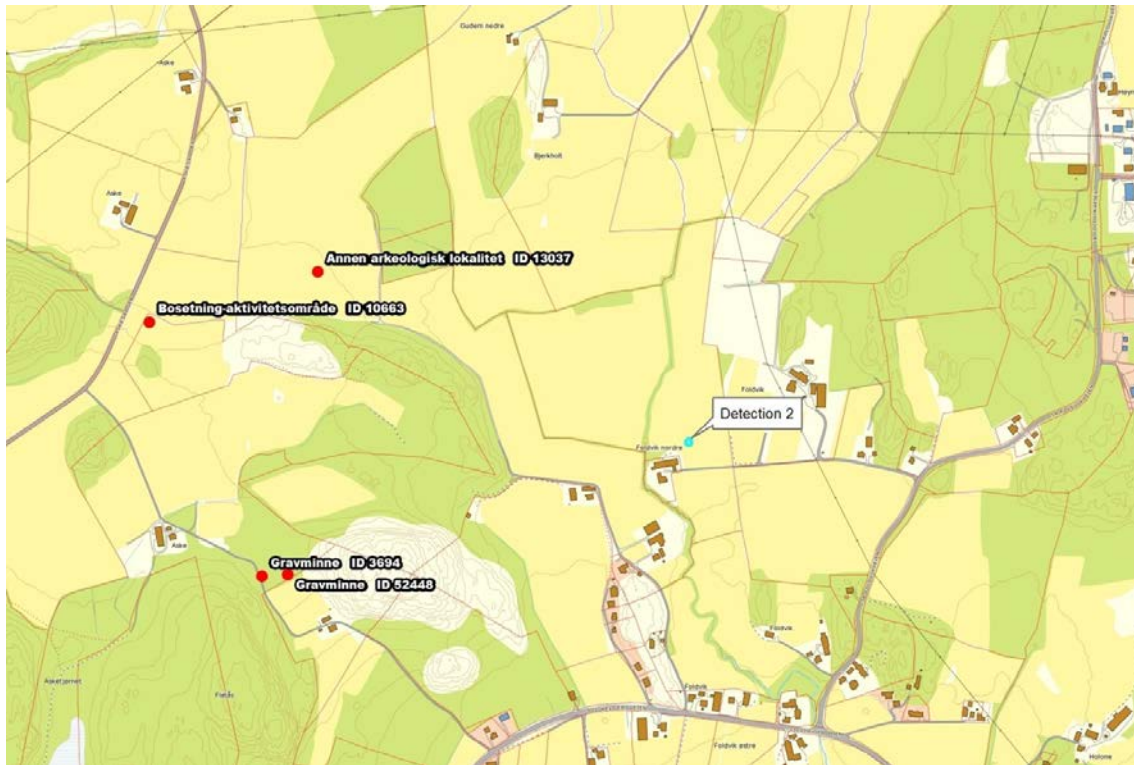


Figure 56. Detection 2 and surrounding cultural heritage sites.



Figure 57. Detection 2 with an unclosed ringditch and what seems like a conserved central (a bit askew to the north) grave inside ringditch.

3.1.2.4 Manual detection in satellite images from 2010

In addition to reviewing the results from CultSearcher, archaeologists at Vestfold County Council manually reviewed the satellite images taken 2010. Archaeologist Trude Aga Brun initially identified sites of potential in the images. Then, at a later stage together with archaeologist Christer Tønning, the detected areas were classified in three categories; Certain (Sikker), uncertain (usikker) and possible (mulig). The grading of the sites was based upon following criteria:

- **Certain:** Clear definite ringditch revealing the location of an over plown grave mound
- **Uncertain :** Faint or weak ringditch, possible location for over plown grave mound
- **Possible :** Weak traces of ringditch or other cropmark wich could indicate over plown grave mound, or other cultural heritage site which could not be defined further.

The complete lists of manual detections contain the UTM zone 32 coordinates and references to the previous tables of automatic detections (Table 4-Table 9), and are grouped on the category (Table 10-Table 12). The 32 observations that are classified as certain (sikre) coincide in many cases with the certain observations of Cultsearcher. 63 of the observations are classified as uncertain (usikker), and 18 of the observations are classified as possible (mulig). Several of the detections are close to previously known cultural heritage sites (Figure 62-Figure 65).

Table 10. Certain manual detections in the Vestfold images of 2010. Auto ID refers to the detection id in Table 4-Table 9, with manual detections from those tables in parentheses.

Man. ID	North	East	Image	Auto ID
1	6544253	556539	Brunlanes	-
14	6542485	554995	Brunlanes	-
15	6542494	555009	Brunlanes	-
16	6542489	555021	Brunlanes	-
17	6542497	555029	Brunlanes	-
18	6542487	555032	Brunlanes	-
19	6542647	555220	Brunlanes	-
21	6542522	552756	Brunlanes 7 Aug 2010	2
22	6542534	552810	Brunlanes	-
33	6540022	555791	Brunlanes 7 Aug 2010	(12)
41	6539165	556607	Brunlanes 7 Aug 2010	1
42	6539159	556592	Brunlanes	-
43	6539059	555636	Brunlanes	-
46	6547047	564325	Tjølling 7 Aug 2010	11
47	6547701	568955	Tjølling 7 Aug 2010	2
48	6547706	568980	Tjølling 7 Aug 2010	3
49	6547686	568964	Tjølling 7 Aug 2010	8
50	6544748	569594	Tjølling 7 Aug 2010	4
53	6547342	568029	Tjølling 7 Aug 2010	1
62	6546633	563214	Tjølling 7 Aug 2010	(15a)
63	6546627	563225	Tjølling 7 Aug 2010	(15b)
64	6546619	563234	Tjølling 7 Aug 2010	(15c)
67	6551309	561140	Tjølling 7 Aug 2010	-
68	6551318	561147	Tjølling 7 Aug 2010	-
69	6551308	561151	Tjølling 7 Aug 2010	-
70	6546527	567732	Tjølling 7 Aug 2010	5
100	6563445	555424	Lågendalen 7 Aug 2010	-
101	6563409	555488	Lågendalen 7 Aug 2010	(7)
106	6562275	555278	Lågendalen 7 Aug 2010	(6)
107	6562283	555264	Lågendalen 7 Aug 2010	(5)
108	6562295	555265	Lågendalen 7 Aug 2010	(4)
109	6562452	555326	Lågendalen 7 Aug 2010	(3)



Figure 58. Manual detection no. 1, in the Brunlanes images. Left:: image of 16 July 2010, right: image of 7 August 2010.



Figure 59. Manual detections nos. 14-18, in the Brunlanes images. Top: from 16 July 2010, bottom: from 7 August 2010.

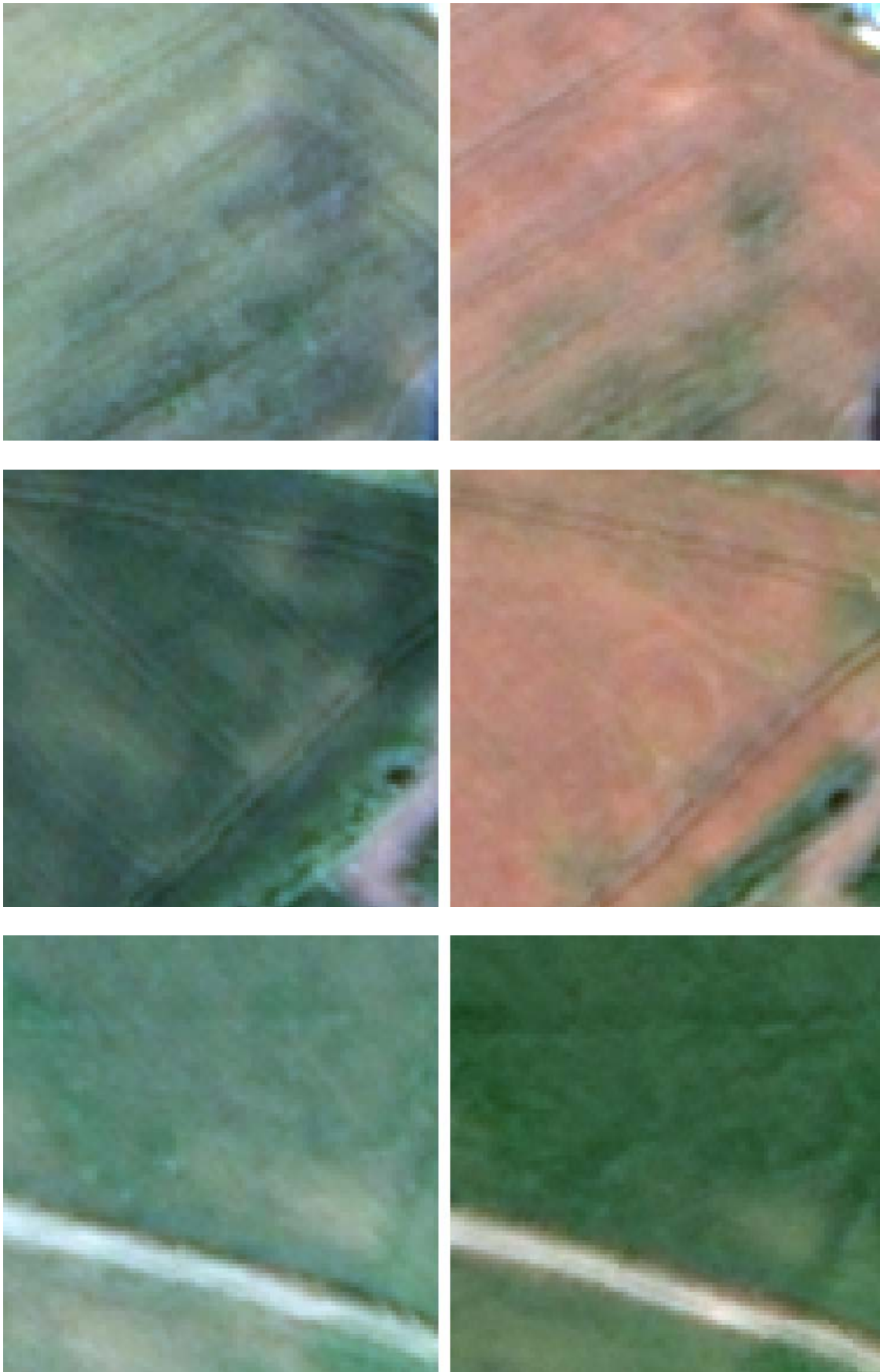


Figure 60. Manual detections nos. 19 (top), 22 (middle), and 42 (bottom), in the Brunlanes images. Left column: from 16 July 2010, right column: from 7 August 2010.



Figure 61. Manual detections nos. 43, in the Brunlanes image (top), 67-69, in the Tjølling image(middle), and 100, in the Lågendalen image; all images of 7 August 2010.

Table 11. Uncertain manual detections in the Vestfold images of 2010.

Man. ID	North	East	Image	Man. ID	North	East	Image	Aut. ID
0	6541473	558162	Brunlanes	60	6545594	563252	Tjølling 7 Aug 2010	
2	6543789	553597	Brunlanes	65	6546585	563903	Tjølling 7 Aug 2010	(14)
3	6543802	553603	Brunlanes	66	6547595	563198	Tjølling 7 Aug 2010	
4	6543817	553622	Brunlanes	71	6546497	567727	Tjølling 7 Aug 2010	
5	6543831	553573	Brunlanes	72	6546500	567700	Tjølling 7 Aug 2010	
6	6543799	553616	Brunlanes	73	6547313	568231	Tjølling 7 Aug 2010	
7	6543776	553603	Brunlanes	74	6547327	568216	Tjølling 7 Aug 2010	
8	6543781	553604	Brunlanes	75	6547329	568225	Tjølling 7 Aug 2010	
9	6543810	553573	Brunlanes	76	6556172	566240	Marum 7 Aug 2010	
10	6543813	553557	Brunlanes	77	6556173	566255	Marum 7 Aug 2010	
11	6543823	553562	Brunlanes	78	6556174	566299	Marum 7 Aug 2010	
13	6543164	554526	Brunlanes	79	6556174	566274	Marum 7 Aug 2010	
20	6542728	554014	Brunlanes	80	6556174	566286	Marum 7 Aug 2010	
23	6542486	552730	Brunlanes	86	6549223	567564	Marum 7 Aug 2010	
25	6542182	552538	Brunlanes	87	6549238	567545	Marum 7 Aug 2010	
26	6542197	552537	Brunlanes	88	6549234	567585	Marum 7 Aug 2010	
27	6542218	552529	Brunlanes	89	6549274	567563	Marum 7 Aug 2010	
28	6542154	552559	Brunlanes	90	6549201	567546	Marum 7 Aug 2010	
30	6541563	552467	Brunlanes	91	6549203	567552	Marum 7 Aug 2010	
31	6541546	552477	Brunlanes	92	6568155	554458	Lågendalen 7 Aug 2010	
34	6539645	553231	Brunlanes	93	6568166	554454	Lågendalen 7 Aug 2010	
35	6539671	553242	Brunlanes	94	6568183	554446	Lågendalen 7 Aug 2010	
36	6539756	555846	Brunlanes	95	6568192	554443	Lågendalen 7 Aug 2010	
37	6539476	549445	Brunlanes	96	6564680	556460	Lågendalen 7 Aug 2010	
38	6539421	549443	Brunlanes	97	6564656	556452	Lågendalen 7 Aug 2010	
39	6539271	553374	Brunlanes	98	6564677	556426	Lågendalen 7 Aug 2010	
40	6539319	553382	Brunlanes	103	6562938	556439	Lågendalen 7 Aug 2010	
44	6537448	547334	Brunlanes	104	6562937	556452	Lågendalen 7 Aug 2010	
45	6538118	557131	Brunlanes	105	6562926	556459	Lågendalen 7 Aug 2010	
51	6547379	568038	Tjølling 7 Aug 2010	110	6562503	555570	Lågendalen 7 Aug 2010	
52	6547415	568028	Tjølling 7 Aug 2010	102	6563472	555446	Lågendalen 7 Aug 2010	
54	6549002	567518	Tjølling 7 Aug 2010					

Table 12. Possible manual detections in the Vestfold images of 2010.

Man. ID	North	East	Image
12	6543372	557533	Brunlanes
24	6542647	552992	Brunlanes
29	6541661	552153	Brunlanes
32	6540416	554604	Brunlanes
55	6549019	567483	Tjølling 7 Aug 2010
56	6549741	562090	Tjølling 7 Aug 2010
57	6549682	562083	Tjølling 7 Aug 2010
58	6549686	562102	Tjølling 7 Aug 2010
59	6545586	563253	Tjølling 7 Aug 2010
61	6543802	563520	Tjølling 7 Aug 2010
81	6553314	566322	Marum 7 Aug 2010
82	6553328	566334	Marum 7 Aug 2010
83	6549574	566304	Marum 7 Aug 2010
84	6549599	566306	Marum 7 Aug 2010
85	6549153	567399	Marum 7 Aug 2010
99	6564235	554738	Lågendalen 7 Aug 2010
111	6562474	555591	Lågendalen 7 Aug 2010
112	6562465	555595	Lågendalen 7 Aug 2010

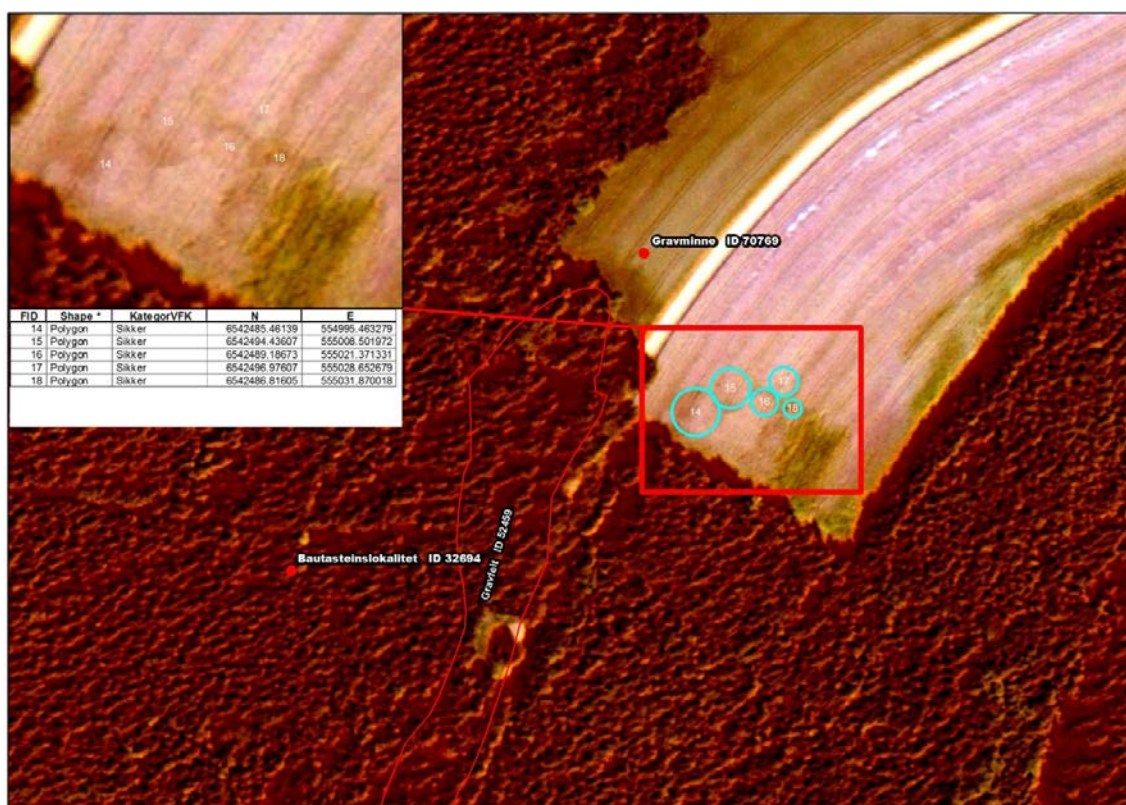


Figure 62. A manually detected grave field with five circles (nos. 14-18). This gravefield lies in connection with registered gravefield ID 52459 and ID 70769. The latter is a excavated ironage grave (flatmarksgrav).

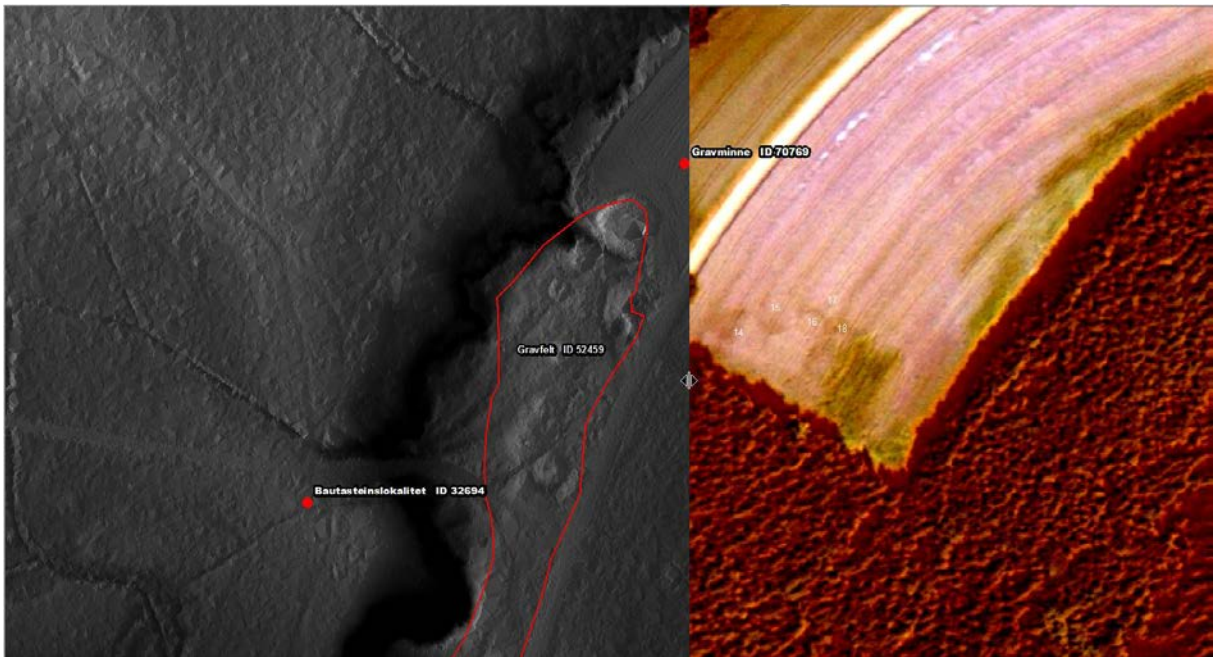


Figure 63. The same grave field as in Figure 62, with the satellite image replaced by a lidar height relief image in the left part of the illustration. Note the heaps, which are grave mounds in the forest, and the lines, which are roads.

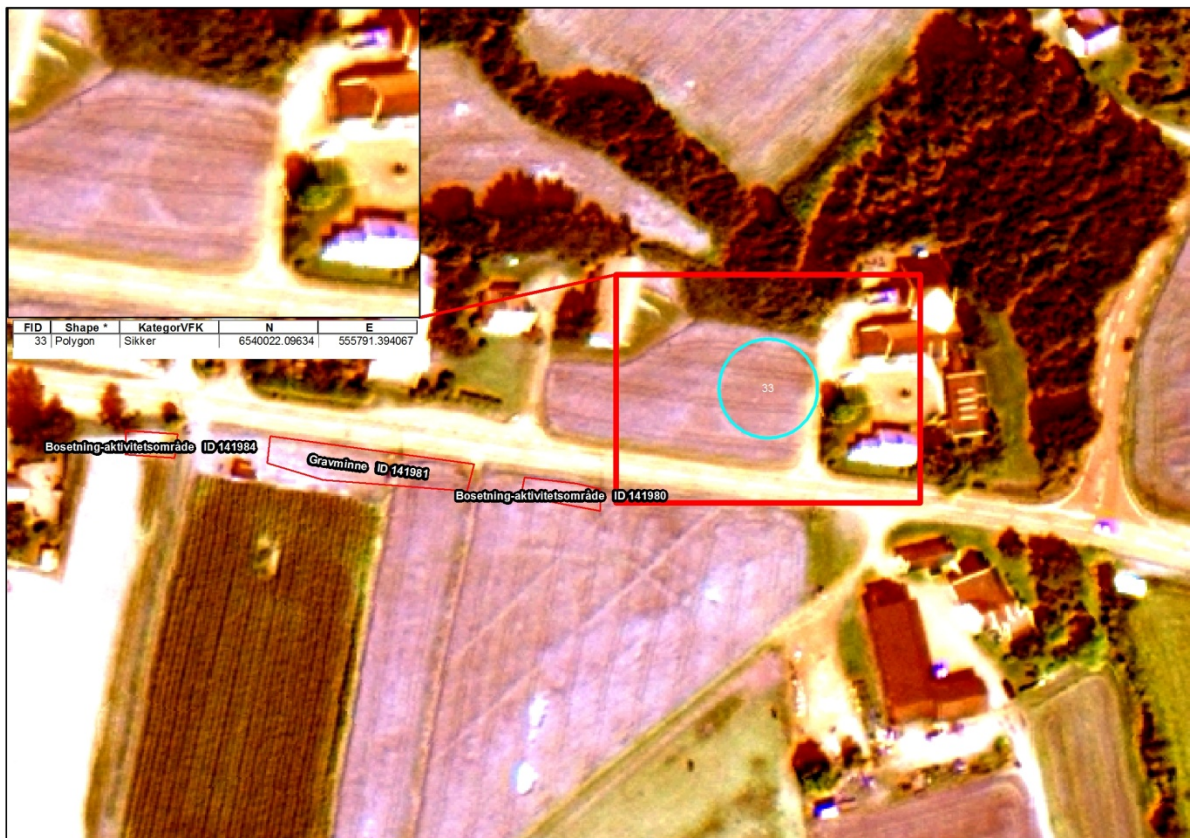


Figure 64. Manual detection no. 33 and surrounding registered cultural heritage sites. ID 141980 and 141984 are leveled remains of housing (cooking pits, fireplace, postholes), while ID 141981 is a leveled grave.



Figure 65. Manually detected ring ritches, detections nos. 62-64. To the south: a gravefield (ID 68437). and to the west: a gravemound (ID 68436).

3.1.3 Detections in Worldview-2 images in Oppland County

3.1.3.1 Possible crop mark detections in the Granavollen image of 24 July 2010

CultSearcher automatically detected 97 potential crop marks, and 91 of these are obvious misclassifications. The remaining six detections are checked by archaeologist Kjetil Loftsgarden (Table 13).

Table 13. Cultsearcher detections in the Granavollen image of 24 July 2010.

CultSearcher detection no.	UTM zone 32		Farm name	Comment by archaeologist
	east	north		
1	582499.5	6692379.0	Lunde nordre	Unlikely. Large amount of clouds on the satellite image. Possible detection is cluster of trees combined with clouds.
2	586198.5	6691648.5	Melbustad	Possible detected grave. No clear other options
3	587111.5	6691143.0	Haslerud	Less possible. The detections are light round areas and not really rings. The surrounding areas has several ringshaped areas of different sizes.
4	587624.5	6695138.5	Framstad nordre	Unlikely. The "Ring" is situated in an industrial area. Deposit of soil from road constructions etc defines the "ring".
5	588657.5	6693720.0	Morstad østre	Possible. A known site with several cookingpits (ID 94869) is situated approx 70 m NW of the detection. The ring is about 12 m in diameter. The southern part seems to have been removed in the construction of the road
6	588754.5	6692298.0	Vennolum	Less possible. Diffuse, but no clear other option.



Figure 66. Detection no. 1 in the Granavollen image of 24 July 2010.



Figure 67. Detections nos. 2 (top), 3 (middle), and 4 (bottom) in the Granavollen image of 24 July 2010.



Figure 68. Detections nos. 70 (top) and 71 (bottom) in the 24 July 2010 image of Granavollen.

3.1.3.2 Granavollen image of 7 August 2010

CultSearcher automatically detected 143 potential crop marks. Of these, 138 are regarded as obvious misclassifications, and the remaining five detections are forwarded to the archaeologist for verification (Table 14).

Table 14. CultSearcher detections in the Granavollen image of 7 August 2010.

CultSearcher detection no.	UTM zone 32		Farm name	Comment by archaeologist Kjell Loftsgarden
	east	north		
1	588846.0	6692448.5	Vennolum	Possible. The ring is clear and about 10 meters in diameter. No other clear options.
2	582296.5	6698675.0	Juli-Ødegården mellom/vest	Possible. The ring is clearly more green than the surroundings, and is about 10 meters in diameter. No other clear options
3	581526.0	6697920.5	Bilden vestre	Less possible. The detection was not clearly ringshaped, however approx 200 m to the NW there is a much better defined ring that was not detected
4	580653.0	6695418.5	Staksrud	Less possible. Looks more quadratic than circular. No other shapes in the field, except a possible ring to the left of the detection is observed.
5	581953.5	6698218.5	Solbjør	Unlikely. No clear ring detection. Detection is likely to be a combination of clouds and vegetation



Figure 69. Detection no. 1 in the Granavollen image of 7 August 2010.



Figure 70. Detections nos. 2 (top), 3 (middle), and 4 (bottom) in the Granavollen image of 7 August 2010.



Figure 71. A ring that was missed by CultSearcher is located about 200 m north-west of detection no. 3.



Figure 72. Detection no. 5 in the Granavollen image of 7 August 2010.

3.1.3.3 Summary after the validation of detections

In the two Granavollen images of 24 July and 7 August 2010, CultSearcher detects six and five rings, respectively, that are to be examined by archaeologists. After validation, four of them are considered to be possible, however none of them are considered certain detections of prehistoric graves.

The images were analyzed in ENVI and as stated in previous report we feel that using ENVI demands a high degree of knowledge of the software. When the operator seldom uses the

program, maybe once or twice a year, it is time consuming "getting back in shape" for operating the program. The interface and use of windows are being perceived as challenging. ESRI's ArcGIS was used to evaluate the detections in relation to the surrounding areas, topography and whether or not known heritage sites were present. Different types of maps, aerial images (Norge i bilder) and the National database for Cultural Heritage Monument, Askeladden, was used in this process.

3.1.3.4 The manual analysis of the satellite images of the Granavollen area

A grid with 500 x 500 m squares were established in ENVI for controlling the examination. To mark possible structures the "regions of interests" (ROI) function in ENVI was used. ROI can also be exported from ENVI as shapefile for use in ArcGIS. These shapefiles were used when evaluating the areas with most potential for finds, together with aerial photos, maps and Riksantikvarens database Askeladden. After the visual analysis in ENVI and in ArcGIS there were 10 observations left and they appear on both satellite images (see table 1). Each ID in the table refer to the corresponding Id in the shapefile in ArcGIS. None of these 10 observations were detected by CultSearcher.

In the following the areas that have been marked as possible on *both* images is presented (Table 15, Figure 73-Figure 93). Area ID 3 and 31 must be considered as areas with the highest potential. Also ID 12 and 14 should be seen as part of this. The rest of the observations are more uncertain.

Table 15. Manual detections in the two Granavollen images. The four most promising detections are ranked 1-4. The remaining five detections are more uncertain.

ID	East	North	Farm	rank	comment
1	579282	6691425	Hvinden vestre		Possible tracks from tractor (turningpoint)
2	580997	6693262	Blakstad		Possible modern. Clearly visible on aerial photo
3	587122	6694756	Horgen nord	1	Situated 25 m SE of gravemound ID7 1136
6	580836	6695396	Staksrud		Several tractor tracks (turningpoints) in the area
12	588165	6692099	Gisleberg	3	Situated 100 m S of Burials ID23040
14	587090	6692461	Hov	4	Part of burial mound ID 52695
27	579279	6695183	Hov søndre		Circular observation
28	584186	6696149	Røisum nordre		Situated 60 m S of Cultural heritage site ID 22975
31	580426	6697229	Askim nordre	2	Circular observation
34	584114	6697598	Dvergsten		Circular observation

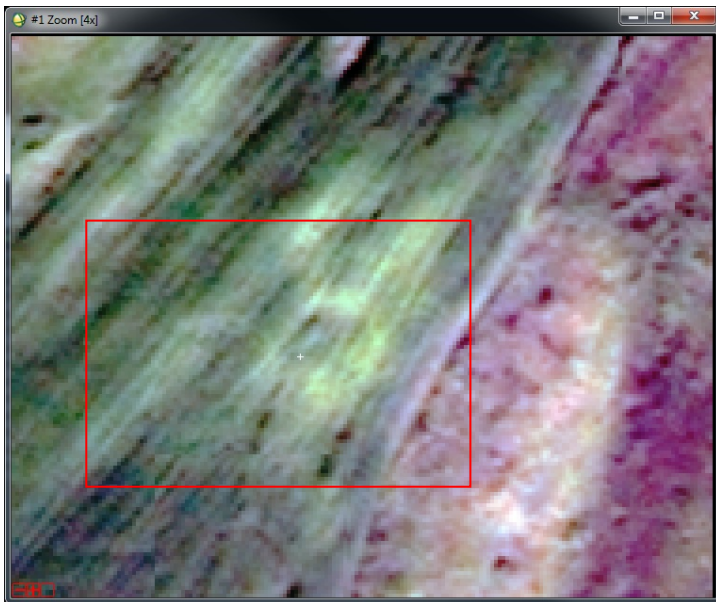


Figure 73. Manual detection no. 1 at Hvinden vestre in 24 July image. The circular pattern may be due to tractor track turns.

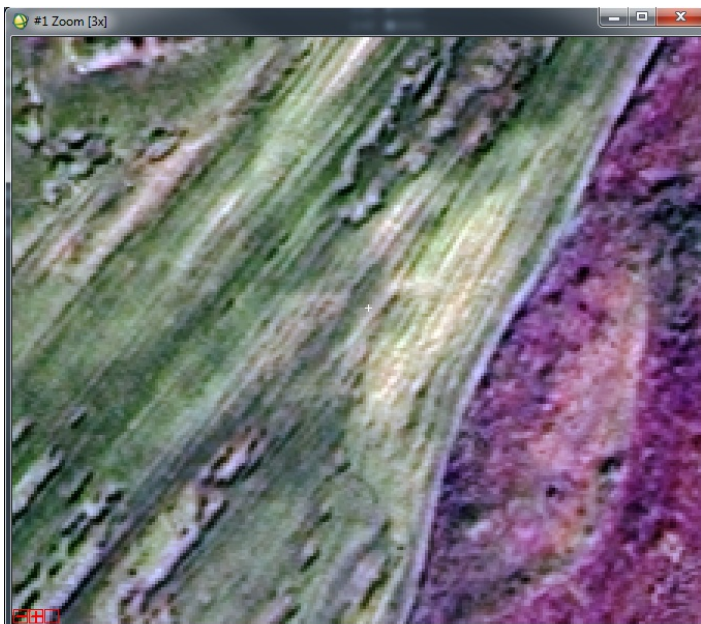


Figure 74. Manual detection no. 1 at Hvinden vestre in 7 August image. The circular pattern may be due to tractor track turns

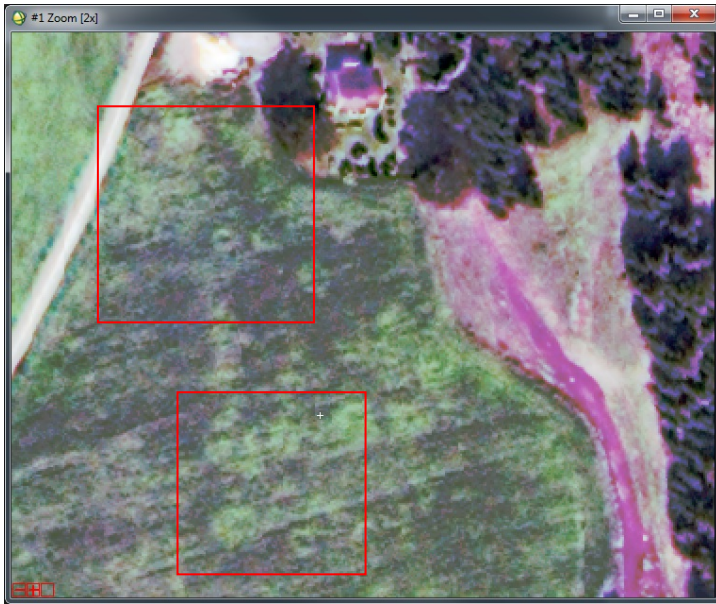


Figure 75. Detection no. 2, in the 24 July image, with circular patterns at Blakstad, possibly of modern origin. They are clearly visible in a digital orthophoto of 7 May 2010 (Figure 77).



Figure 76. Detection no. 2 at Blakstad in Worldview-2 image of 7 August 2010.



Figure 77. Top: Circular patterns at Blakstad in orthophoto of 7 May 2010, with 10 cm ground resolution. Bottom: Close-up of four of the circular patterns at Blakstad.



Figure 78. Detection no. 3 at Horgen nord in 24 July image. The detection is located 25 m south-east of a grave mound with Askeladden ID 71136.

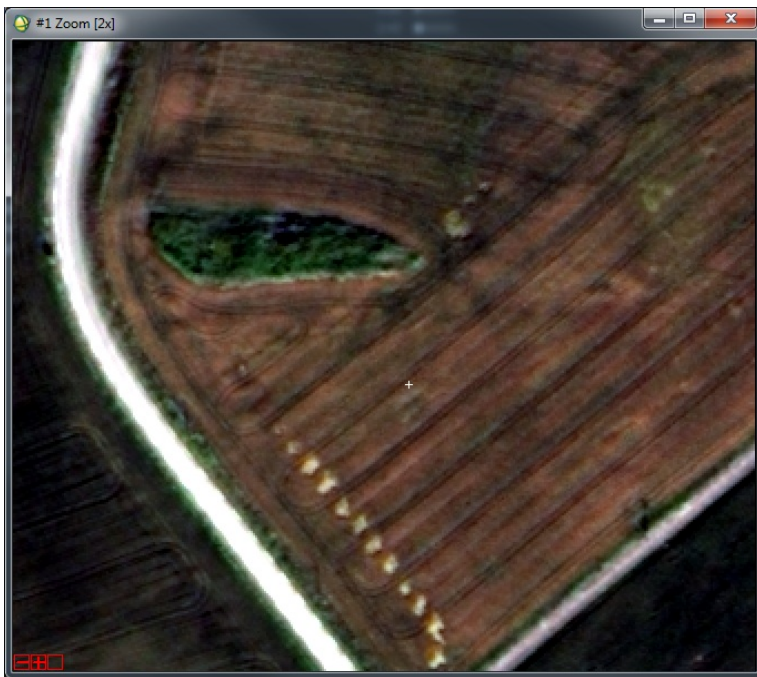


Figure 79. Detection no. 3 at Horgen nord in 7 August image.

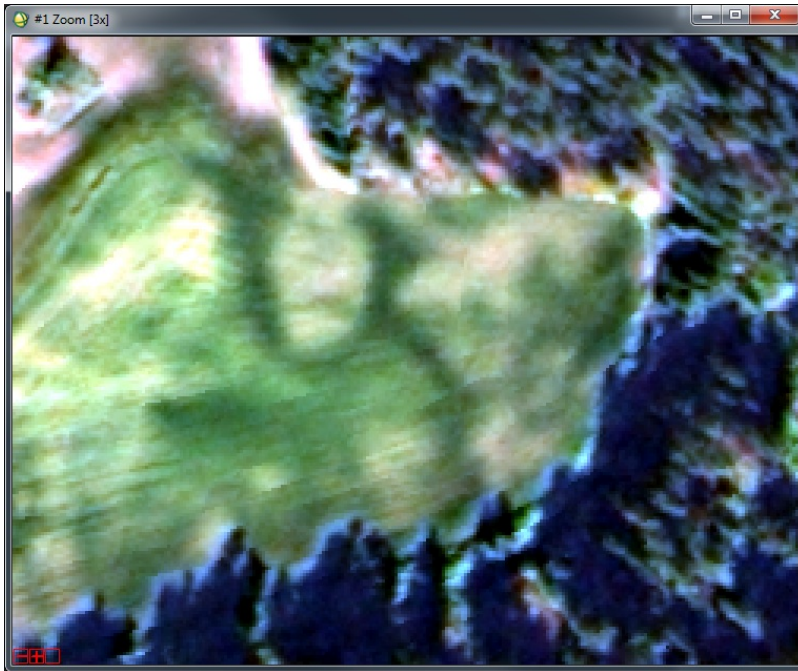


Figure 80. Detection no. 6 at Staksrud in the 24 July image. There are several tractor track turns in the area.



Figure 81. Detection no. 6 at Staksrud in the 7 August image.

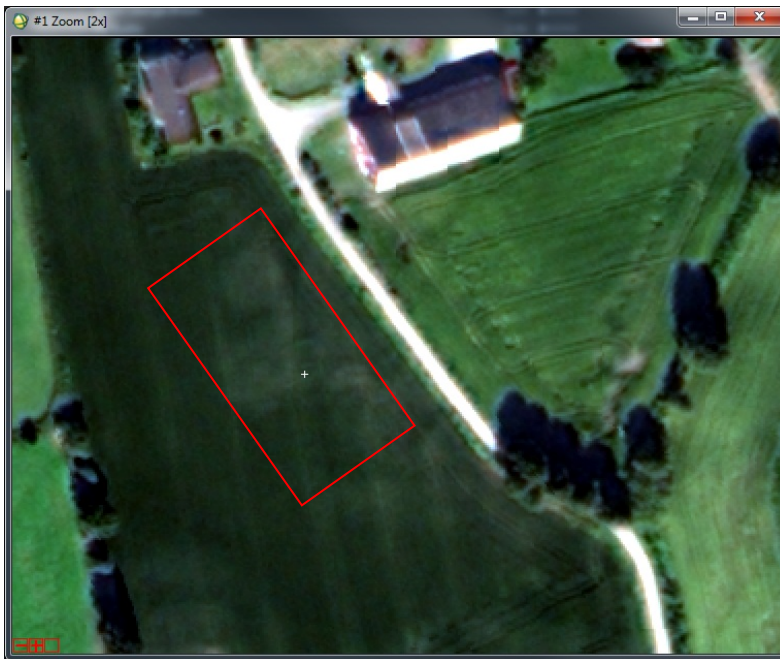


Figure 82. Detection no. 12 at Gisleberg in the 24 July image. The detection is located 100 m south of burial mounds with Askeladden ID 23040.

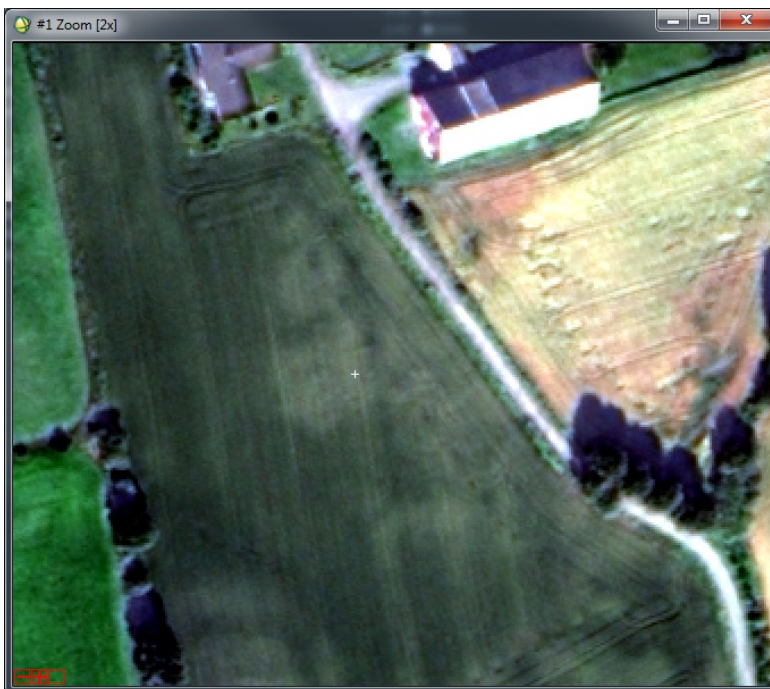


Figure 83. Detection no. 12 at Gisleberg in the 7 August image.

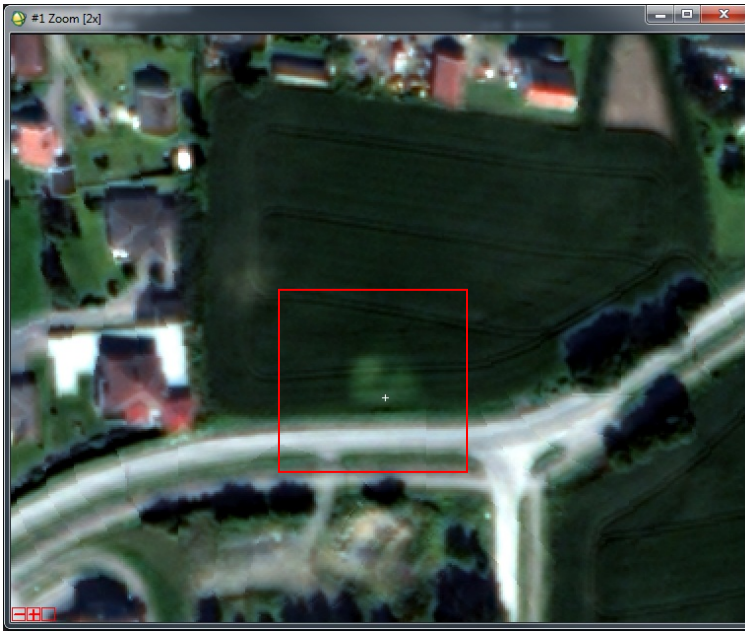


Figure 84. Detection no. 14 at Hov in the 24 July image. The detection is inside a known burial mound site, with Askeladden ID 52695.

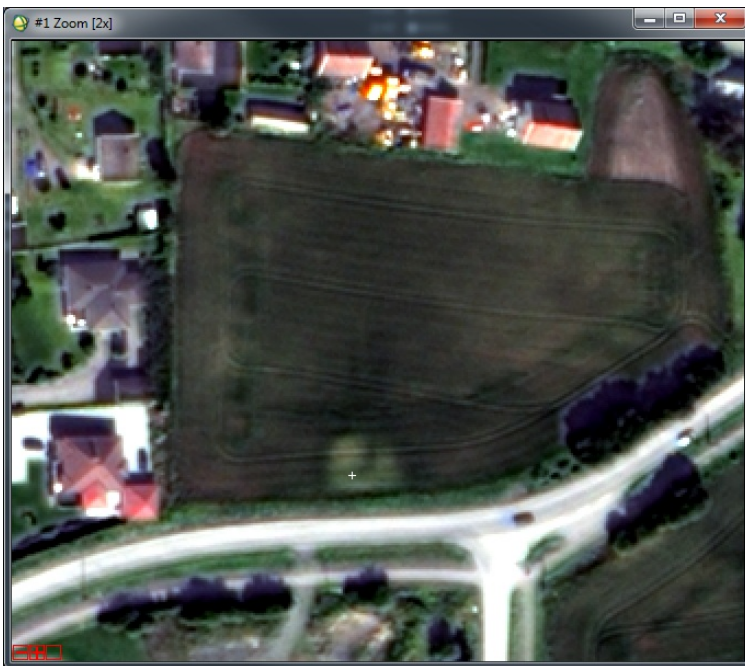


Figure 85. Detection no. 14 at Hov in the 7 August image.

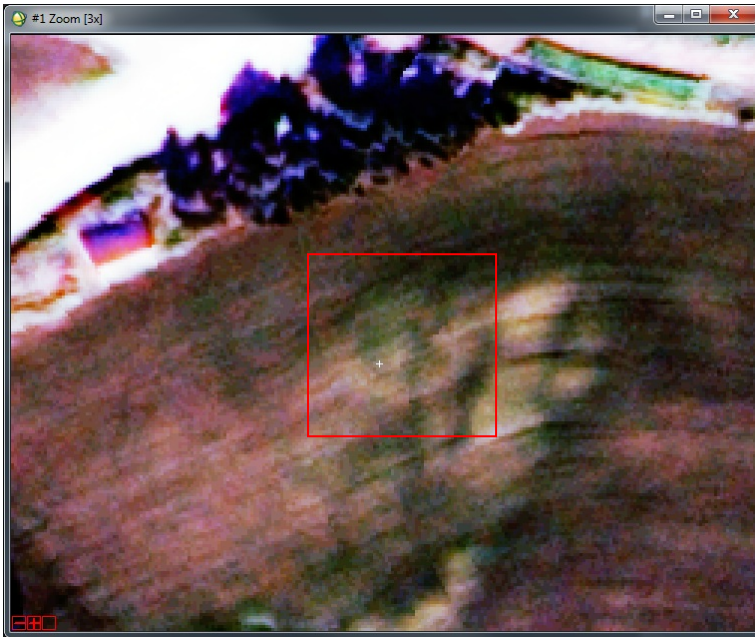


Figure 86. Detection no. 27, a circular pattern at Hov søndre in the 24 July image.

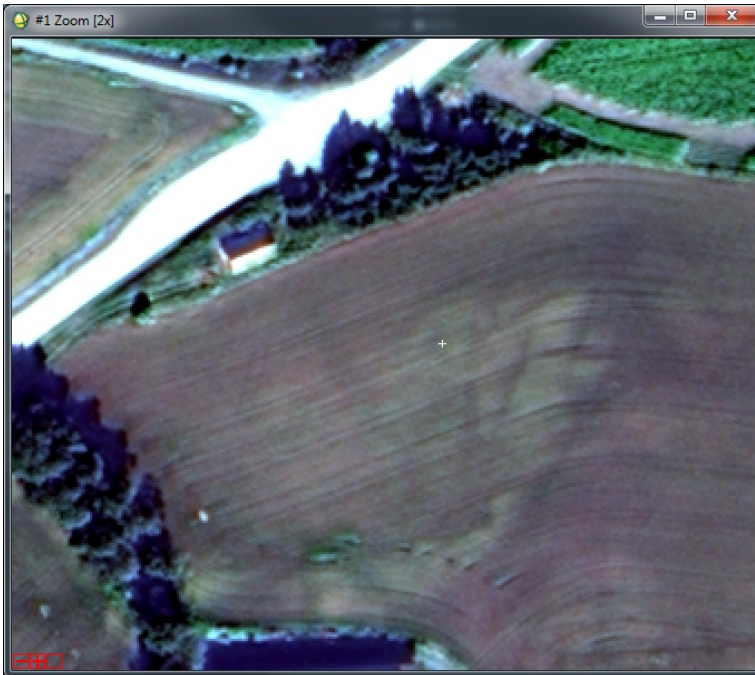


Figure 87. Detection no. 27 at Hov søndre.



Figure 88. Detection no. 28 at Røisum nordre in the 24 July image. The detection is located 60 m south of a cultural heritage site with Askeladden ID 22975. The detection is probably modern.

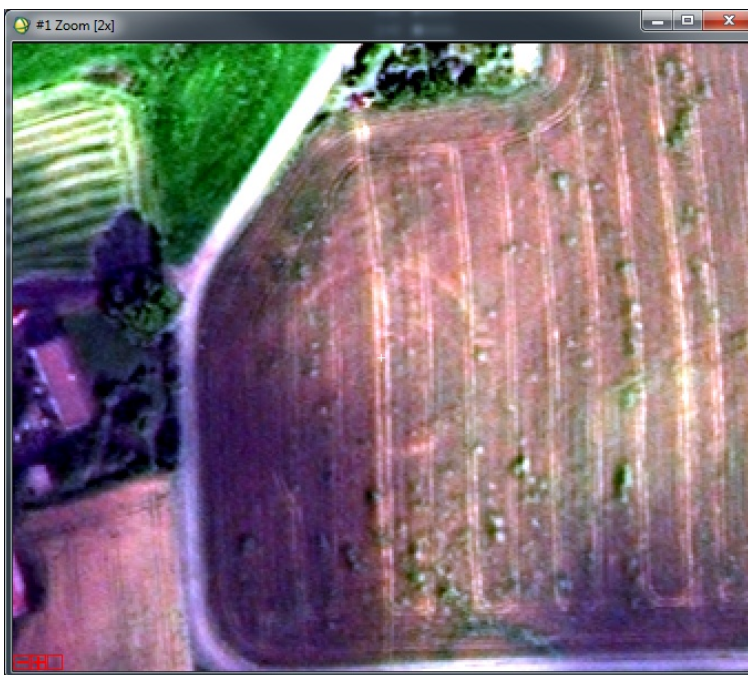


Figure 89. Detection no. 28 at Røisum nordre in the 7 August image.

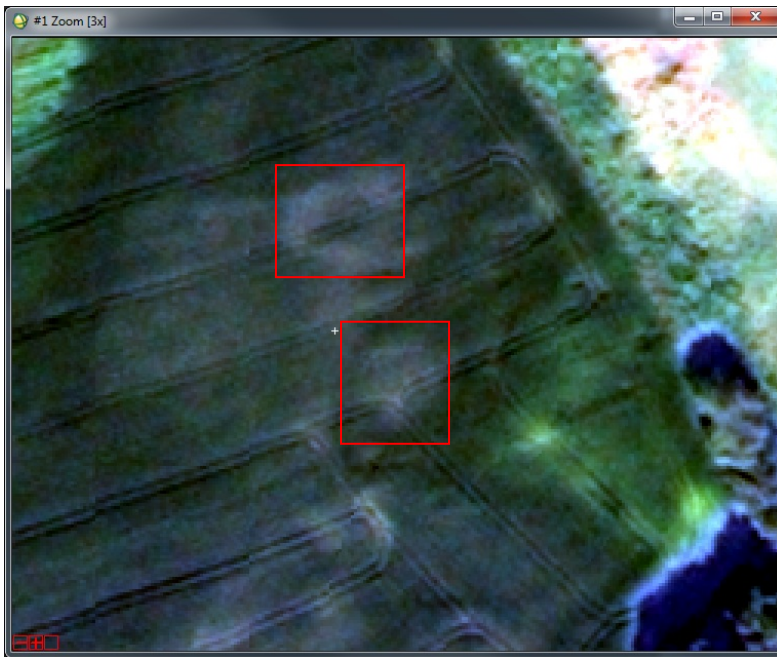


Figure 90. Detection no. 31, two circular patterns at Askim Nordre in the 24 July image.

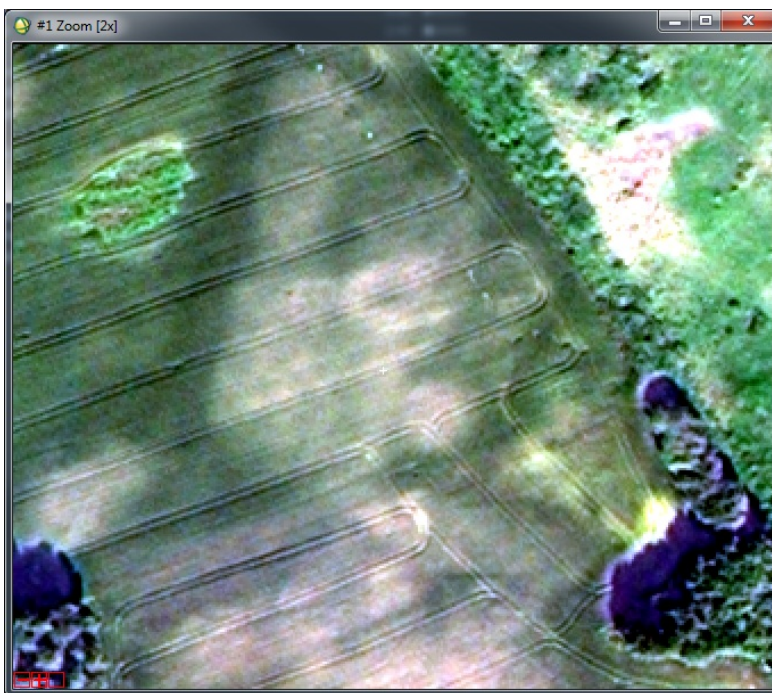


Figure 91. Detection no. 31 in the 7 August image.

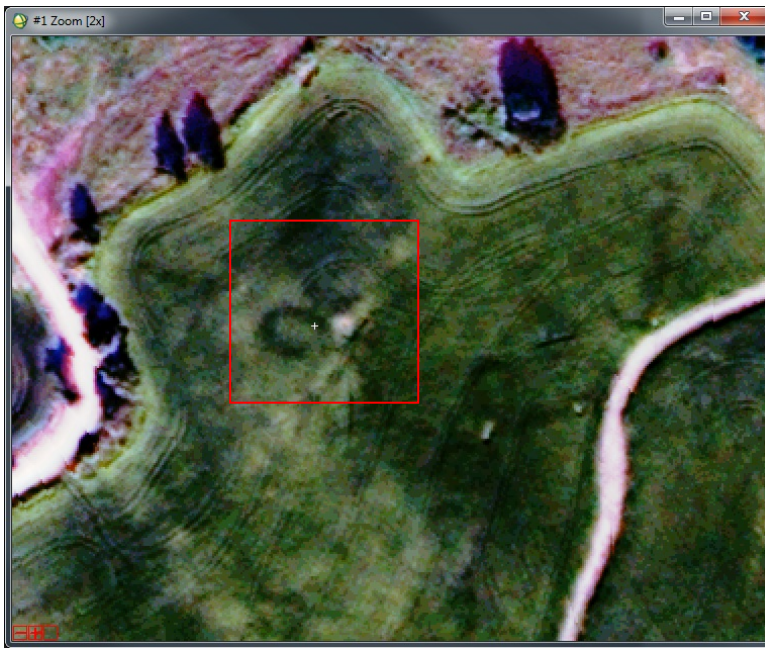


Figure 92. Detection no. 34, a circular pattern at Dvergsten in the 24 July image.



Figure 93. Detection no. 34 at Dvergsten in the 7 August image.

3.1.3.5 Summary after manually visual analysis of the satellite images of the Granavollen area.

There were 10 observations of ring structures that had not been detected by CultSearcher and that the operator defined as interesting. Out of these are four more likely to be indicating remains from prehistoric graves.

As a conclusion, the analysis made by KHM shows that CultSearcher detects ring structures that can be remains of grave mounds. Of the detections done by Norsk Regnesentral, approximately 50 % have a possible or less possible rating. As KHM receives the already "washed" ROI-file its difficult to give a number of true hits. None of the detected structures can be said showing absolutely true detections of remains of prehistoric grave mounds. The visual analysis showed that there are ringshaped structures that CultSearcher do not detect. Several of these are likely to be remains of prehistoric grave mounds. This indicates that to be sure of not missing any potesial structures the operator still has to use visual analysis in this work. The time spent using the software, with all its challenges, validating detections and the necessary manually visual control of the *whole* image must be taken in consideration when using the system.

3.1.4 Detections in Worldview-2 images in Sør-Trøndelag

Two image acquisitions of Ørland from the summer of 2010 are available: 5 June and 19 August. The acquisitions represent both the start of the growing season and the peak, before harvest. Automatic detections with CultSearcher are done in both images.

3.1.4.1 Ørland image of 5 June 2010

CultSearcher automatically detects 31 potential crop marks. 28 of these are regarded as obvious misclassifications, whereas 3 of them are checked by an archaeologist (Table 16). The archaeologist regards all three to be possible cultural heritage sites. None of them are visible on orthophotos in *Norge i bilder* (www.norgebilder.no).

Table 16. Automatic detections (aut. det.), confirmed automatic detections (conf.a.d.) and manual detections (man.det.) in the Ørland image of 5 June 2010.

det. no.	UTM zone 32		diam. [m]	aut. det.	conf. a.d.	man. det.	Farm name	Comment by archaeologist
	east	north						
1	536382	7063618	17	x	x		Skjeggghaug gnr 82/80	Bright ring, possible cultural heritage site
2	533837	7068463	9	x	x		Døsvik gnr 77/7	Bright ring, dark interior. Possible cultural heritage site
3	531480	7065689	9	x	x		Rønne gnr 71/14	Dark ring, bright interior. Possible cultural heritage site.
4	531539	7063746	15			x	Vik gnr 70/2	Bright ring. Not visible in August image. Possible cultural heritage site.
5	532993	7067009	7			x	Berg gnr 78/4	Dark ring, crop mark. Visible also on August image (weaker) Possible cultural heritage site.

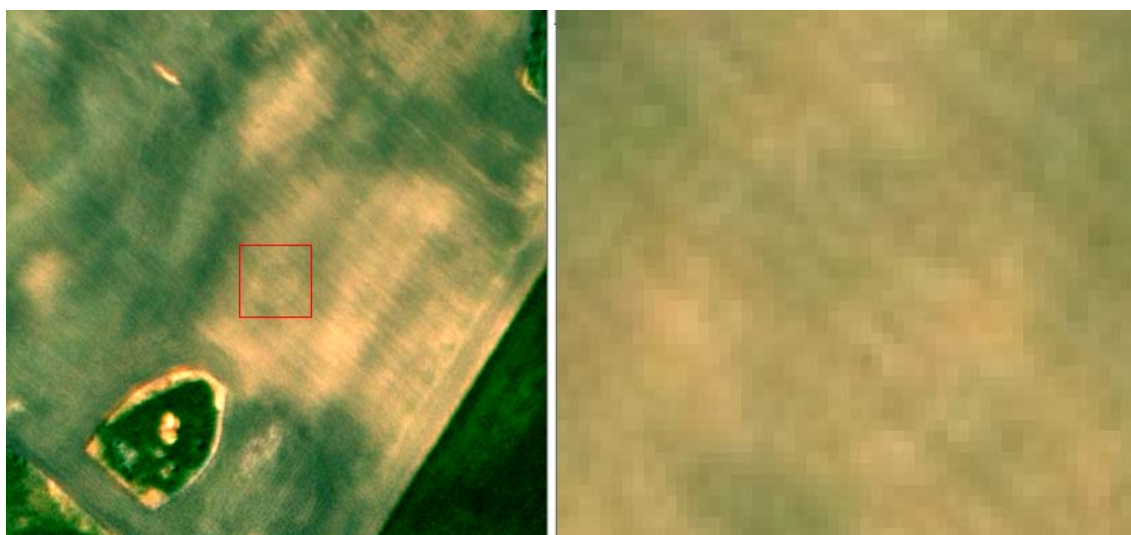


Figure 94. Detection no. 1 in the Ørland image of 5 June 2010.



Figure 95. Detections nos. 2 (top) and 3 (bottom) in the Ørland June image.

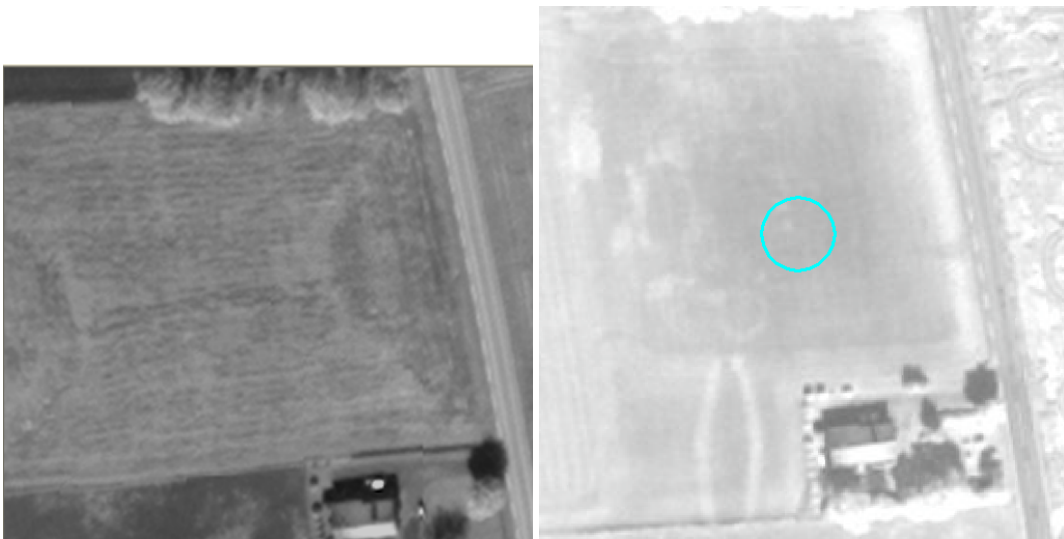


Figure 96. Left: Detection no. 4, at Vik, in the Ørland June image. Right: the new detection at Vik, superimposed on a Quickbird image from 7 August 2007, which shows a leveled grave field including an elongated grave mound.

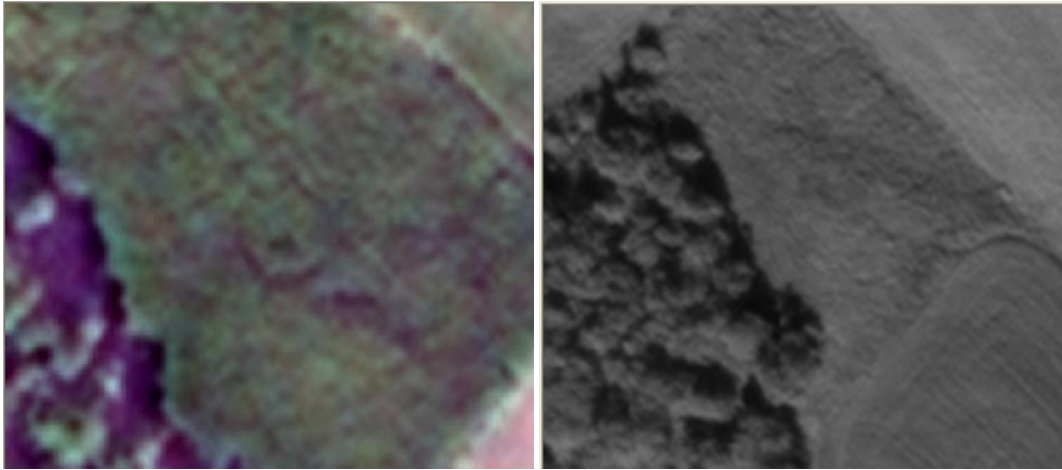


Figure 97. Left: detection no. 5, at Berg, in the Ørland June image. Right: the crop mark is less visible in the August image.

3.1.4.2 Ørland image of 19 August 2010

CultSearcher automatically detected 76 potential crop marks. 72 of these are regarded as obvious misclassifications, whereas 4 of them are considered as interesting and checked by an archaeologist (Table 17).

Table 17. CultSearcher detections in the Ørland image of 19 August 2010.

det. no.	UTM zone 32		diam [m]	aut. det.	conf. a.d.	man. det.	Farm name	Comment
	east	north						
1	531010	7065795	12,0	x	x		Fagervoll gnr 75/20	Dark ring, partially bright interior. Possible cultural heritage site.
2	531332	7064482		x			Vik gnr 70/12	Bright, partial ring, might be tractor tracks. Most likely not a cultural heritage site.
3	535128	7064991	8,0	x			Nordlund gnr 82/69	Dark polygon. Curcular, but part of a larger structure. May be a moist part of the field. Most likely not a cultural heritage site.
4	534514	7064214	7,5	x	x		Ørland gnr 82/416	Bright ring. Several similar, somewhat larger rings near by. Possible cultural heritage site. Grave field?

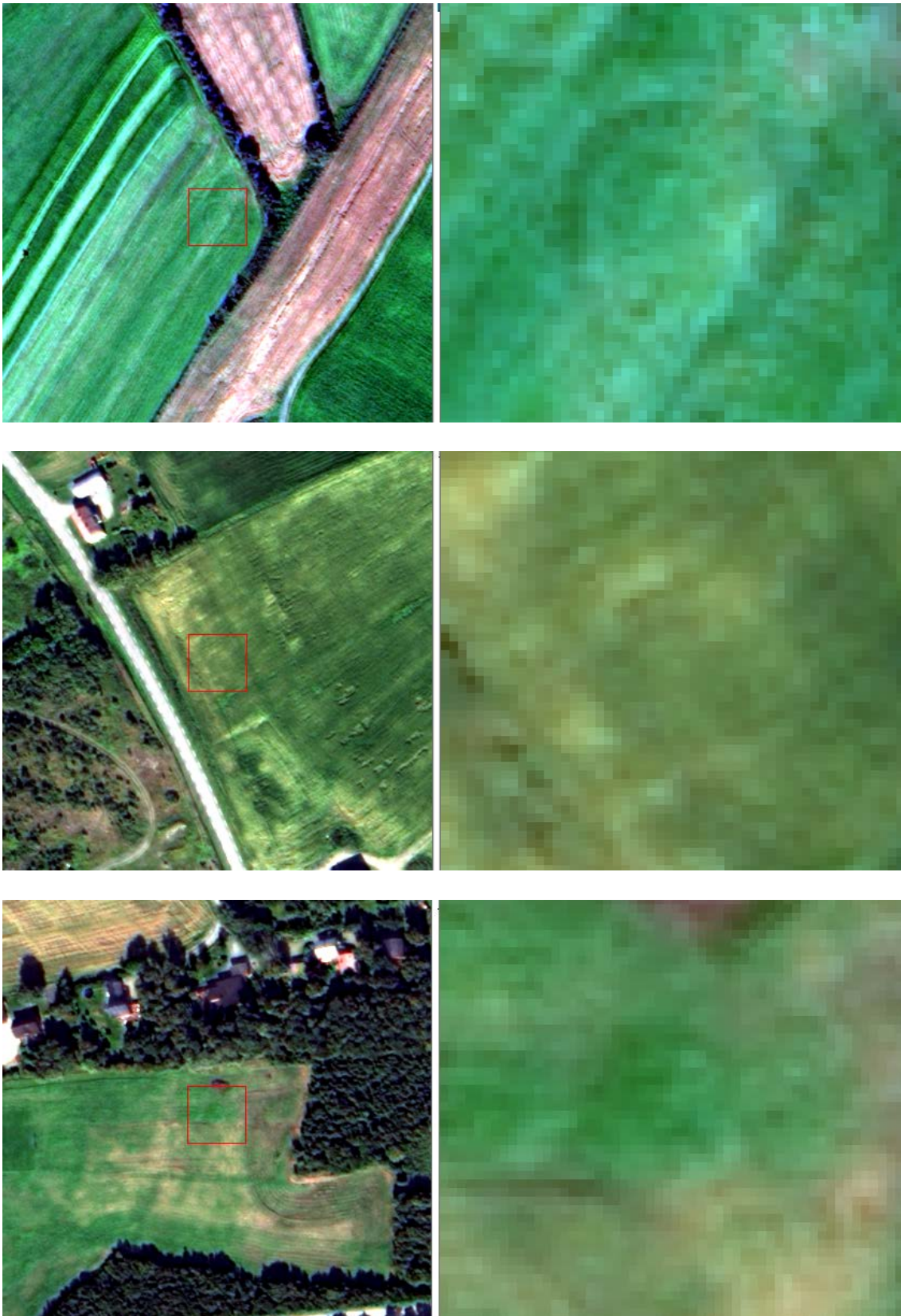


Figure 98. Detections nos. 1 (top), 2 (middle), and 3 (bottom) in the Ørland image of 19 August 2010.



Figure 99. Detection no. 4 in the 19 August image of Ørland.

3.1.4.3 Comments on visual inspection of Ørland images

Of the in total nine detections in the two image acquisitions, seven are regarded as possible or likely leveled grave mounds by visual inspection by the archaeologist. However, none of these can be confirmed without field inspections.

Detection no. 4 in the June image, at Vik, is a very interesting detection. It is located in a field with a known historical grave field, which is now leveled. Nothing is visible on the surface at present. However, there exists historical records of the grave field. In addition, an archive Quickbird image shows marks of an elongated leveled grave mound and several circular leveled grave mounds. These are also documented by oblique aerial images.

None of the detections coincide with existing detections in the Askeladden cultural heritage database.

3.1.4.4 Sources of error

A large number of the detections are located at or close to tractor tracks, commonly occurring in fields. Especially at ends and corners of fields, vehicle track curves and turns may cause false detections. Another source of false detections are mobile, circular feeding stations for cattle. These result in circular patterns of 8-10 m diameter, which coincides with a common size of many leveled grave mounds. However, the feeding stations are in most cases easy to spot during manual verification of the automatic detections.

Ørland municipality has many defense installations, some dating back to the 1940s. A number of canon and machine gun posts are scattered across the landscape. Some are abandoned and partly removed. The shape and size may in many cases coincide with leveled grave mounds, especially the one that have been abandoned, and filled with, say, soil or sand, may cause false detections.

Another source of misdetections is tree shadows. These are, however, easy to spot during visual inspection.

The detection at Vik illustrates a drawback with relying on remote sensing imagery to detect cultural heritage sites in the form of crop marks and soil marks. Soil humidity conditions and

vegetation cover may change dramatically by time. Older image acquisitions reveal distinct structures under the soil, where as in other acquisitions they are not visible. A possible solution is to acquire images on a regular basis over a time period in order to overcome the variations of soil and vegetation conditions and the varying presence of soil marks and crop marks.

As a conclusion, the two acquisitions during the summer of 2010 resulted in one likely and six possible leveled grave mounds previously not registered in the Askeladden cultural heritage database. Archaeological field inspections are, however, necessary to confirm these.

3.1.5 Detections in the Quickbird image of Gardermoen of 29 July 2003

A few years back, the project acquired an archive Quickbird image of Gardermoen of 29 July 2003. For the purpose of initial testing, agricultural masks were hand drawn for portions of the image, and CultSearcher processed those subimages at that time. The project has finally received GIS data from Jessheim, Nannestad and Gjerdrum municipalities, enabling the processing of the entire Gardermoen image of 29 July 2003.

CultSearcher automatically detected 372 potential crop marks, whereas 19 of them are considered as interesting and need to be checked by an expert (Table 18).

Table 18. CultSearcher detections in the Gardermoen image.

CultSearcher detection no.	UTM zone 32		Farm name	Comment
	east	north		
1	618451.8	6669946.2		Known site, part of training set, sub2
2	618694.2	6671305.8		Known site, part of training set, sub2
3	610852.2	6674989.2		Previously unknown?
4	618319.2	6669849.0		
5	611107.8	6678521.4		Part of training set, sub1, but not a crop mark!
6	614358.0	6681243.0		
7	612254.4	6673231.2		
8	613665.0	6672692.4		
9	612943.8	6677019.6		
10	608672.4	6676575.6		
11	610567.8	6676124.4		
12	611334.6	6680698.8		Part of training set, sub1
13	611055.0	6679169.4		
14	611357.4	6672708.6		Part of training set, sub3
15	611039.4	6672627.0		
16	614317.2	6672033.6		
17	617181.6	6668586.0		
18	611340.0	6679755.0		
19	617282.4	6669263.4		



Figure 100. Detection no. 1 in the Gardermoen image of 29 July 2003.

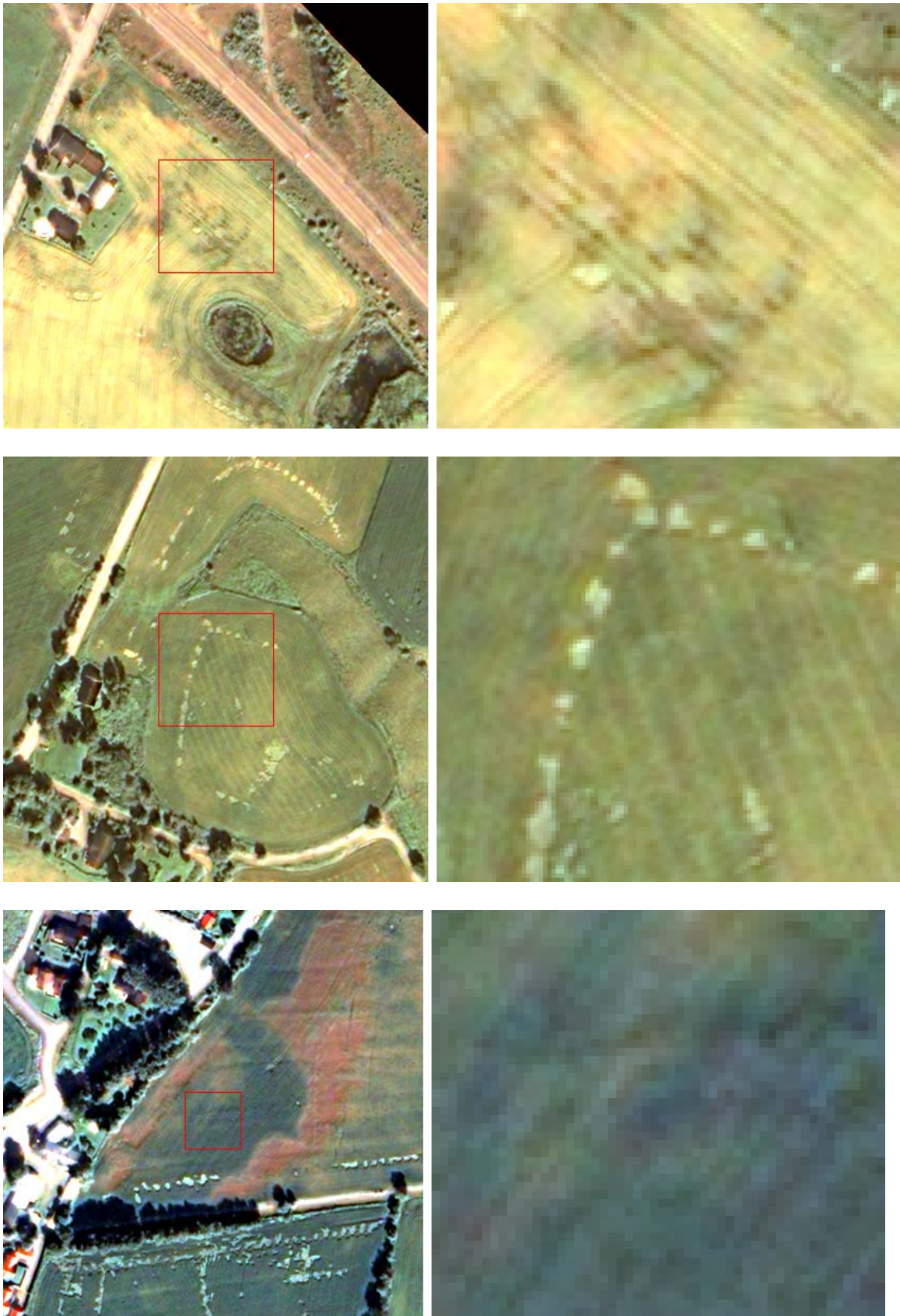


Figure 101. Detections nos. 2 (top), 3 (middle), and 4 (bottom) in the Gardermoen image of 29 July 2003.

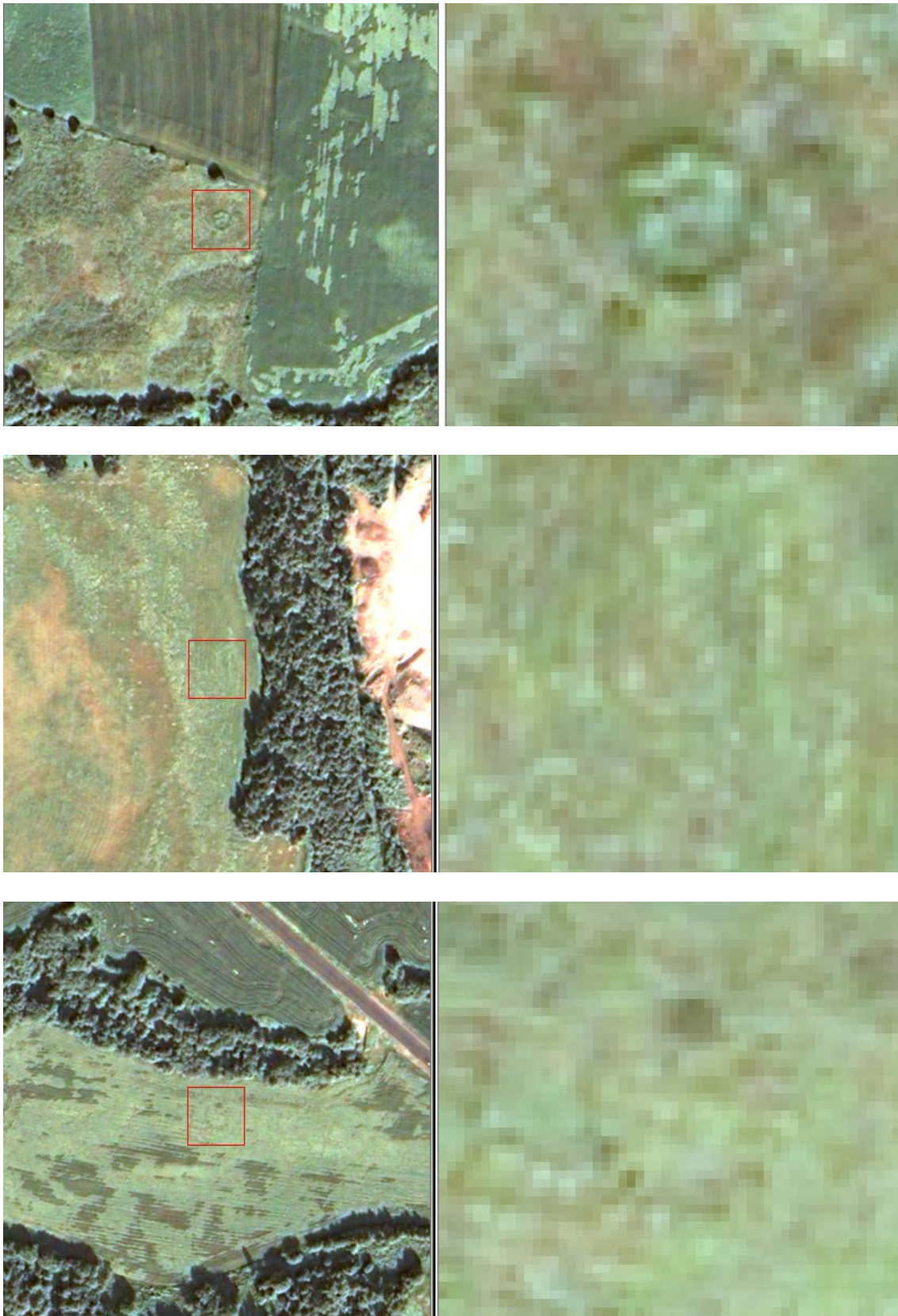


Figure 102. Detections nos. 5 (top), 6 (middle), and 7 (bottom) in the Gardermoen image of 29 July 2003.

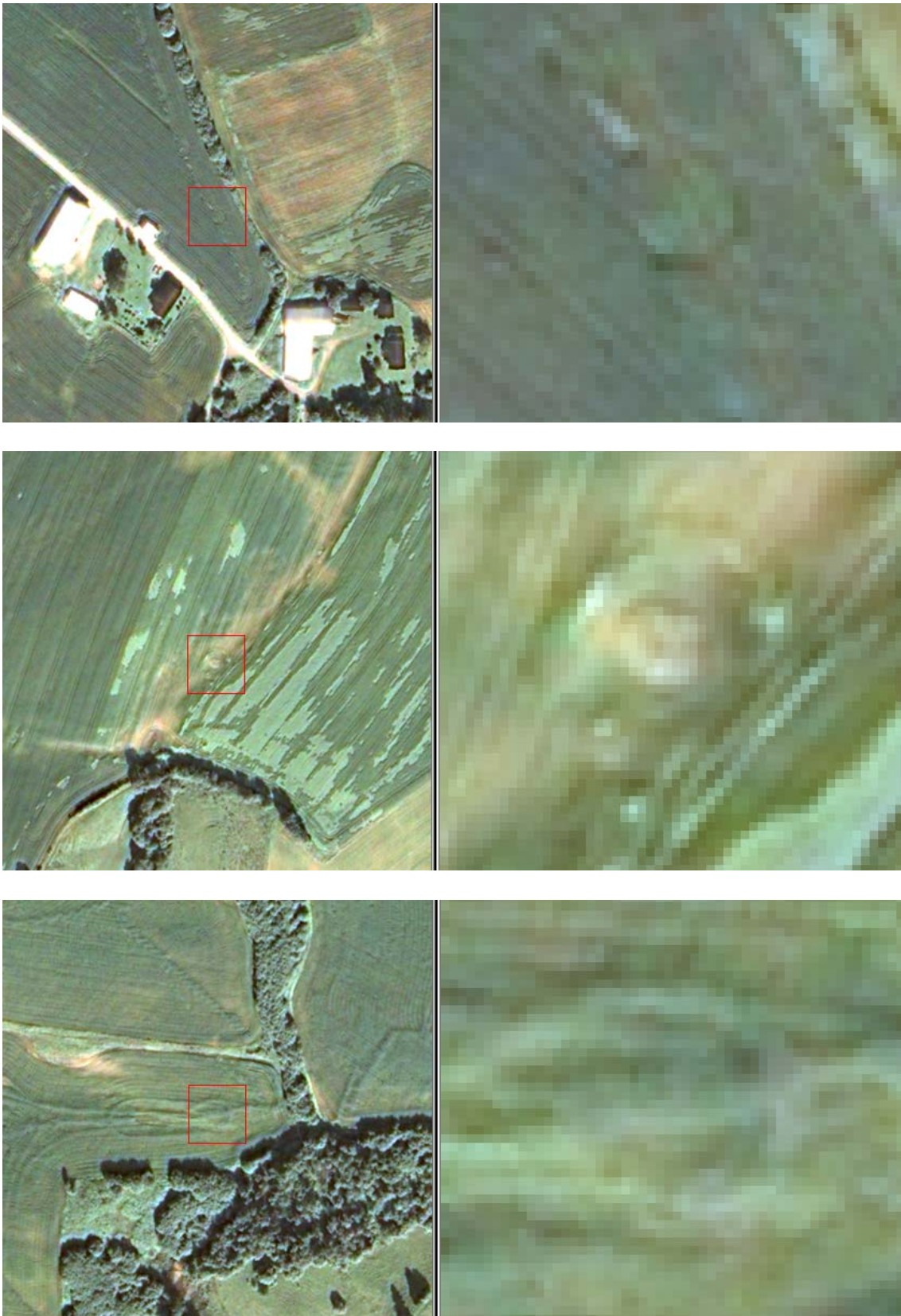


Figure 103. Detections nos. 8, (top), 9 (middle), and 10 (bottom) in the 29 July 2003 image of Gardermoen.



Figure 104. Deetctions nos. 11 (top), 12 (middle), and 13 (bottom) in the 29 July 2003 image of Gardermoen.

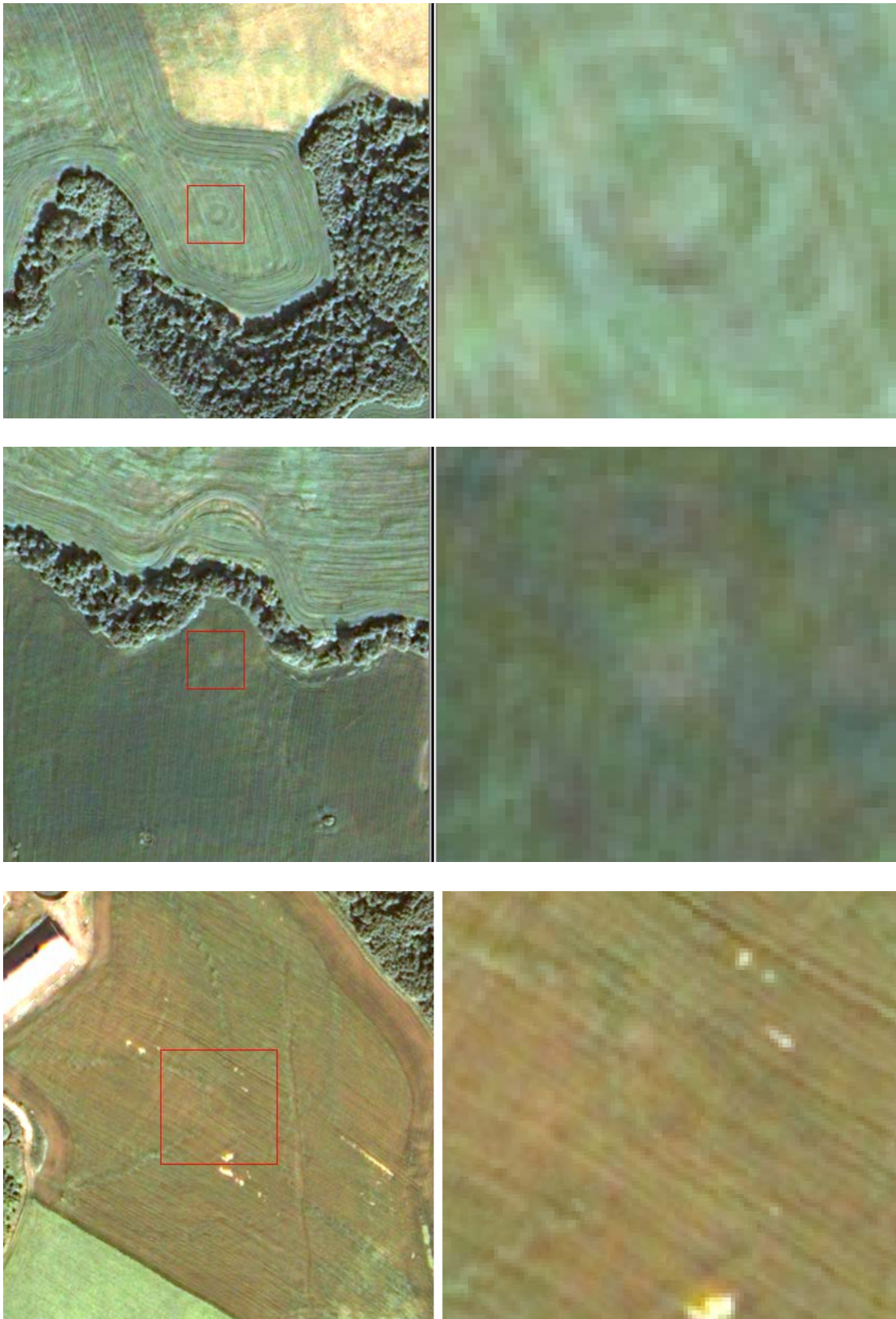


Figure 105. Detections nos. 14, (top), 15 (middle), and 16 (bottom) in the Gardermoen image of 29 July 2003.

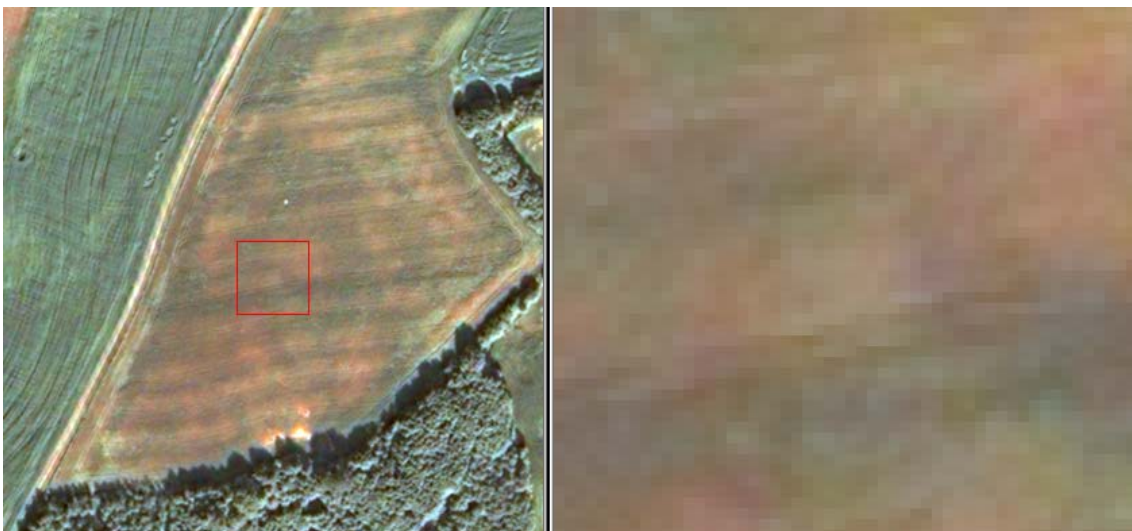
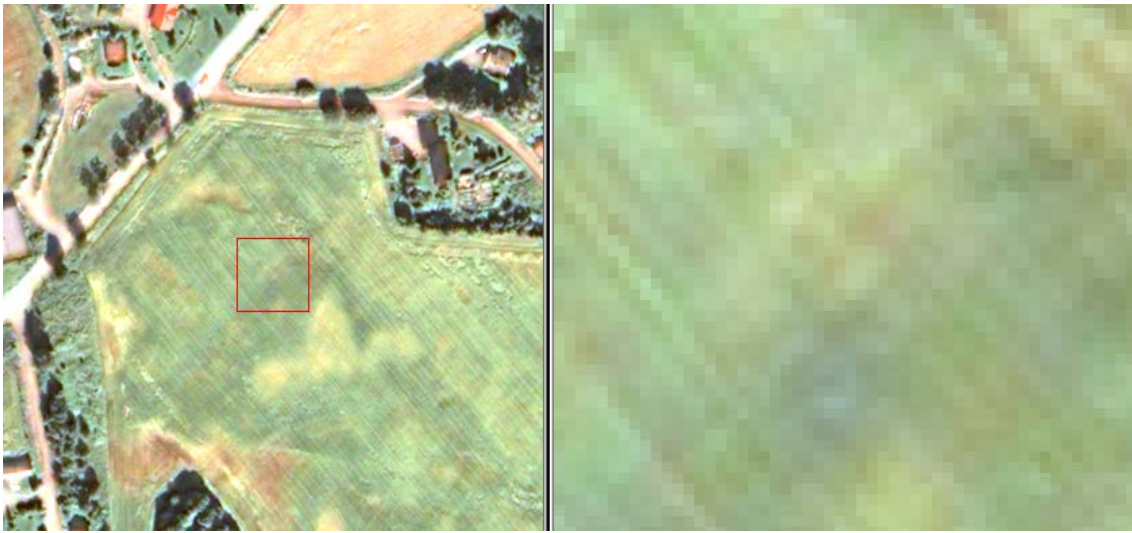


Figure 106. Detections nos. 17 (top), 18 (middle), and 19 (bottom) in the Gardermoen image of 29 July 2003.

3.1.6 Detections in aerial ortophotos in Vestfold

Aerial images, covering most of the Tjølling satellite image, were downloaded from Norge i bilder (www.norgebilder.no), resampled from 0.2 m to 0.6 m resolution, and processed by CultSearcher.

Two of the detections from the Worldview-2 image were found by the automatic algorithm (Table 19). However, the correlation threshold had to be set to 50 instead of 55. In addition to the two true detections, we have picked two doubtful ones. The two other sites of the 2010 Worldview-2 detections, Fjellvik and Eide, were not visible in the 2002 ortophoto. Perhaps 15 July 2002 was a little early for these locations to have the crop marks developed.

Table 19. Detections in Tjølling area of the 2002 Vestfold ortophoto acquisitions.

TBC detection no.	UTM zone 32		Farm name	Acquisition date	Comment
	east	north			
1	568980.0	6547705.6	Store Sandnes	July 15, 2002	Also detected in 2010 Worldview-2 image
2	568052.4	6547114.0	Klepåker	July 15, 2002	Partial ring
3	568161.6	6547252.6	Eide	July 15, 2002	Uncertain
4	567730.8	6546525.4	Nedre Klåstad	July 15, 2002	Also detected in 2009 Quickbird and 2010 Worldview-2 images.



Figure 107. Detection no. 1 in the aerial orthophoto of 15 July 2002 of parts of Vestfold.

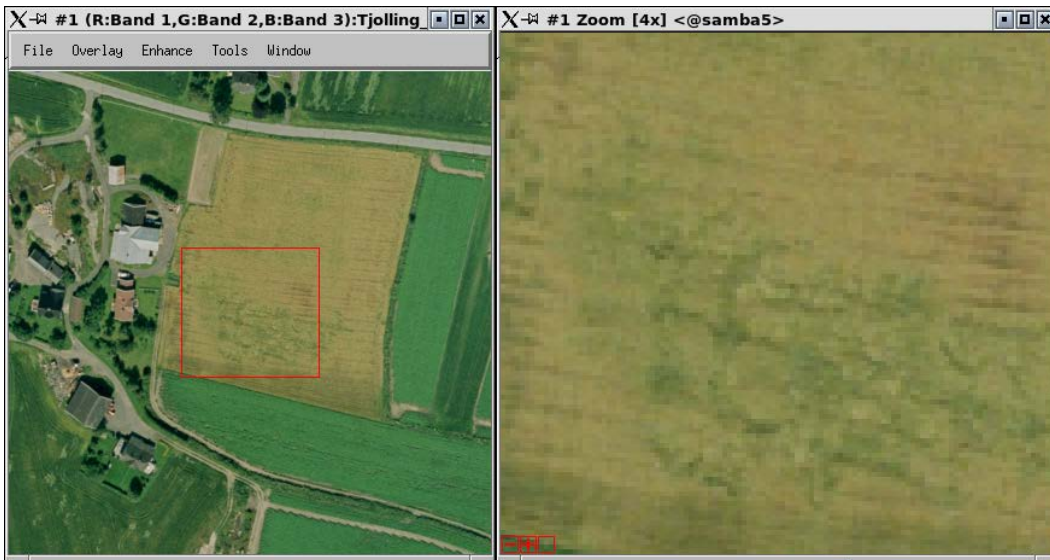


Figure 108. Detections nos. 2 (top), 3 (middle), and 4 (bottom) in the aerial orthophoto of 15 July 2002..

3.2 Automatic detection of pitfall traps in lidar data

The automatic pit detection method was run on the two images 32-1-503-169-6 (Figure 110) and 32-1-503-169-7 (Figure 111). By using the default values for the search parameters (Table 20), 12 pits are detected in 32-1-503-169-6 and six pits in 32-1-503-169-7.

Table 20. Default values for advanced pit search parameters.

parameter	default	unit	relaxed
minimum radius	1.2	meter	
maximum radius	3.6	meter	
radSpacing	0.2	meter	
pixel size	0.2	meter	
max number of pits	1000		
minimum similarity	20		10
edge width	2	pixels	

parameter	default	unit	relaxed
min depth	4	pixels	0 or 1
max dev from U-shape	0.03333		1
max dev from V-shape	0.1		1
masking	0		
find heap	0		
find pit	1		

Table 21. CultSearcher detections of pits in the lidar height image 32-1-503-169-6. The shaded rows are removed manually before field work.

id	east [meter UTM 32N]	north [meter UTM 32N]	radius [m]	score	norm corr	correlation	min depth [feet]	avg depth [feet]	stdev edge [feet]	rms U	rms V	amplitude
1	519665.6	6815531.0	3.4	600.608	30.133	51.227	6	6.404	0.491	0.018	0.009	51.227
2	519612.0	6815592.5	3.2	500.520	27.908	44.654	5	5.785	0.692	0.021	0.012	44.654
3	519627.4	6815592.0	3.2	500.513	27.596	44.153	5	5.867	0.497	0.021	0.012	44.153
4	519721.2	6815465.0	3.4	500.549	27.551	46.837	5	6.395	0.563	0.018	0.011	46.837
5	519978.0	6815453.0	3.2	400.500	27.002	43.203	4	5.423	0.531	0.019	0.015	43.203
6	519807.2	6815411.0	3.2	500.481	26.115	41.784	5	6.129	0.512	0.023	0.012	41.784
7	519665.8	6815563.0	3.0	400.445	26.076	39.115	4	5.982	1.112	0.029	0.023	39.115
8	519793.8	6815435.0	2.8	500.406	25.857	36.200	5	6.247	0.469	0.028	0.020	36.200
9	519766.8	6815457.5	3.4	500.494	25.144	42.745	5	5.827	0.666	0.021	0.012	42.745
10	519645.0	6815590.0	3.2	500.457	25.010	40.015	5	6.044	0.569	0.021	0.012	40.015
11	519947.8	6815433.0	3.2	400.424	23.480	37.568	4	6.063	1.173	0.032	0.029	37.568
12	519670.8	6815498.0	3.2	400.423	23.407	37.452	4	4.848	0.610	0.021	0.014	37.452
13	519947.6	6815433.0	3.4	400.448	23.145	39.346	4	6.359	1.388	0.034	0.031	39.346
14	519450.6	6815654.5	2.4	300.217	17.016	22.121	3	3.807	0.654	0.034	0.025	22.121
15	519531.0	6815627.0	2.4	300.182	16.280	19.536	3	3.589	0.643	0.036	0.032	19.536
16	519484.4	6815790.5	3.4	100.254	14.653	24.909	1	3.331	1.532	0.040	0.040	24.909
17	519484.0	6815790.5	2.8	100.176	13.626	19.076	1	2.764	1.114	0.045	0.045	19.076
18	519369.2	6815730.0	2.2	100.120	13.593	14.952	1	3.196	1.230	0.050	0.046	14.952
19	519352.4	6815748.0	2.2	200.114	13.170	14.487	2	2.714	0.463	0.041	0.032	14.487
20	519483.8	6815791.0	2.4	100.149	13.162	17.111	1	2.588	1.018	0.044	0.043	17.111
21	519390.4	6815472.0	3.4	100.196	12.115	20.596	1	3.385	2.623	0.048	0.048	20.596
22	519577.8	6815837.5	1.6	200.047	11.943	9.554	2	2.500	0.502	0.062	0.047	9.554
23	519390.4	6815459.0	3.4	100.185	11.640	19.788	1	2.323	1.031	0.038	0.036	19.788
24	519334.8	6815427.0	3.4	100.177	11.305	19.219	1	3.731	2.772	0.049	0.048	19.219
25	519909.8	6815924.0	3.4	100.175	11.197	19.034	1	2.647	0.956	0.035	0.033	19.034
26	519419.2	6815887.0	2.2	100.077	10.710	11.781	1	2.505	1.096	0.058	0.059	11.781
27	519425.2	6815914.0	1.4	100.019	10.625	7.437	1	2.600	1.946	0.104	0.105	7.437
28	519484.8	6815417.0	3.4	100.158	10.436	17.741	1	2.863	2.146	0.046	0.046	17.741
29	519651.6	6815828.5	3.4	100.156	10.358	17.608	1	2.517	1.164	0.038	0.036	17.608
30	519422.0	6815958.0	1.6	100.028	10.146	8.117	1	2.097	0.683	0.076	0.078	8.117
31	519804.2	6815970.0	2.8	100.108	10.028	14.040	1	2.649	1.050	0.047	0.045	14.040
32	519396.2	6815478.0	3.2	100.134	10.006	16.010	1	2.551	1.237	0.043	0.042	16.010

By setting *minimum similarity* to 10, and relaxing three other parameters as follows: *minimum depth*=0, *max dev from U-shape* =1 and *max dev from V-shape* =1, a total of 237 detections are made in image 32-1-503-169-6. By raising *minimum depth* to 1 (feet), this number is reduced to 32 detections (Table 21). Of these 32, if sorted by *normalized correlation*, the following are redundant detections and should have been removed by CultSearcher: nos. 13, 17, and 20. In addition, it was obvious from the lidar hill shade image that detections nos. 25 and 31 were at road edges (Figure 109), and thus not cultural heritage sites.

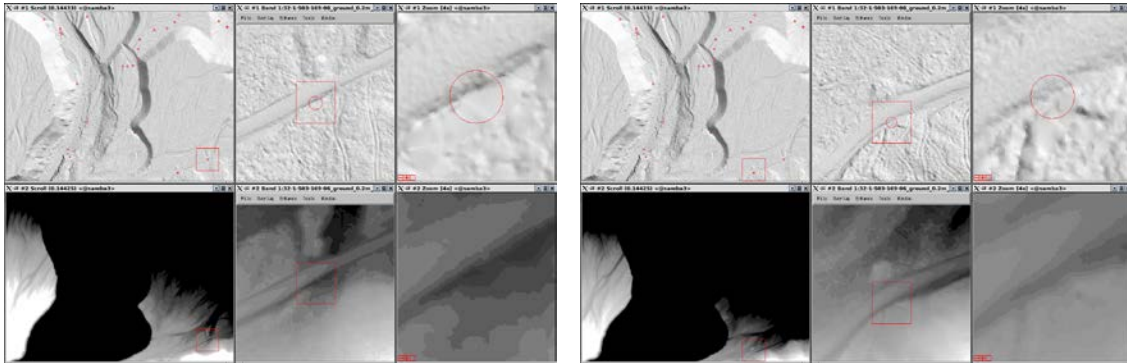


Figure 109. Detections at road edges.

By removing these five detections manually, 27 detections were left for archaeological field work (Figure 110). The 27 remaining detections are re-numbered 1-27 for convenience.

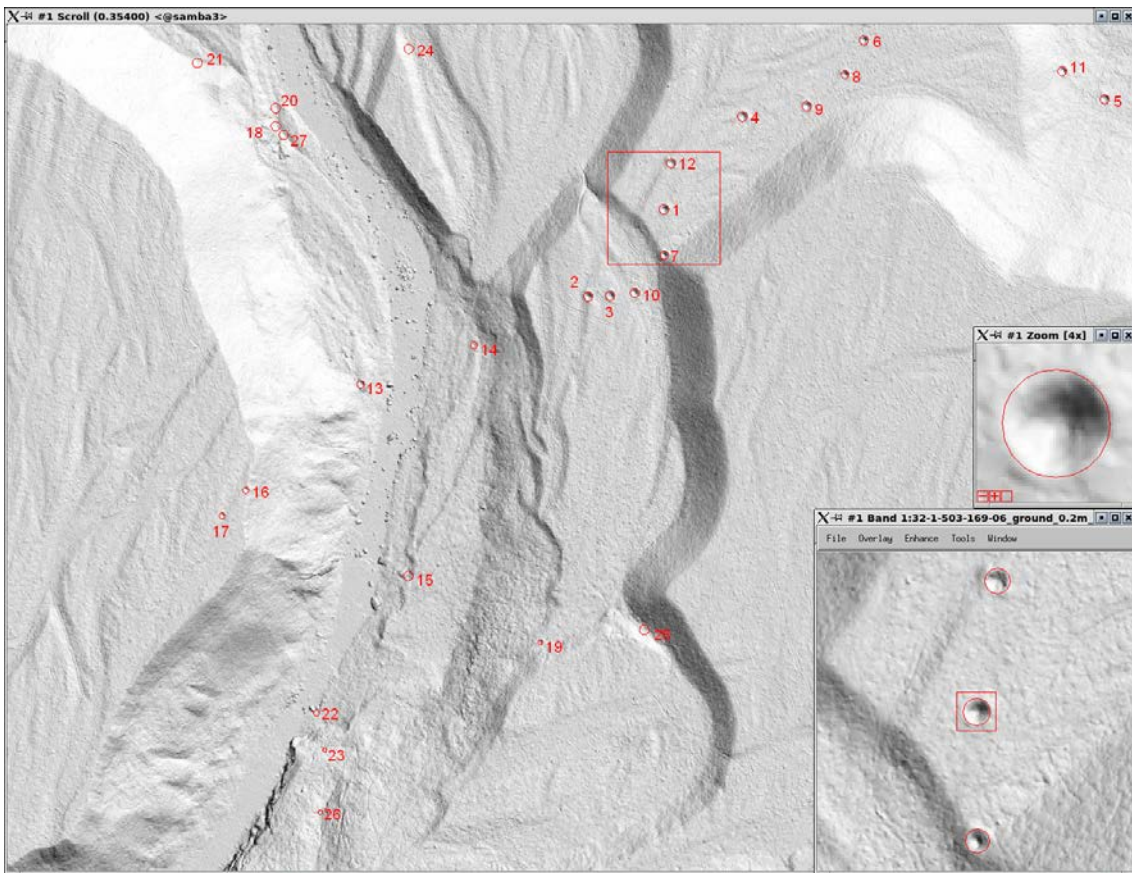


Figure 110. The top 27 detections in image 32-1-503-169-6, with the strongest detection enlarged. The detections are labeled in order from the strongest (1) to the weakest (27).

We also relax the advanced pit search parameters (Table 20) for image 32-1-503-169-7. By using *min depth* =0, a total of 922 detections are made. By raising *min depth* to 1, the number of detections is reduced to 97. The six strongest detections have *min depth* from 6 to 9. The seventh strongest detection has *min depth*=2, but is an obvious road edge. The remaining 90 detections are regarded weak, and excluded from archaeological field inspection. Only the six strongest detections from image 32-1-503-169-7 are checked in the field (Figure 111).

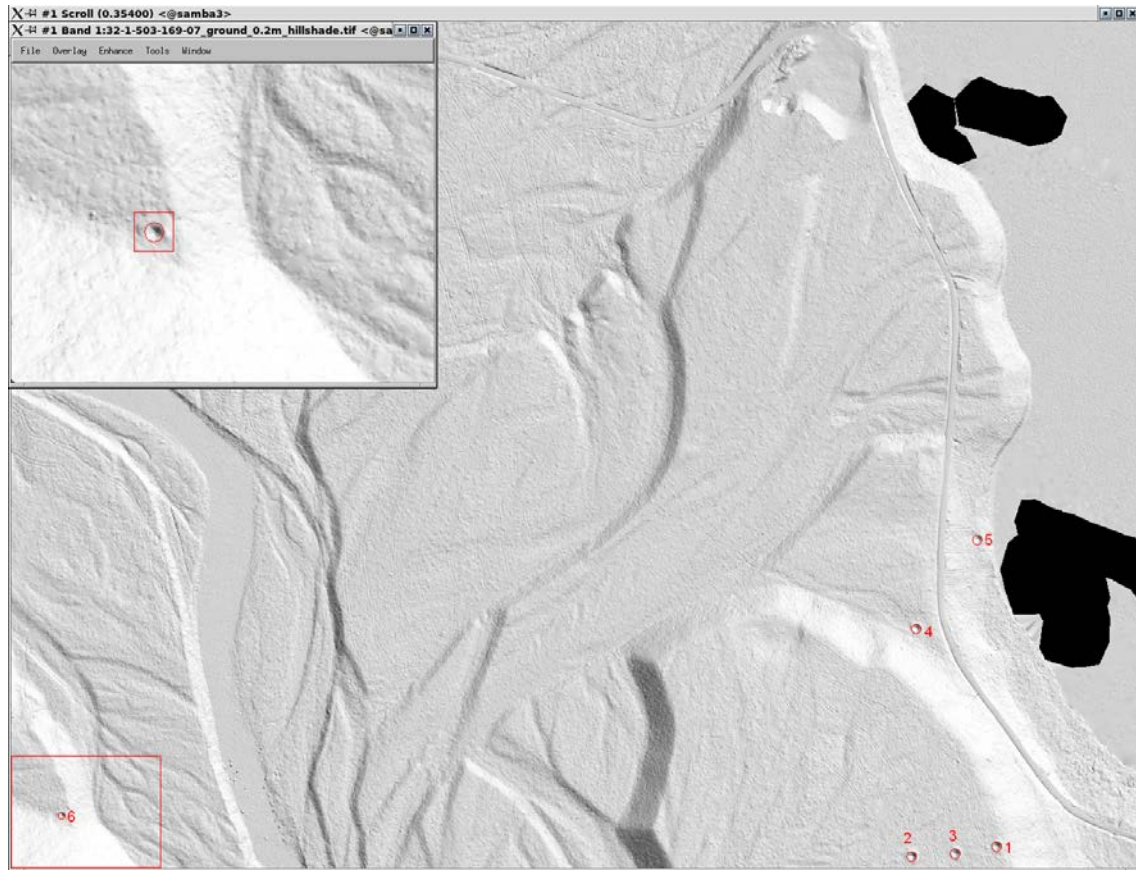


Figure 111. The top 6 detections in image 32-1-503-169-7, with the strongest detection enlarged. The detections are labeled in order from the strongest (1) to the weakest (6).

3.2.1 Field inspection of pitfall traps

On 20 October 2010, Lars Holger Pilø and Anne Engesveen drove by car from Lillehammer to Nord-Fron and inspected the 27 detections in image 32-1-503-169-6 and the six detections in image 32-1-503-169-7. The detections from CultSearcher were labeled on hill shade images (Figure 110-Figure 111) and lists with coordinates and measurements from CultSearcher were used in addition. All six detections in image 32-1-503-169-7 were confirmed to be true detections. Of the 27 detections in image 32-1-503-169-6 (Figure 112-Figure 124), 17 were confirmed to be true detections, and ten were false detections (Table 22).

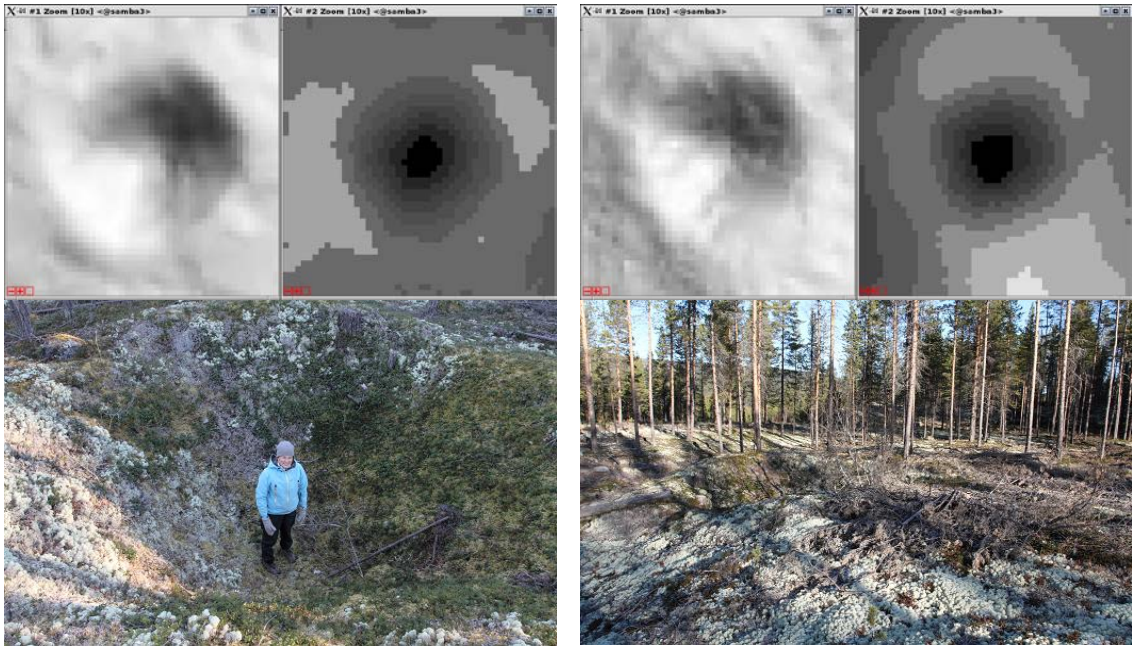


Figure 112. This and the following five figures show the top 12 detections in image 32-1-503-169-6. For each detection, the hill shade image is above left, the elevation image is above right, and the field image is below. In the elevation image, each gray tone level represents a separate integer elevation value in feet (0.3048 m). This figure: detections nos. 1 (left) and 2 (right).

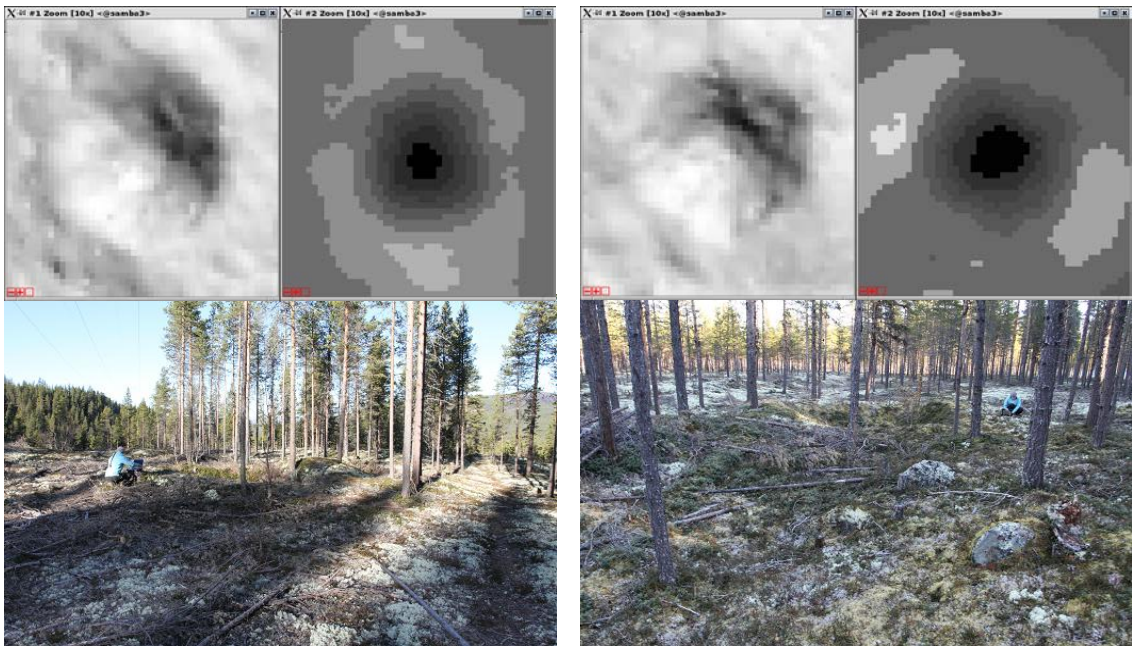


Figure 113. Detections nos. 3 (left) and 4 (right).

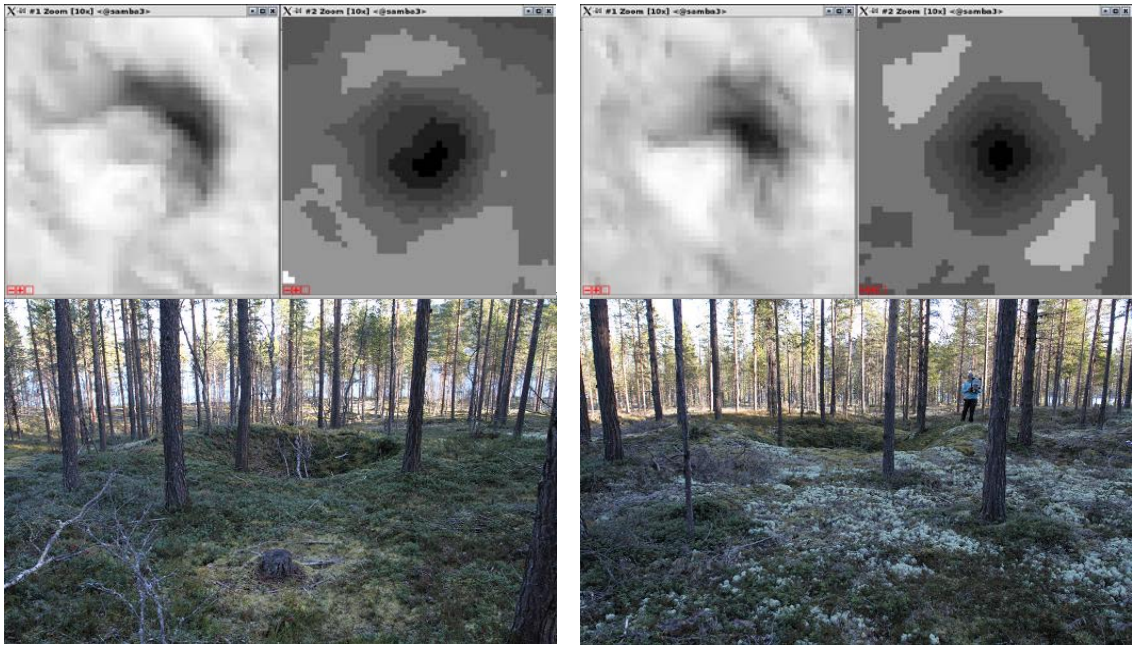


Figure 114. Detections nos. 5 (left) and 6 (right).

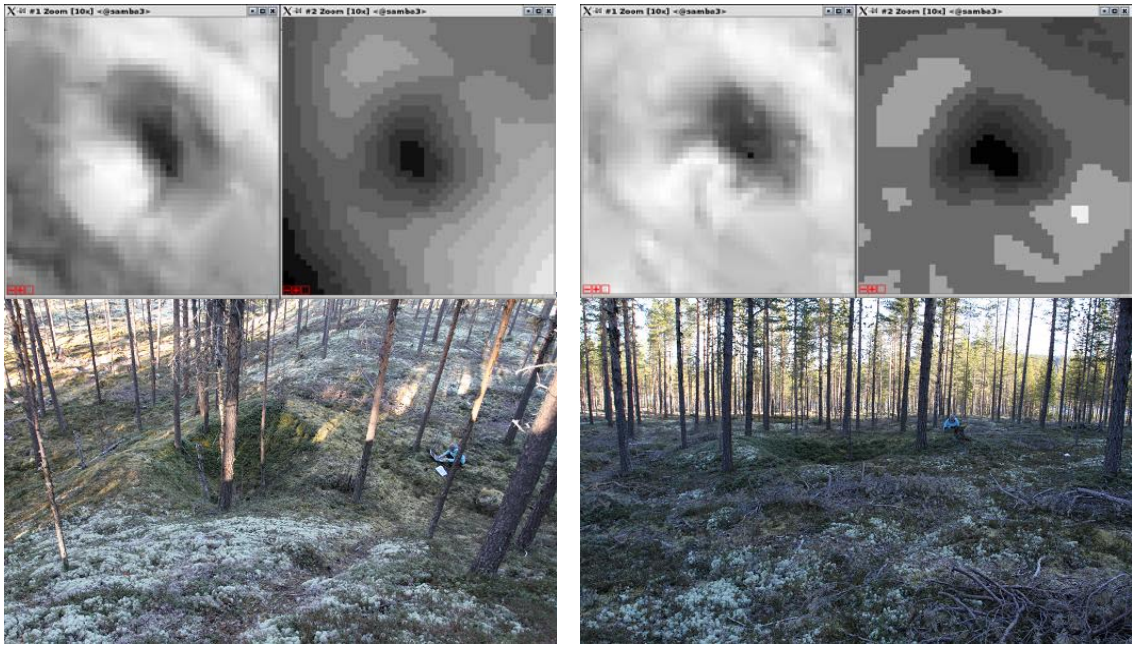


Figure 115. Detections nos. 7 (left) and 8 (right).

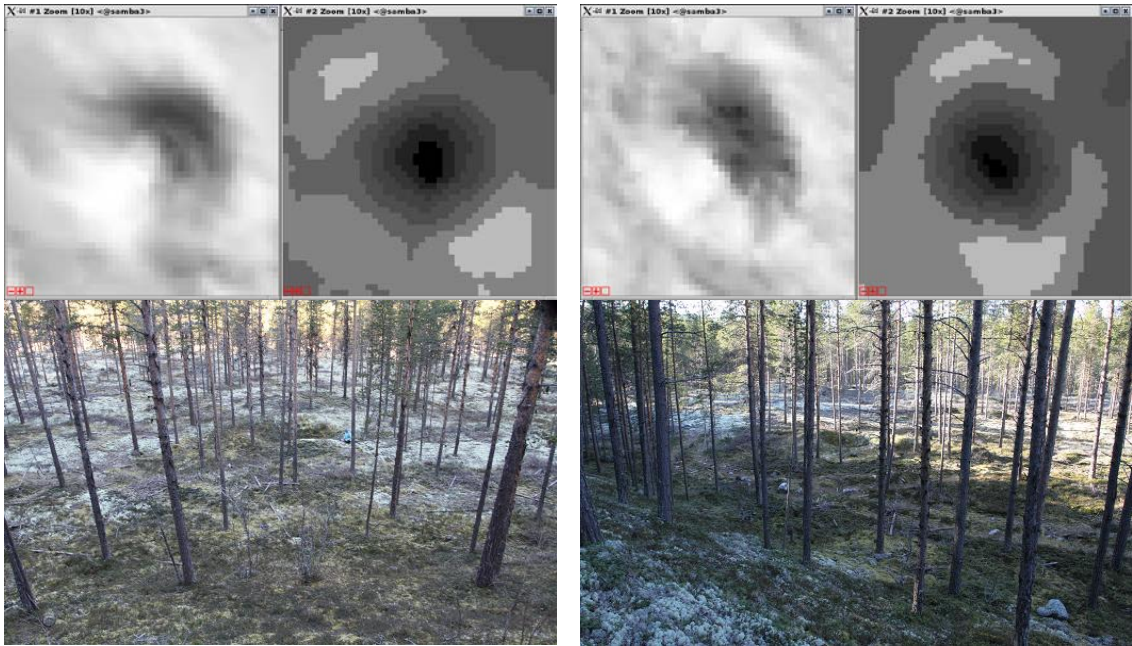


Figure 116. Detections nos. 9 (left) and 10 (right).

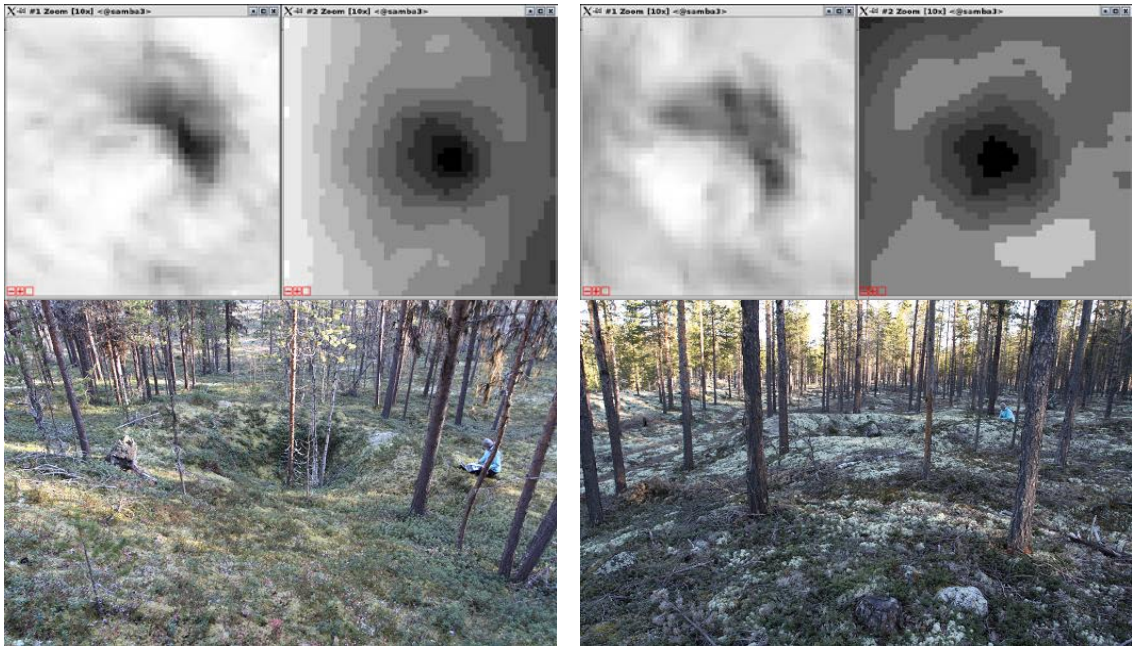


Figure 117. Detections nos. 11 (left) and 12 (right).

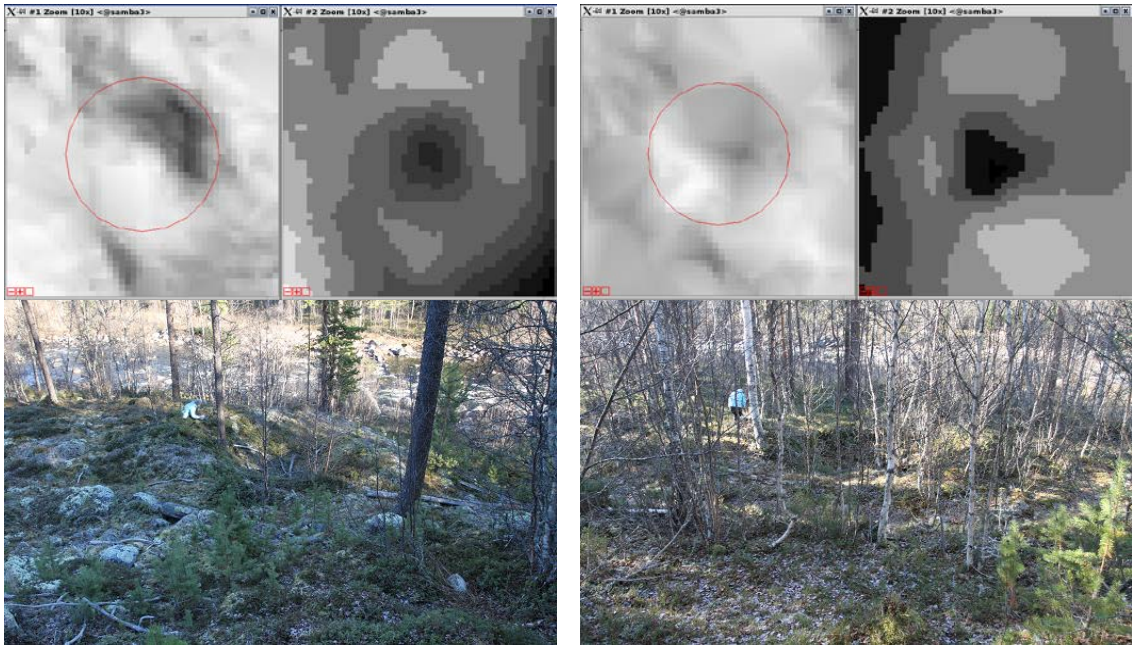


Figure 118. This and the two next figures show five less clear detections. However, all five were confirmed by field inspection. Here: detections nos.13 (left) and 14 (right).

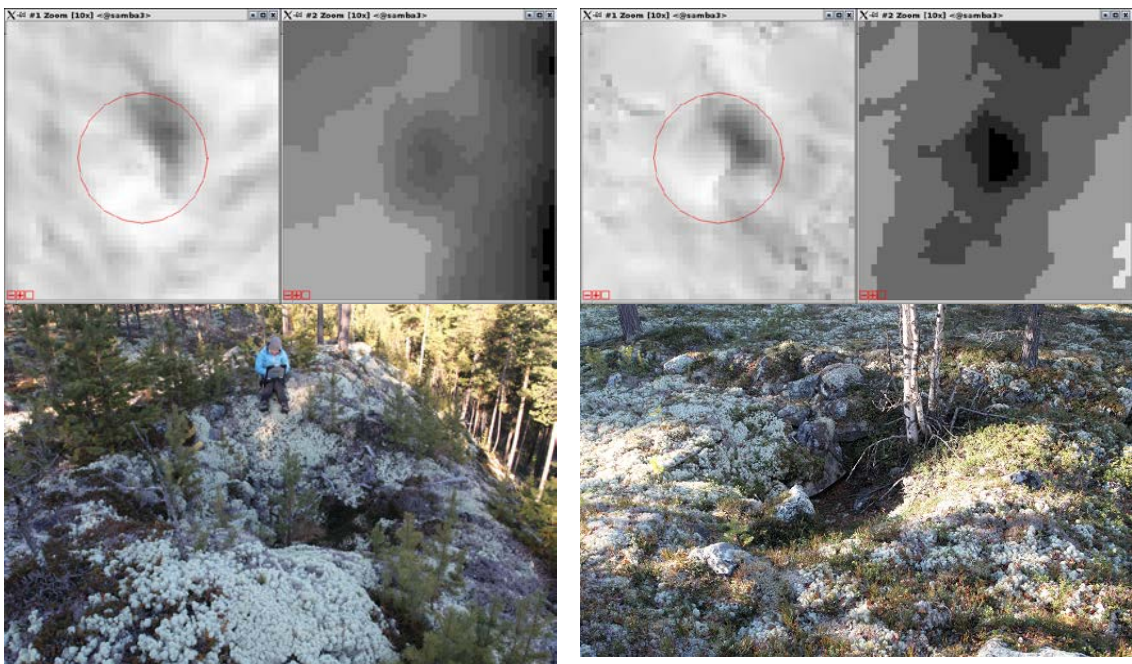


Figure 119. Detections nos. 16 and 17.



Figure 120. Detection no. 19. This detection was not found during the initial visual inspection of the laser data, but detected by CultSearcher, and confirmed in the field.

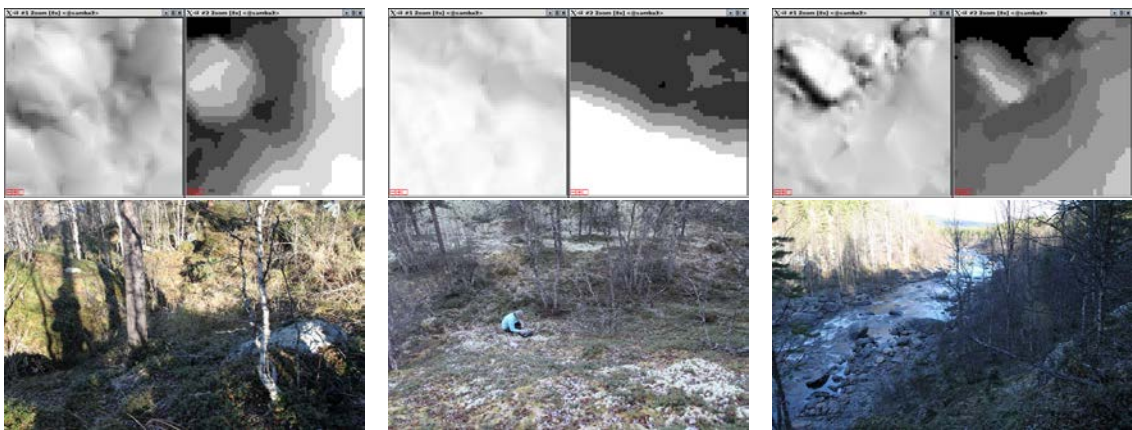


Figure 121. False detections. Nos. 15 (left) , 21 (middle), and 22 (right).



Figure 122. False detections: detections nos. 23 (left) and 24 (right).

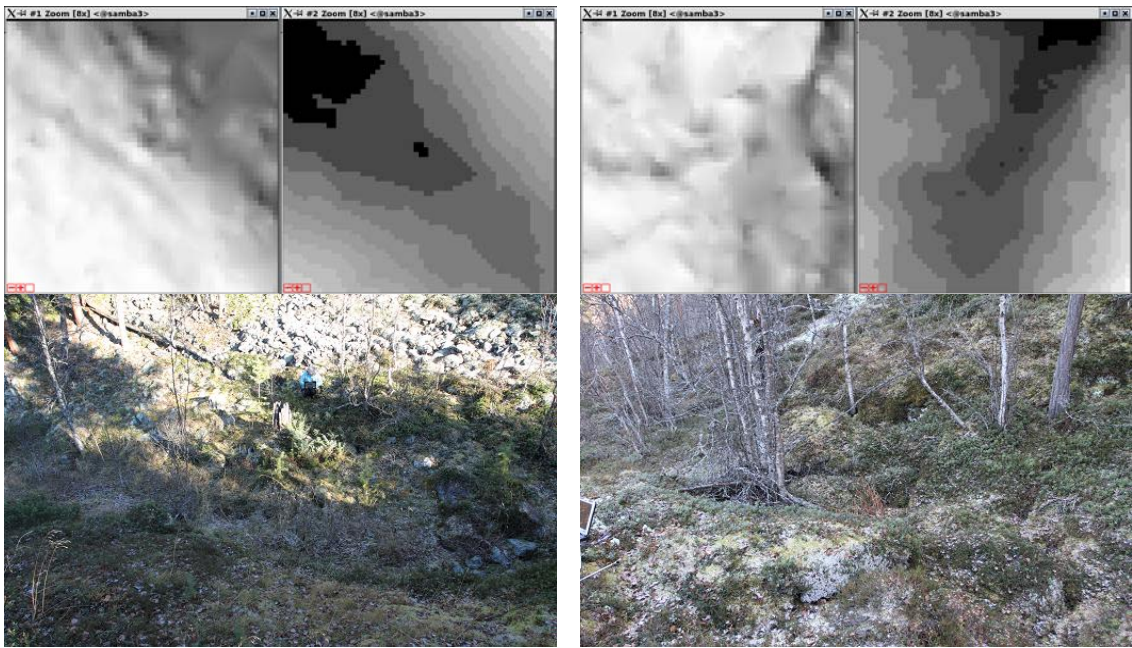


Figure 123. False detections: detections nos. 25 (left) and 26 (right).

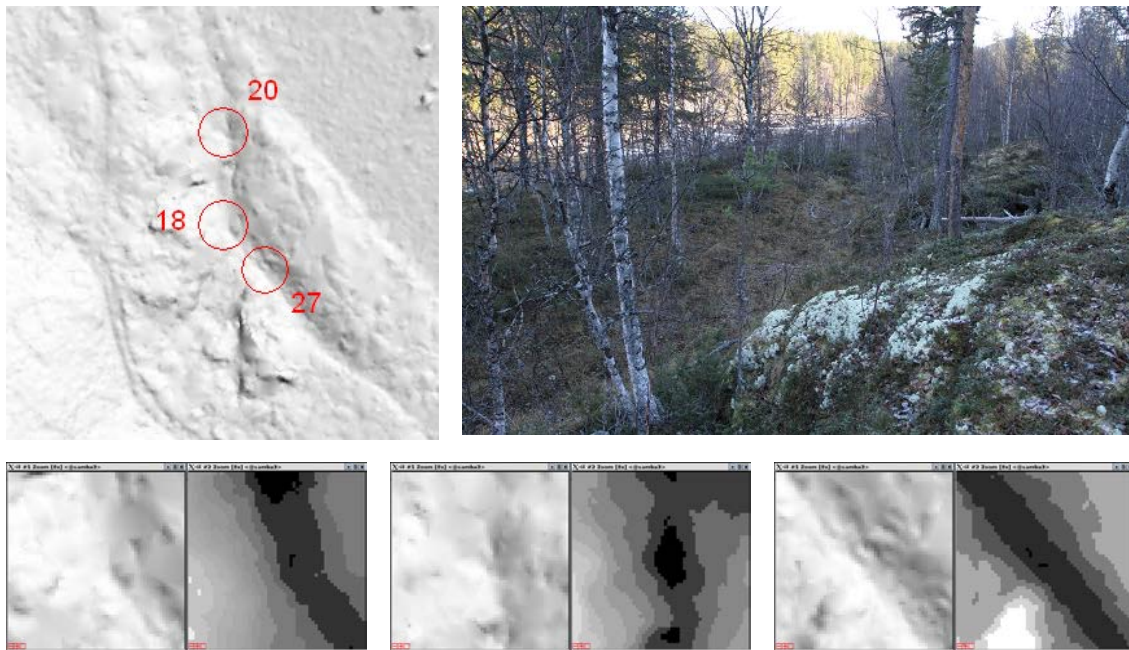


Figure 124. False detections: nos. 18 (bottom left), 20 (bottom middle) and 27 (bottom right). Top left: the three false detections are located in the same small valley. Top right: section of the small valley, with a large river and a sunlit tree-covered hillside in the background.

Table 22. The result of the field inspection. The green rows denote valid detections, and the pink rows denote false detections. The detections are sorted by *normalized correlation*, the 6th column.

id	east [meter UTM 32N]	north [meter UTM 32N]	radius [m]	score	norm corr	correlation	min depth [feet]	avg depth [feet]	stdev edge [feet]	rms U	rms V	amplitude
1	519665.6	6815531.0	3.4	600.608	30.133	51.227	6	6.404	0.491	0.018	0.009	51.227
2	519612.0	6815592.5	3.2	500.520	27.908	44.654	5	5.785	0.692	0.021	0.012	44.654
3	519627.4	6815592.0	3.2	500.513	27.596	44.153	5	5.867	0.497	0.021	0.012	44.153
4	519721.2	6815465.0	3.4	500.549	27.551	46.837	5	6.395	0.563	0.018	0.011	46.837
5	519978.0	6815453.0	3.2	400.500	27.002	43.203	4	5.423	0.531	0.019	0.015	43.203
6	519807.2	6815411.0	3.2	500.481	26.115	41.784	5	6.129	0.512	0.023	0.012	41.784
7	519665.8	6815463.0	3.0	400.445	26.076	39.115	4	5.982	1.112	0.029	0.023	39.115
8	519793.8	6815435.0	2.8	500.406	25.857	36.200	5	6.247	0.469	0.028	0.020	36.200
9	519766.8	6815457.5	3.4	500.494	25.144	42.745	5	5.827	0.666	0.021	0.012	42.745
10	519645.0	6815590.0	3.2	500.457	25.010	40.015	5	6.044	0.569	0.021	0.012	40.015
11	519947.8	6815433.0	3.2	400.424	23.480	37.568	4	6.063	1.173	0.032	0.029	37.568
12	519947.6	6815433.0	3.4	400.448	23.145	39.346	4	6.359	1.388	0.034	0.031	39.346
13	519450.6	6815654.5	2.4	300.217	17.016	22.121	3	3.807	0.654	0.034	0.025	22.121
14	519531.0	6815627.0	2.4	300.182	16.280	19.536	3	3.589	0.643	0.036	0.032	19.536
15	519484.4	6815790.5	3.4	100.254	14.653	24.909	1	3.331	1.532	0.040	0.040	24.909
16	519369.2	6815730.0	2.2	100.120	13.593	14.952	1	3.196	1.230	0.050	0.046	14.952
17	519483.8	6815791.0	2.4	100.149	13.162	17.111	1	2.588	1.018	0.044	0.043	17.111
18	519390.4	6815472.0	3.4	100.196	12.115	20.596	1	3.385	2.623	0.048	0.048	20.596
19	519577.8	6815837.5	1.6	200.047	11.943	9.554	2	2.500	0.502	0.062	0.047	9.554
20	519390.4	6815459.0	3.4	100.185	11.640	19.788	1	2.323	1.031	0.038	0.036	19.788
21	519334.8	6815427.0	3.4	100.177	11.305	19.219	1	3.731	2.772	0.049	0.048	19.219
22	519419.2	6815887.0	2.2	100.077	10.710	11.781	1	2.505	1.096	0.058	0.059	11.781
23	519425.2	6815914.0	1.4	100.019	10.625	7.437	1	2.600	1.946	0.104	0.105	7.437
24	519484.8	6815417.0	3.4	100.158	10.436	17.741	1	2.863	2.146	0.046	0.046	17.741
25	519651.6	6815828.5	3.4	100.156	10.358	17.608	1	2.517	1.164	0.038	0.036	17.608
26	519422.0	6815958.0	1.6	100.028	10.146	8.117	1	2.097	0.683	0.076	0.078	8.117
27	519396.2	6815478.0	3.2	100.134	10.006	16.010	1	2.551	1.237	0.043	0.042	16.010

3.2.2 Detection of pitfall traps in reduced versions of lidar data

The analysis described in Section 2.5.5 was performed on the entire Olstappen dataset (Table 23).

Table 23. Detection results on reduced point density datasets. Detection categories are from a manual inspection of the detection results on the full resolution dataset, with '9' being a certain true detection of a cultural heritage pit, '5' being in doubt, and '1' being a certain false detection. Categories 2-3 are probable false detections, with something resembling a pit. Categories 6-8 are probable cultural heritage pits.

point density		detection category										
factor	per m ²	1	2	3	4	5	6	7	8	9	Sum 5-9	
1	7.277	1756	164	42	0	35	6	59	53	109	262	100.00 %
0.9	6.549	1458	141	40	0	33	5	58	53	109	258	98.47 %
0.8	5.822	1295	136	33	0	32	5	56	52	107	252	96.18 %
0.7	5.094	1170	124	32	0	30	6	56	52	107	251	95.80 %
0.6	4.366	1065	108	28	0	29	4	52	53	107	245	93.51 %
0.5	3.638	947	97	28	0	26	4	49	52	106	237	90.46 %
0.4	2.911	806	79	24	0	21	4	49	50	103	227	86.64 %
0.3	2.183	636	75	17	0	19	4	46	46	103	218	83.21 %
0.25	1.819	559	62	18	0	17	4	44	44	105	214	81.68 %
0.2	1.455	482	53	13	0	15	3	37	42	101	198	75.57 %
0.15	1.092	360	43	16	0	11	2	31	41	91	176	67.18 %
0.1	0.728	252	33	9	0	6	2	23	34	82	147	56.11 %
0.08	0.582	198	29	9	0	6	0	21	29	74	130	49.62 %
0.06	0.437	143	22	6	0	6	0	14	21	71	112	42.75 %
0.04	0.291	94	16	3	0	3	0	9	12	47	71	27.10 %
0.02	0.146	35	4	0	0	1	0	1	3	26	31	11.83 %
0.01	0.073	15	1	0	0	2	0	0	3	9	14	5.34 %
0.005	0.036	6	0	0	0	0	0	0	0	1	1	0.38 %
0.003	0.022	2	0	0	0	0	0	0	0	0	0	0.00 %
0.001	0.007	0	0	0	0	0	0	0	0	0	0	0.00 %

For the purpose of measuring the reduced detection on the datasets with reduced point density, one may consider detections of categories 5-9, spanning the detections labeled 'in doubt', 'probable detection' and 'certain detection'. These are 262 in total. For the datasets of reduced point densities, the number of detections are given in the two rightmost columns of Table 23 as absolute and relative figures.

By plotting the detection percentages, relative to the full resolution dataset, as a function of point density per m² (Figure 125), it is evident that the recognition rate drops slowly from 100% to 82% as the point density is reduced from 7.3 to 1.8 ground points per m². When the point density is reduced further below 1.8 points per m², the recognition rate drops more rapidly, reaching 50% at around 0.6 ground points per m².

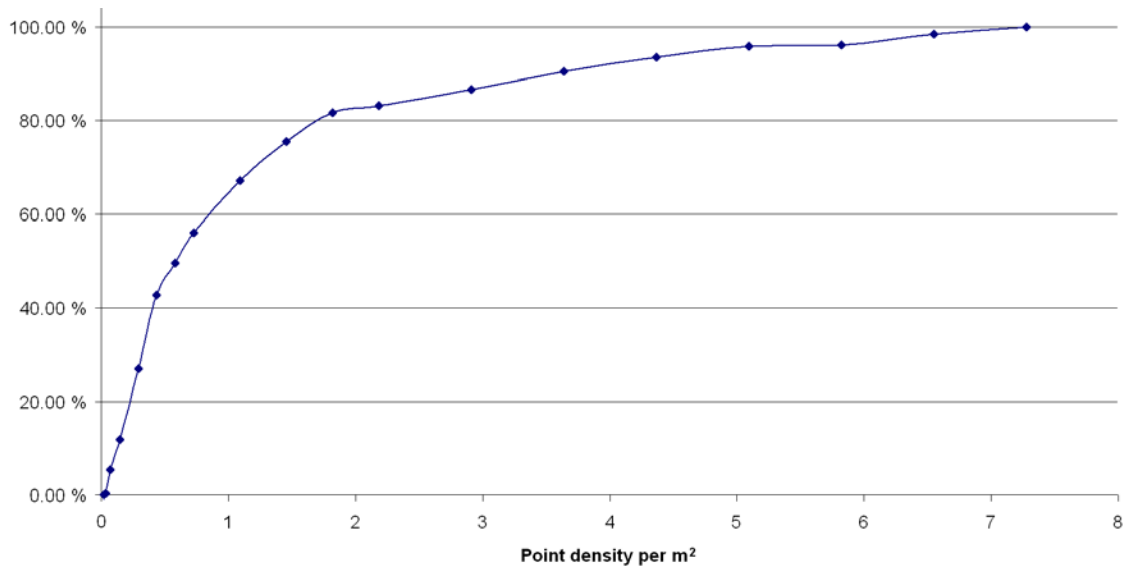


Figure 125. Detection rates as a function of point density, relative to the full resolution dataset.

4 Discussion

4.1 Detection of circular soil marks and crop marks in optical images

The detection method has been further improved during the 2010 project to further reduce the number of false detections and provide a meaningful ordering of the reported detections. The reported detections still contain more false than true detections, calling for a manual verification step after the automatic detection step. However many of the false detections are obvious, and can be quickly discarded.

The 2010 project was able to acquire many new 0.5 m resolution satellite images from the new WorldView-2 satellite. This, in turn, resulted in many new detections of leveled grave mounds. An obvious limitation of the method is that the leveled grave mounds be manifested as crop marks or soil marks in the images in order to be detected. The presence or absence of such marks is highly dependent of the level of humidity in the ground and the ability to predict the time at which crop marks will be visible at the time images are ordered. In addition, presence of clouds in the images reduces the area that can be searched.

4.2 Detection of pitfall traps in lidar data

Prior to the field work, it was quite obvious that the 12 strongest detections in image 32-1-503-169-6 were true detections. Detections nos. 13, 14, 16, 17 and 19 were all regarded as probable true detections. However, detection no. 14 appeared to have only one lidar hit inside the pit, and could thus be the result of artifacts due to too few ground hits and/or confusion between ground hits and low vegetation. Detection no. 19 was not found during the initial visual inspection of the laser data, but detected by CultSearcher, and confirmed in the field.

4.3 Point density of lidar data

The results of the experiments with reducing the point density of lidar data indicate that 1.8 ground returns per m² is a minimum requirement for the detection of pitfall traps. It should be stressed that the point densities in the experiments are ground returns, excluding vegetation and building returns. The specifications of the datasets refer to the number of emitted pulses, some of which never reach the ground. Therefore, when the experiments suggest that at least 1.8 ground hits per m² is needed, this means that the total number of emitted pulses per m² may need to be higher. How much higher depends on the vegetation density: denser vegetation needs a higher number of emitted pulses to maintain the same ground return density.

The Norwegian Mapping Authority has started a national lidar data acquisition in order to produce a new national digital elevation model, with an acquisition resolution of 0.7 emitted pulses per square meter. For the Olstappen dataset, this would result in about 50-55% recognition rate.

Three other effects are not addressed in the point reduction experiment. First, the flying height is higher when acquiring lower point densities, meaning that the footprint on the ground of each emitted laser pulse is larger, which means that the measured elevation is averaged over a larger area. Second, the shape of the pitfall traps and other pits are more distorted (Figure 126), meaning that the manual inspection of the detection results could be more difficult. In the present experiment, one had the luxury of doing the manual inspection on the full resolution dataset. Third, the number of false detections may increase.

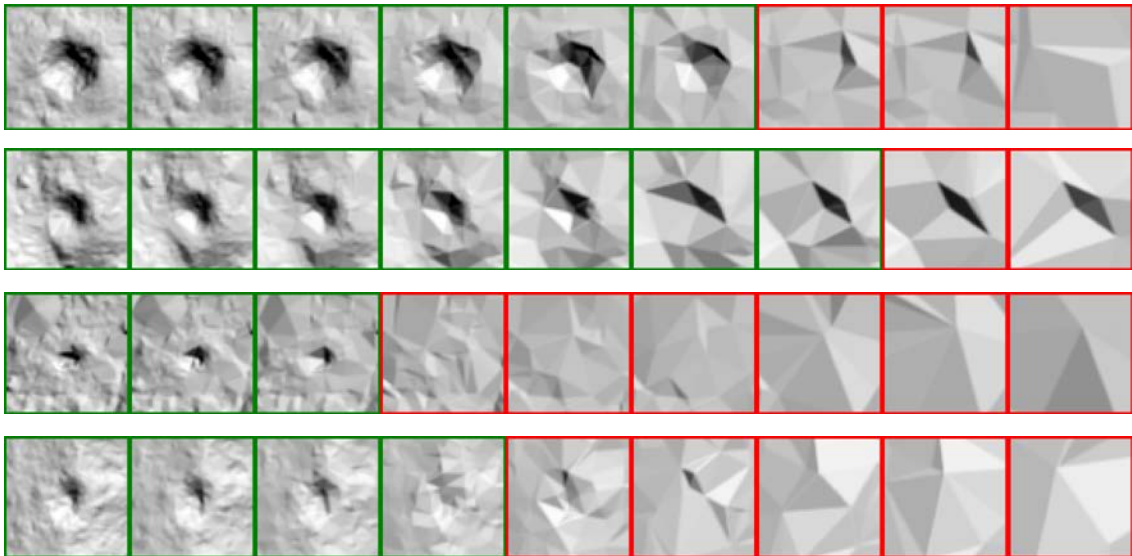


Figure 126. Four pitfall traps at nine different point densities. From left to right: original dataset with 7.3 ground points per m^2 , reduced dataset with 3.6 points per m^2 , 1.8 points per m^2 , 0.73, 0.29, 0.15, 0.073, 0.036, and 0.007 points per m^2 . A green frame indicates that the pitfall trap is detected at this resolution, while a red frame indicates that it is not detected.

In the point reduction experiment, a detection can be moved by up to two meters and still be valid. We have not investigated how much the detections actually moved in the reduced datasets. Obviously, if detections are moved, this has implications on the accuracy of the center coordinates of pits. Similarly, reduced point density has implications on the measured radii and depths of pits.

5 Concluding remarks

We think that the detection method has reached a level of maturity that makes it suitable for implementation in a pre-operational pilot, in which privileged users may log on, upload their images, run the detection method and get a shapefile with detection results back.

One current drawback with the current method is that if it is to be run on satellite images, these will have to be orthorectified manually, which takes time and is not always accurate. The process takes a couple of hours for one satellite image by the combined use of a digital elevation model (DEM) and manually digitized ground control points with known heights. The current national DEM has 25 m grid spacing, which means that some residual errors still remain in the orthorectified image, and the image will not align perfectly with GIS data. For example, we have observed that masks for agricultural fields may be off by a meter or two, thus including some strips of forest, with the possibility of misclassifying a tree crown as a circular object. However, the Norwegian Mapping Authority is creating a new national DEM based on laser scanning at 0.7 emitted pulses per m². This will provide a much more accurate DEM.

This drawback is not present when the detection method is run on aerial orthophoto or lidar height data, since these data are already correctly geocoded. Therefore, the first implementation of the pre-operational pilot could be made to operate on these data formats

Vestfold County has acquired lidar data of forested areas that are known to contain intact grave mounds. The detection method for lidar height data could be extended to detect such grave mounds.

The project should continue to acquire very high resolution satellite images (Worldview-2) for a few selected areas, e.g., Tjølling and Brunlanes. Especially for the Tjølling area, each new image has revealed new crop marks due to previously unknown leveled grave mounds.

Further, the project should continue to detect pitfall traps in lidar data. Oppland County has several datasets on which the detection method could be run. Many of these are of the same resolution as the Olstappen dataset, and it would be interesting to observe if equally good recognition performance could be obtained on these datasets. Also, there are some older datasets with lower point density, and it would be interesting to compare the detection performance with the reduced Olstappen data of the same point density.

References

References for soil and crop mark detection method

Aase, J. K., Siddoway, F. H., 1981. Assessing winter wheat dry matter production via spectral reflectance measurements. *Remote Sensing of Environment* 11, pp. 267-277.

Campbell, J. B., 2006. *Introduction to Remote Sensing, Fourth Edition*. Taylor and Francis, Oxon, UK.

Jenssen, R. and Principe, J. C. (2010). Information theoretic clustering. *Scolarpedia*, to appear 2010 (URL: http://www.scolarpedia.org/article/Information_theoretic_clustering).

Townshend, J. R. G., Goff, T. E., Tucker, C. J., 1985. Multitemporal dimensionality of images of normalized difference vegetation index at continental scales. *IEEE Transactions on Geoscience and Remote Sensing* 23 (6), pp. 888-895.

Varma, M. and Zisserman, A. (2004). A statistical approach to texture classification from single images. *Int. J. Computer Vision*, vol. 62(1-2), pp. 61-81.

References for detection methods on lidar data

Bewley, R. H., Crutchley, S. P., Shell, C. A., 2005. New light on an ancient landscape: lidar survey in the Stonehenge World Heritage Site. *Antiquity* 79, pp. 636-647.

Coluzzi, R., Masini, N., Lasaponara, R., 2010. Flights into the past: full-waveform airborne laser scanning data for archaeological investigation. *Journal of Archaeological Science*, in press.

Devereux, B. J., Amable, G. S., Crow, P., Cliff, A. D., 2005. The potential of airborne lidar for detection of archaeological features under woodland canopies. *Antiquity* 79, pp. 648-660.

Devereux, B. J., Amable, G. S., Crow, P., 2008. Visualisation of lidar terrain models for archaeological feature detection. *Antiquity* 82, pp. 470-479.

Hastie, T., Tibshirani, R., Friedman, J., 2009. *The Elements of Statistical Learning. Data Mining, Inference, and Prediction*. Second Edition. Springer: New York.

Hesse, R., 2010. Lidar-derived local relief models – a new tool for archaeological prospection. *Archaeological Prospection* 17, pp. 67-72.

Somol, P., Pudil, P., Novovičová, J., Paclík, P., 1999. Adaptive floating search methods in feature selection. *Pattern Recognition Letters* 20, pp. 1157-1163.